Physical uplink layer for NVIS remote sensor networks in hostile channels

Tomás González Fontán

http://hdl.handle.net/10803/688595

Data de defensa: 25-05-2023

UNIVERSITAT RAMON LLULL

DOCTORAL THESIS

Title	Physical uplink layer for NVIS remote sensor networks in hostile channels
Presented by	Tomás González Fontán
Centre	La Salle Digital Engineering School
Department	Engineering
Directed by	Joan Lluís Pijoan Vidal

"I thank …

"...first and foremost, to my family, who have always supported me at all times and in all circumstances".

"...to the GRITS research group. Without the guidance or support of its members I would not have written this thesis. Joan Lluís Pijoan, David Badia, Agustín Zaballos and Joan Navarro (my personal psychologist)."

"...to my friends of the project, Joaquim Porté, Jordi Malé and Joan Gómez. Above all I want to emphasize my friends Adrià Mallorquí and Josep Masó, with whom we shared the hard and great Antarctic experience".

"...And finally, to my unconditional friend since I moved to Barcelona city, Marc Diez".

ABSTRACT

The objective of this thesis is to study and improve the physical layer of an NVIS system in order to use this technology within a remote sensing ecosystem over hostile channels. The thesis has been developed during the SHETLAND-NET project which aimed to deploy an NVIS sensor network for the South Shetland Islands archipelago. The aim was to install a low-cost, low-power platform capable of transmitting signals by ionospheric propagation, with the objective of communicating two Antarctic islands to transfer sensor data.

A study of the current bibliography has been carried out and supported with previous studies on the topics: (1) HF channel sounding with different robustness improvement techniques, (2) modulations used in HF and in the new communication standards, outside the HF bandwidth and (3) common antennas in these systems and improvements in miniaturization.

With these three points, it is desired to improve the capabilities of NVIS technology, making a channel sounding with two propagation modes in order to use the Polarization Diversity technique and thus improve robustness.

On the other hand, from this channel survey, the SC-FDE modulation is designed, which is presented as the alternative to OFDM in the ascending layers, because it considerably reduces the PAPR effects generated by the subdivision of subcarriers and is able to maintain the advantages of OFDM.

Finally, the improvement proposed is the miniaturization of the antennas used in these systems, proposing a 15-meter antenna of Horizontal Dipole type that is buried underground, in order to reduce the current pollution generated by these antennas putting in context that they are antennas of sizes of minimum 15 meters long.

All these tests have been tested experimentally between the radio link of Barcelona and Cambrils at the disposal of the Escuela Técnica Superior de Ingeniería de La Salle (Ramon Llull University) which are approximately 100 meters apart.

As a final test, part of these studies have been tested in the Antarctic Research Campaign 2021-2022.

RESUMEN

El objetivo de esta tesis es estudiar y mejorar la capa física de un sistema NVIS con el fin de utilizar esta tecnología dentro de un ecosistema de sensores remotos sobre canales hostiles. La tesis se ha desarrollado en el transcurso del proyecto SHETLAND-NET que tenía como objetivo desplegar una red de sensores NVIS para el archipiélago de las islas Shetland del Sur. Se pretendía instalar una plataforma de bajo coste y consumo, el cual sea capaz de transmitir señales mediante propagación ionosférica, con el objetivo de comunicar dos islas Antárticas para poder transferir datos de sensores.

Se ha realizado un estudio de la bibliografía actual y sustentada con estudios anteriores de los temas: (1) Sondeo de canal HF con diferentes técnicas de mejora de robustez, (2) modulaciones utilizadas en HF y en los nuevos estándares de comunicación, fuera del ancho de banda de HF y (3) antenas comunes en estos sistemas y mejoras en la miniaturización.

Con estos tres puntos, se desea mejorar las capacidades de la tecnología NVIS, haciendo un sondeo de canal con dos modos de propagación con el objetivo de utilizar la técnica de Diversidad de Polarización y así mejorar la robustez.

Por otro lado, a partir de este estudio de canal, se diseña la modulación SC-FDE la cual es presentada como la alternativa de la OFDM en las capas ascendentes, debido a que reduce considerablemente los efectos del PAPR que genera la subdivisión de subportadoras, y es capaz de mantener las ventajas de la OFDM.

Por último, la mejora que se propone es la miniaturización de las antenas que se utilizan en estos sistemas, proponiendo una antena de 15 metros de tipo Dipolo Horizontal que se entierra bajo tierra, con el fin de reducir la contaminación actual que generan estas antenas poniendo en contexto que son antenas de tamaños de mínimo 15 metros de largo.

Todas estas pruebas han sido probadas de manera experimental entre el radioenlace de Barcelona y Cambrils a disposición de la Escuela Técnica Superior de Ingeniería de La Salle (Universidad Ramon Llull) que distan aproximadamente 100 metros.

Como prueba final, parte de estos estudios se han podido probar en la Campaña de Investigación Antártica 2021-2022.

RESUM

L'objectiu d'aquesta tesi és estudiar i millorar la capa física d'un sistema NVIS, amb la finalitat d'utilitzar aquesta tecnologia dins d'un ecosistema de sensors remots sobre canals hostils. La tesi s'ha desenvolupat en el transcurs del projecte SHETLAND-NET, que tenia com a objectiu desplegar una xarxa de sensors NVIS per a l'arxipèlag de les illes Shetland del Sud. Es pretenia instal·lar una plataforma de baix cost i consum, el qual sigui capaç de transmetre senyals mitjançant propagació ionosfèrica, amb l'objectiu de comunicar dues illes Antàrtiques per a poder transferir dades de sensors.

S'ha realitzat un estudi de la bibliografia actual i sustentada amb estudis anteriors dels temes: (1) Sondeig de canal HF amb diferents tècniques de millora de robustesa, (2) modulacions utilitzades en HF i en els nous estàndards de comunicació, fora de l'amplada de banda de HF i (3) antenes comunes en aquests sistemes i millores en la miniaturització.

Amb aquests tres punts, es desitja millorar les capacitats de la tecnologia NVIS, fent un sondeig de canal amb dues maneres de propagació amb l'objectiu d'utilitzar la tècnica de Diversitat de Polarització i així millorar la robustesa.

D'altra banda, a partir d'aquest estudi de canal, es dissenya la modulació SC-FDE la qual és presentada com l'alternativa de la OFDM en les capes ascendents, pel fet que redueix considerablement els efectes del PAPR que genera la subdivisió de subportadores, i és capaç de mantenir els avantatges de la OFDM.

Finalment, la millora que es proposa és la miniaturització de les antenes que s'utilitzen en aquests sistemes, proposant una antena de 15 metres de tipus Dipol Horitzontal que s'enterra sota terra, amb la finalitat de reduir la contaminació actual que generen aquestes antenes posant en context que són antenes de grandàries de mínim 15 metres de llarg.

Totes aquestes proves han estat provades de manera experimental entre el radioenllaç de Barcelona i Cambrils a la disposició de l'Escola Tècnica Superior d' Enginyeria de La Salle (Universitat Ramon Llull) que disten aproximadament 100 metres.

Com a prova final, part d'aquests estudis s'han pogut provar en la Campanya de Recerca Antàrtica 2021-2022.

TABLE OF CONTENTS

ACRONYMS

ADC	Analog-Digital Converter
BER	Bit-error rate
BPF	Band Pass Filter
CDF	Cumulative Distribution Function
CFR	Crest Factor Reduction
CP	Cyclic Prefix
CPU	Central Processing Unit
CR	Clipping Ratio
DAC	Digital-Analog Converter
DFT	Discrete Fourier Transform
DL	Downlink
Ds	Delay Spread
DTN	Delay Tolerant Network
EbNo	Energy per bit to Noise power spectral density ratio
EVM	Error Vector Magnitude
FDMA	Frequency Division Multiple Access
FFT	Fast Fourier Transform
FSK	Frequency Shift Keying
FPGA	Field-programmable gate array
FOT	Frequency of optimum transmission
HF	High Frequency
IBI	Inter-Block Interference
IBO	Input Back-off
ICI	Inter-Carrier Interference
IDFT	Inverse Discrete Fourier Transform
IFFT	Inverse Fast Fourier Transform
IoT	Internet of Things
ISI	Inter-symbolic interference
ITU	International Telecommunications Union
LNA	Low Noise Amplifier.
LoS	Line of Sight
MIMO	Multiple Input Multiple Output.
MMSE	Minimum Mean Squared Error.
MUF	Maximum Useful Frequency
NVIS	Near Vertical Incidence Skywave
OFDM	Orthogonal Frequency Division Multiplexing
OFDMA	Orthogonal Frequency Division Multiple Access
OSI	Open Systems Interconnection

PAPR	Peak to Average Power Ratio.
PN	Pseudo-Noise
PSK	Phase Shift Keying
QAM	Quadrature Amplitude Modulation
SC-FDE	Single Carrier Frequency Domain Equalization
SC-FDMA	Single Carrier Frequency Domain Multiple Access
SDR	Software Defined Radio.
SIMO	Single Input Multiple Output.
SNR	Signal to Noise Ratio.
TDMA	Time Division Multiple Access
ZF	Zero Forcing

FIGURE LIST

TABLE LIST

A. Introduction

1 Thesis introduction

In this chapter, the author explains where and how he became involved in the research activity, where he was able to participate in several engineering projects. Then, the background of the school and the research group is presented in order to put this thesis in context. Finally, the objectives of the thesis are presented from the hypotheses proposed.

1.1 Motivation

Mr. Tomas Gonzalez received his MSc. degree in Telecommunications Engineering from La Salle - Ramon Llull University (URL) in 2020. He is lecturer at Telecommunication Engineering Department of La Salle URL where he is lecturing "Signals and transmission systems", "Programming Methodology and Technology "and "Projects of Telecommunication Subsystem Design I" of the Master of Science in Telecommunication Engineering. He is currently a member of the Smart Society Group and participates in several R&D projects.

His motivation started when he first joined the Group of Research in Internet Technologies and Storage of the same University (GRITS). He was always interested in the evolution of communication standards such as 4G and 5G, and the project that GRITS was working on at the time he joined, were studies of the modulations that these standards involve in their schemes. This fact, and the involvement of Antarctica, the decision was not difficult.

1.2 Previous Work

La Escuela Técnica Superior de Ingeniería de La Salle (Universidad Ramon Llull) has been involved in research projects related to ionospheric communications for about 20 years. This type of communication works by bouncing High Frequency (HF) signals using the intrinsic properties of the ionosphere, linking distant locations. The first objectives of the project were defined in order to create very long-range communications for remote areas with oblique communications. These objectives were more than fulfilled using different types of modulations and signal processing techniques, achieving communication between the Antarctic Base Juan Carlos I and Catalonia (>12,000 km). The course of this study is described below:

In 2000, an advanced digital HF communications system using spread-spectrum technique was proposed as an alternative to satellite communication. This system should be fully configurable for any modulation (analogue and digital) and with error correction techniques. It had to be fast enough to transmit voice and data such as e-mail, but always with security as a priority. Finally, this system had to be as optimal as possible in terms of power. Finally, a system capable of transmitting at 100 bps was obtained [1]. A new blind multipath detection algorithm was presented in [2] that could both cancel the multipath interference and estimate the multipath channel response blindly. The method was especially designed for low coherence bandwidth channels, such as the ionospheric channel, and has very low computational requirements. The same authors presented in [3] new combined blind equalization and detection schemes for a DS-SS system that improved the bit-error rate compared to traditional RAKE receivers in multipath time-varying channels. Later, in 2003, the study described above began to be extrapolated, and the aim was to increase the supply of this communication. The project characterized an ionospheric radio-link channel from the Spanish Antarctic Base (62.6°S, 60.4°W) to the Observatori de l'Ebre (40.8°N, 0.5°E) in Spain. The paper [4] presents the final results of the project corresponding to the 2006/2007 survey. These results were used to design the physical layer of a low data rate transmission system to send the information acquired by a geomagnetic sensor in Antarctica. Such were these studies that resulted in the doctoral thesis of the author Carles Villella [5].

During this project, more authors participated in this thesis who later also presented their thesis following their contributions in papers such as [6] and [7] where a new technique was presented to reduce the PAPR generated by OFDM by separating the symbols into subcarriers. This was done with minimal additional computational cost and without the receiver needing additional information. Once the PAPR study was completed, the use of adaptive multicarrier clustered CDMA with adaptive modulation for the downlink was investigated to increase the user capacity of the system while maintaining satisfactory BER performance. In the paper [8] a physical layer based on DS-SS signalling for low SNR links is presented where preliminary transmissions were performed on a high frequency link between Antarctica and Spain. Up to 55.7% error-free transmissions were achieved using a transmission bandwidth of 5156Hz, a coded bit rate of 57 bps and a transmission power of 200W on an ionospheric link. The final contribution to Marc Deumal's thesis [9] were the papers [10][11] that presented an OFDM-based channel estimation between Spain and Antarctica and the proposals of two multicarrier transmission schemes based on measured channel transfer functions and noise and interference registers. Special attention is paid to the design of the pilot pattern in order to maximize system performance while ensuring high power and bandwidth efficiency.

In [12] a study of the time interleaving effect applied to OFDM symbols transmitted through a multipath time-varying long-haul ionospheric channel is studied. Following this study, it was extended to a 24-hour analysis for the entire HF band. In addition, new

measurements of the absolute propagation time and Doppler frequency shift were introduced at [13].

In [14] a comparison has been made between digital transmission techniques, direct sequence spread spectrum and orthogonal frequency division multiplexing, which can provide a low power, low speed ionospheric data link from Antarctica. As a conclusion spread spectrum techniques can be used to transmit data at low speed when the channel forecast is poor, but when the channel forecast is good multicarrier techniques can be used to transmit sporadic bursts of data at higher speed.

SC-FDE is also explored as a modulation for long distances under the channel between Spain and Antarctica [15], presenting promising first results. In [16] a study of narrowband and wideband channel was made by making a sweep in the whole band achieving a wider measure of channel availability than the previous ones. In [[17] a channel study is performed using an oblique incidence sounder (OIS) and measurements from several vertical incidence sounding (VIS) stations. The results show correlations that may lie in the fact that the frequency of highest availability can be estimated from VIS sounding measurements.

Paper [18] presents the BER performance comparison between SC-FDE, OFDMA and SC-FDMA in a long-distance HF data link with low SNR. The paper [19] closes the physical layer design, by studying the channel error and synchronization performance, and concludes with a new physical layer proposal for the oblique ionospheric probe.

The first NVIS analysis [20] starts with a channel sounding with raw data provided by Digisonde DSP-4D, developed by the University of Lowell. With these data, Doppler Spread and Doppler Shift evaluations are performed, as well as SNR for ordinary waves and X-ordinary. The use of phase modulations beyond the 3 KHz bandwidth has been tested too.

NVIS research by the school is explained in the state of the art because multiple references are made.

1.3   Context and hypothesis

Around 2013, studies have been focused on the integration of Internet of Things (IoT) networks to ionospheric communications using Near Vertical Incidence Skywave (NVIS) technology. For example the proposal of a low-cost NVIS system tested between one of the Andean communities of the Sacred Valley of the Incas in Peru and Urubamba [21]. This system communicates with a smartphone, running a messaging application, so low resolution texts and images can be sent. In this way a remote village can communicate with a nearby village.

This technology is a variant of ionospheric communications where signals are transmitted at an angle of incidence between 70 and 90 degrees, creating a coverage area

of radius 250 km. The use of this technology has been defined several times as an alternative to satellite, due to its low cost and ease of installation. The term IoT refers to the automation of common tasks through the use of sensors and the definition of specific communication standards. This fact has been transported to Antarctica as it is one of the most remote places in the world. Specifically, the motivation became the communication of two Antarctic islands transferring sensor data with the use of IoT and NVIS technologies. Internet use in Antarctic stations has a high cost per year, excluding maintenance costs and taking into account a connection speed of between 1 and 2 Mb for the entire station (in the case of the Spanish station Juan Carlos I). As a result of this context, of Antarctica, IoT, and satellite alternatives, an NVIS communication link was implemented, and its optimization was researched.

In summary, the goal of this thesis was to implement a communication system that could be used as an alternative to satellite and that could operate in remote areas such as Antarctica. In addition, this system had to meet the following requirements: (1) be low-cost, to be more cost effective than a satellite, (2) be able to manage IoT sensors, (3) be quickly and easily deployed, and (4) have a low power consumption, since all electricity in Antarctica comes from hybrid systems combining genset and renewable energies.

First of all, in order to know the characteristic effects of the ionosphere as a communication channel, it is necessary to know parameters such as channel availability, optimal frequencies, multipaths, etc.

From this point on, the following hypothesis are put forward:

> **Hypothesis 1:** *Can polarization diversity be exploited to reduce transmit power and/or antenna size?*
>
> *The ionosphere has a very dynamic behaviour. This intrinsic behaviour motivates us to define two fixed frequencies, one for daytime and another for night-time transmissions. In the absence of a system that can predict the state of the ionosphere and automatically change the frequency to the most efficient one, a study of the effects of ionospheric communication is needed. This thesis studied the two propagation modes (Ordinary and Extraordinary) that the ionosphere possesses. In this way we also seek to improve the robustness of the communication by leveraging polarization diversity to incorporate both modes; when the modes are added constructively, the quality of communication improves considerably.*

In order to define a physical layer for the NVIS technology, a transmission scheme based on HF standards (STANAG and MIL-STD) is followed. However, for a hostile environment, without including the suppression of effects such as multipath or fading, these standards are not entirely valid.

After completing the ionospheric sounding to obtain the channel parameters, we proceed to study and/or improve the modulation to be used. Until now, these

communications have used typical digital modulations such as Frequency Shift Keying (FSK), Phase Shift Keying (PSK) and Quadrature Amplitude Modulation (QAM), all with a drawback for real-time implementation: The equalization in time makes implementation complicated. It is true that current transmission schemes avoid channel effects by increasing the transmit power obtaining high Signal to Noise Ratio (SNR), however they do so in the time domain. In a sensor network we cannot use such schemes due to power consumption and the need for simple receivers. For this reason, the equalization will be done in the frequency domain.

We proceeded to use the multicarrier technique Orthogonal Frequency Division Multiplexing (OFDM) in order to try to solve the equalization problem, since it is done in the frequency domain. The study in [22] showed that the OFDM multicarrier technique improved FSK, PSK and QAM for a specific Energy per bit to Noise power spectral density ratio (EbNo). However, OFDM introduced two complications: on the one hand the technique needs to use class A linear amplifiers due to the nature of the signal, and on the other hand it has a very high Peak-to-average power ratio (PAPR).

Furthermore, the following hypothesis is also put forward:

Hypothesis 2: *It is possible to establish a low-power network of sensors between the Spanish Antarctic Base Juan Carlos I on Livingston Island and the Uruguayan Antarctic Base Artigas on King George Island. The network can be operational all-year round by using a modulation with equalization in frequency-domain and can outperform OFDM.*

OFDM is a modulation technique to protect against unwanted channel effects, such as multipath and fading, due to its design and the nature of the signal it forms. However, in systems requiring low power consumption, the PAPR of OFDM is critical. The proposed alternative to this technique, Single Carrier Frequency Domain Equalization (SC-FDE), is the same type of modulation that is already defined in some current communications standards such as 4G, 5G, and NB-IoT. While SC-FDE does not correct the channel effects as well as OFDM does, it does protect more from the most common interference in communication channels (noise). Additionally, it maintains the advantage of doing the equalization in the frequency-domain instead of the time-domain.

On the hardware side, radio platforms have improved greatly and are becoming more versatile, especially with the introduction of radio front ends with Software Defined Radio (SDR) technology. Despite the improvements, these systems still require large antennas. Assuming the most commonly used antenna in HF (horizontal $\lambda/2$ dipole), and taking into account that ionospheric communications using NVIS have a frequency range between 2 and 10 MHZ, the antennas will have a size of 75 m and 15 m. The only studies and advances on the reduction of antenna size are in the military field, related to developing smaller antennas for use in their vehicle fleet.

From this point on, the following hypothesis is put forward:

Hypothesis 3: *Invisible antennas could work for NVIS IoT communications.*

There have long been disputes about visual pollution with the number of antennas deployed in large cities. A scenario is proposed, where the antenna is completely buried and is able to radiate enough to be used as an NVIS antenna. It is assumed that this antenna will have much less radiation, but this also happens with mobile antennas too. The study will be directly compared with a 30-meter horizontal dipole antenna tuned to 5.4 MHz.

1.4 Objectives of the thesis

1.4.1 Channel Sounding

Being a communication that depends on the state of the ionosphere, which never maintains its characteristics/parameters constantly, a study of the ionosphere as a communication channel is carried out to define the proper signal values to be transmitted. These studies will be carried out with a multi-day survey between Barcelona and Cambrils (transceiver nodes provided and implemented by La Salle). These studies have been previously done in oblique propagation (see State of Art chapter) and in NVIS only without polarization diversity.

The objectives of this item are:

- Previous channel sounding studies review and deduce the thresholds of the values of the parameters to be analysed.
- Evaluate parameters such as the Delay Spread (Ds) in order to know the duration that the protection against multipath must have in order to reduce the transmission power or simply the channel availability.
- Same study for the two propagation modes considered independent in order to also apply diversity techniques with the objective of finding an improvement in the NVIS channel (robustness or antennas size).
- To make a channel model in order to be able to simulate transmissions later on.

1.4.2 Modulation Study

Based on the proposed use of OFDM for NVIS, an attempt will be made to use another modulation in order to reduce the weak points. These studies will be carried out with a multi-day survey between Barcelona and Cambrils and two Antarctica islands. These studies have been previously done in oblique propagation (see State of Art chapter).

The objectives of this item are:

- Design and implement the SC-FDE modulation and perform a survey to compare with the previous OFDM.
- Implement this physical layer for the sensor (uplink layer, UL) in Antarctica in order to propose a use case where an NVIS gateway is designed to link sensor network devices covering large-scale remote areas in a secure manner in the context of ubiquitous sensor networks (USN).
- Study the SC-FDE with non-standard bandwidths in order to improve channel capacity overcoming the current bitrate.

1.4.3 Buried antenna

Considering that the antennas used for all these studies are of large dimensions (HF antennas), we propose the study, simulation, and implementation of a buried antenna. Since this NVIS system is intended for the transfer of sensor information, a small antenna size is desirable. These studies will be carried out with a multi-day survey between Barcelona and Cambrils. So far, the study of HF antenna miniaturization is a field that remains to be exploited. There is not enough literature on buried antennas of this style.

The objectives of this item are:

- Study the feasibility of buried antennas and its dependence on type of ground, depth, construction techniques.
- Simulate different antenna parameters at different heights for a buried antenna.
- Experimental test of a real buried antenna to achieve the trade-off of antenna size reduction and efficiency, as well as possible applications.

2 State of art

This chapter provides context, a conceptual introduction to the problems to be addressed, as well as the latest articles on each topic, in order to define the state of art.

2.1 HF communications

Current communication schemes, such as 5G, have opened up a wide range of possibilities that make all network strategies more flexible and provide much more versatility for using remote sensor applications. These are simple to deploy when service providers' infrastructure is available. In more remote or hostile locations, the communication possibilities become much more complex, being satellite communication the most widely used. Satellites entail a high deployment budget, as well as a complex process, which cannot be deployed comfortably.

HF communications (frequencies between 3 and 30 MHz) were used from the beginning for intercontinental communications, with not very high transmission speeds compensating for the communication distance. These communications are still in use, and scientists keep doing research on them. For example, in this study [23] efforts to mitigate piracy and misuse of the 7 MHz band that is often used for natural disasters and emergencies are discussed. Further considerations to band interference conditions and improper use of certain frequencies/communications are proposed.

Less than a year ago, one of Rohde and Schwarz's Communications and Electronics Engineers stated that HF communications will be the alternative to satellite communication. This is due to the implementation of digital modulations for spectral efficiency, research of new antennas achieving robustness and transmission speed [24].

The evolution of HF communications in the near future is divided into three lines of research and objectives according to the authors of [25]. The three paths mentioned are self-adaptation to an ever-changing environment "intelligent HF radio communication systems", broadband HF communications and heterogeneous networks (see 2.1.1 for more details).

2.1.1 HF history and evolution

Radio communications began to be used more than 100 years ago with radiotelegraph communications for long distances and powers greater than 100 KW. HF communications started out as point-to-point and shortwave and were mostly used by radio amateurs. As systems became more efficient, power and antennas were reduced. So far, three strongly differentiated generations of HF communications have been reflected explained below [26][27].

The first generation went through the need for narrowband HF radios capable of exchanging voice data on a 3 kHz channel. Continuous wave was gradually replaced by Frequency Shift Keying (FSK), Phase Shift Keying (PSK), Quadrature Amplitude Modulation (QAM) which introduced very significant improvements, but still the frequency selection was done manually. Also, satellites were introduced as an alternative communication with higher throughputs.

The second generation returned to the use of traditional HF communications due to attacks on satellites and the introduction of microprocessors that made it possible to switch from the analogue to the digital world. Also, communications became point-to-multipoint. The ALE (Automatic Link Establishment) system was introduced, which became standardized and allowed for reliability and speed of connection in the face of rapid changes in the ionosphere or occupied HF channels. At this point, military organisms such as MIL-STD (US Department of Defense standard for HF communications) or STANAG (North Atlantic Treaty Organization, Military Agency for the Standardization of HF Radio Links) were defined with the objective of standardizing transmission and reception parameters for HF communications. Currently, several studies are focused on improving these standards. For example, the authors of [28] outlined the current robust military waveform, defined in MIL-STD-188-110D, waveform 0, and compares it to the filter bank spread spectrum waveform (FBMC-SS). This comparison is made in order to propose this waveform for communications over ionospheric/cosmic wave HF channels.

The objectives of the third generation and fourth generation (current one) could be applied to today's challenges: linking faster and at lower Signal to Noise Ratio (SNR), more connected users and larger networks, higher speed...

The most significant changes were in the increment of the bandwidth using different techniques and improvement of the ALE system with a much deeper logic. A example of this is the study done in [29] which proposes a system where both the ALE and transmission procedures are fully parallel. They propose the simple "Constrained Greedy" channel allocation schemes and study the performance of a sample network in terms of throughput and message delay for various time-of-day and seasons. Results indicate that performance improvements up to an order of magnitude are possible compared to conventional systems.

With the improvement of ALE systems and the use of higher bandwidth, heterogeneous networks and broadband transmissions were introduced. An example of that is the study in [30] which shows that recently introduced wideband (up to 24 kHz) and multiband (multiple 3 kHz bands) HF communications make sense based on a measurement campaign conducted in Finland.

The current generation tends to use technologies related to artificial intelligence and machine learning, big data in the case of data collection. The motivation to transmit more data led to the use of new standards that make HF communications capable of transmitting with 24 kHz channels. We can see this trend in the study of [31] where a

new low-cost reconfigurable software defined radio (SDR) platform for high frequency (HF) applications is presented with NVIS preliminary results, which can be reprogrammed according to modulation and channel type. The transmission can be adapted to the best propagation frequency at any time by means of a previous analysis even at bandwidths up to 36 kHz.

Another example of the higher bandwidths for HF communications is the investigation of [32]. Based on various performance metrics from two campaigns conducted in the upper Midwest region of the United States of America, a prototype implementation of a Wideband High Frequency (WBHF) Automatic Link Establishment (ALE) protocol is proposed as a frequency, bandwidth and data rate selection function for HF channels ranging from 3 kHz to 48 kHz wide.

Fig. 1 shows the possible research areas in this generation in the near future:

- Intelligent HF Radio
- Wideband HF
- Heterogeneous Networking.

Some results of this point could be checked in the proposal of [33] where a deep learning framework which extracts features along the time axis at each frequency bin, and predicts multiple characteristics of the signal, including the centre frequency and the shape attributes. The unique advantages of the framework are the utilization of all time features and no prior anchor which adapt to the slender shape of signal with a strong generalization ability. Results prove the superiority of the proposed framework both in accuracy and speed.
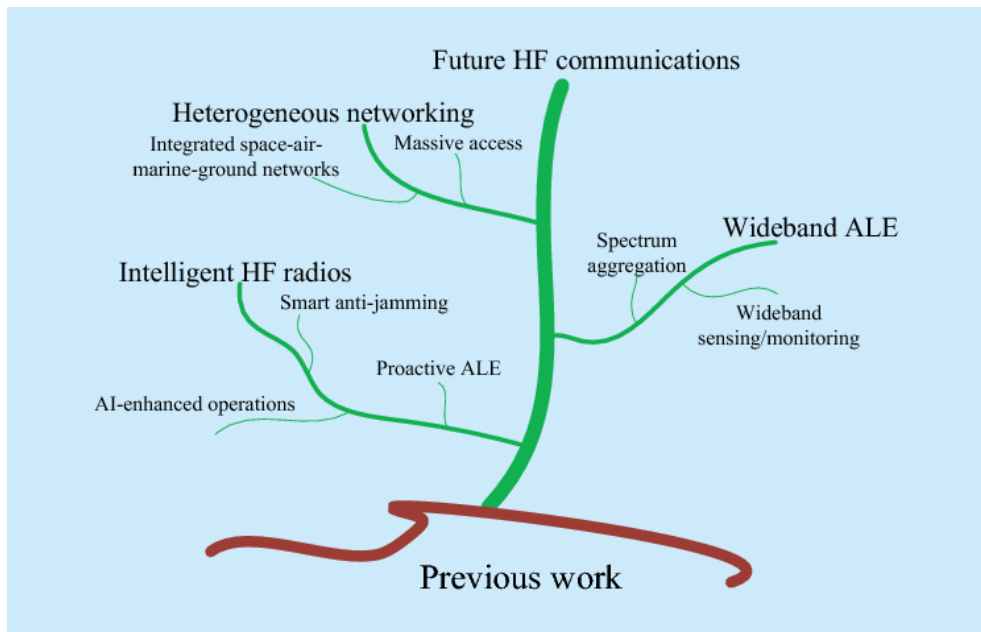
Fig. 1 Research areas in the future of HF communications [26]

Apart from these lines of research/objectives, it is necessary to talk about the multiple applications of these communications. By making transmissions more efficient, it leads to the convergence of many applications. It is here, where the term Internet of Things, mentioned above, benefits from all this: A framework of cooperative multi-station secure transmission in high-frequency skywave communications for wide-area Internet of Things (IoT) applications by simultaneously exploiting the benefits of massive multiple-input multiple-output (MIMO) and coordinated multiple points communications were studied in [34]. Another application could be the article [35] which presents a solution for one-dimensional localization based on magneto-inductive (MI) waves, since passive RFID tags in the HF regime present significant problems, due to the absence of radiating fields at the low frequencies involved. Another example is the U.K.-based amateur radio project involving a network of beacon transmitters and monitoring stations operating at 5.290 MHz [36].

2.2   Ionospheric Communications

HF transmissions are commonly referred to as "direct waves" when there is a clear Line of Sight (LOS). Sometimes, there is no LOS when the location is more remote, or the terrain is more difficult. As an alternative to direct wave communications, "skywave" communications make sense. These communications are also called ionospheric communications and take advantage of the ionosphere as a communication channel. Thanks to solar radiation and other phenomena that influence its state, the ionosphere can reflect shortwave electromagnetic waves. This communication is used as an alternative to costly satellite communication and is employed in remote locations where telecommunications infrastructure is not deployed or is scarce.
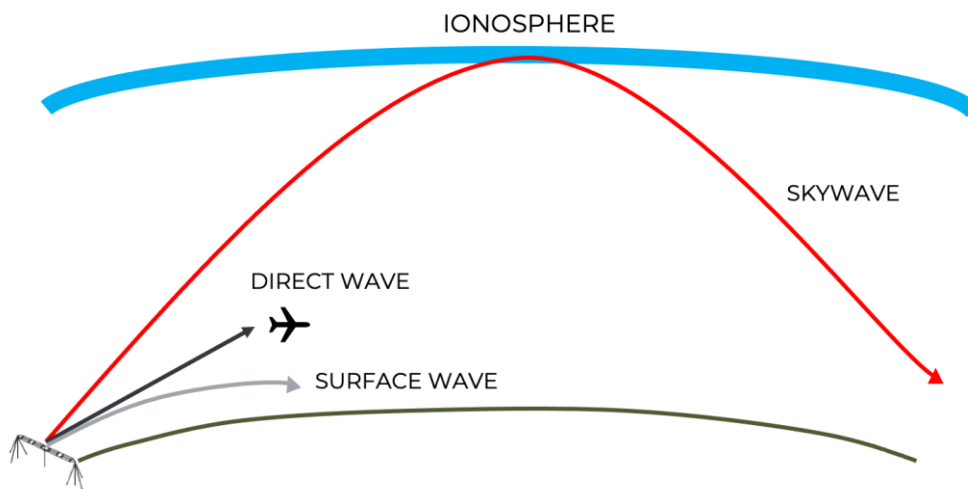
Fig. 2 *HF communication types* [37]

These communications are divided into two main groups depending on the distance to be covered and the bitrate.

- Oblique Communications: These communications are long distance when the beam is focused towards the horizon. The wave could reach less than 4000 Km for one hop having a low incidence angle [38].

  A major disadvantage of this communication is that the signal is very small because of the long distances to be covered and the amount of data to be transmitted is very small. However, in [39] developed an HF band communication system providing digital voice transmission within a bandwidth of about 3 kHz, through ionospheric reflection, mainly OFDM systems. The combination of this feature with CDMA (code division multiple access) spread spectrum type schemes provides an extremely robust modem without the need for powerful codes and long interleavers to guarantee a specific data rate and quality of service. However, [40] investigated the performance of coded and uncoded OFDM and OFDM-CDMA waveforms in various high-frequency channels with multipath and fading.
  For long distance communications, the studies in [18][19] demonstrates its total viability communicating Antarctica with Spain.
  The oblique communications are still being studied, as for example in the study in [41] An empirical virtual height model is proposed for both ionospheric and ground scatter (GS) observations and provides an improved estimate of the ground range to the backscatter location. It is intended for mid-latitude HF space weather radars of the Super Dual Auroral Radar Network (SuperDARN).

- NVIS communications: Military forces discovered a way to communicate which was very easy to deploy and had fewer deployment costs. These communications were based on transmissions in the HF band, directing these signals towards the ionosphere in order to bounce the signal back. This technology has grown in recent years with the arrival of SDR modules due to its high versatility and low cost.
  Following the standards described in MIL-STD and STANAG, extensive research continues done to improve transmission schemes. This technology can be easily used in remote locations, thanks to the lack of direct line of sight. Either if the areas to communicate have difficult access, or these locations lack infrastructure, NVIS communications are a suitable solution. These communications can reach 250 km range, and no direct line-of-sight link can match it, since the longest distance would be about 70-80 km. Of course, the link distance depends on the transmission angle (between 70º and 90º) which also influences the maximum usable frequency (MUF), typically between 3 and 10 MHz [7].
  However, some studies discuss some design patterns. The study in [42] argues that there are errors in existing NVIS transmitter elevation angle calculation methods, thus presenting a synthetic method for predicting the transmitter

elevation angle of these communications links to be used for frequency selection and communication field strength prediction. In addition, the absence of solar cycle in several periods, conduct to observe the channel availability as for example the study in [43] where the motivation to implement NVIS for homeland security or disaster purposes, NVIS performance limiters are determined based on solar conditions, times of day, and geophysical locations. Also, the study in [44] Day-by-day observations were conducted throughout 2019 to examine the existence of an NVIS HF channel using the WSPR method between Surabaya and Jombang which is separated by approximately 70 km away. This motivation comes from the minimum solar cycle period predicted in 2019, which is detrimental to HF propagation.

Regardless of the type of communication used, ionospheric communications transmitters need to have a channel status, even if approximate, due to the multitude of effects produced by these communications. The difficult prediction of the ionosphere has led to the continuous study of the ionosphere. Examples include the following studies: The availability of the NVIS channel in the medium wave band has been thoroughly studied and analysed in [45]. In addition, the optimal period for transmitting this type of signals during the night from Spain is proposed. The proposal in [46] determinates the optimum carrier frequency for NVIS (which changes by the state of the ionosphere) proposes a simple method to visualize the opening channel of the ionosphere using the ionogram data. Also, a BPSK Ionosonde based on the SDR platform is implemented in [47]. Algorithms are determined to measure parameters such as SNR, Delay Spread (Ds) and Doppler spread in an NVIS channel by choosing a suitable and reliable communication channel.

Complex algorithms, as well as multiple machine learning techniques, are being used to try to predict the critical frequency, variations, anomalies, channel effects, among others [48][49][50]. Therefore, the latest studies on ionospheric communications are very focused on the study and prediction of the ionosphere.

In addition, solar activity operates in a cyclic manner and directly affects the behaviour of the ionosphere. These are fluctuations in the amount of energy emitted by the sun, which follows a pattern of approximately 11 years. According to ESA (European Space Agency), July 2025 is expected to be the day with the most sunspots in this cycle [51].
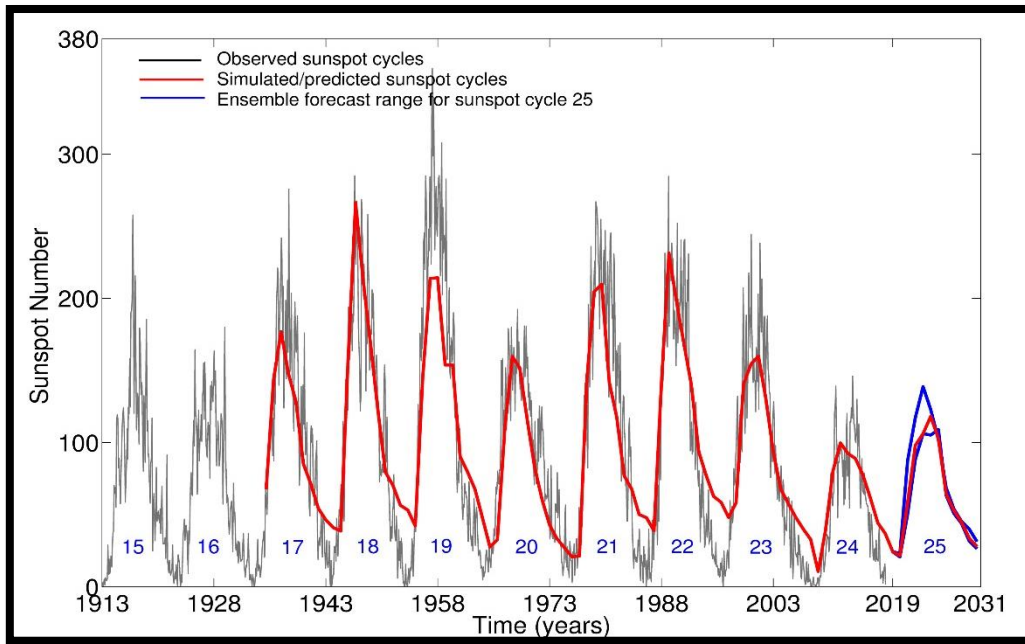
Fig. 3 Prediction of the solar cycle [52]

2.3   Capacity improvement

Many techniques are investigated in order to improve the capacity of these communications. While the theoretical calculation of capacity is limited by Shannon's theorem, this value can be increased by taking advantage of multipath propagation. Multiple propagation is beneficial when there is a decorrelation between signals. The most commonly used decorrelation is special diversity, which consists of increasing the number of antennas in both transmission and reception [53]. An example of that can be seen in Fig. 4.
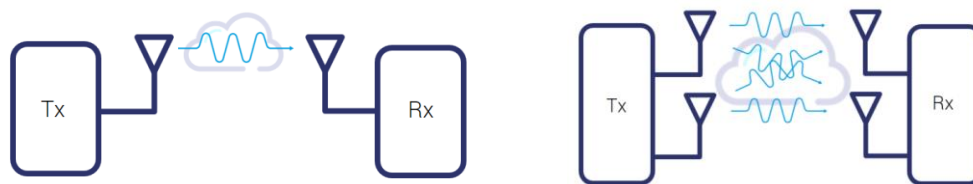
Fig. 4 Example of SISO system and MIMO system 2x2 [54]

This concept is widely used in current communication standards. However, in channels as narrow as those of NVIS, much research has been done on increasing capacity. Some examples are: (1) the paper [55]   proposes the improvement of channel capacity by making use of ordinary (O) and extraordinary (X) circular polarization inherent in NVIS. The implementation of a 2x2 (MIMO) system under a theoretical study improves a SISO

system and simulations are performed in the 7 MHz band. (2) Also, the measurement system in [56] is designed to obtain the channel response as the basis of HF MIMO (2x2) NVIS channel modelling between Surabaya-Malang. (3) In the papers [57][58] the authors focus on HF MIMO bulk communications using OFDM modulation using the sampled direction vector array. Their investigation focuses on the effect of propagation delay through the large-scale antenna array, so they use statistical channel state information (CSI) in the beam domain is frequency independent. They considered a minimum mean-squared error (MMSE) based Uplink (UL) receiver and downlink (DL) precoder with perfect CSI at the base station (BS).

The paper [59]demonstrates why spread-spectrum multicarrier technologies, such as MC-CDMA, are very robust for HF communications versus simple OFDM for delay-sensitive transmissions. The recognition that MC-CDMA could be interpreted as a kind of correlated spatial MIMO.

2.4   Modulations

The evolution of communications in the last two decades has been exponential. In Spain we have evolved from having peak data rates of 384 kbps (peak data rate and only downlink) in 3G standards around 2005, to practically having speeds of 1 Gbps with 5G in less than 20 years. In fact, the most widely used applications in everyday life, such as WIFI or the recent 5G communication schemes, are digital signals and maximum spectral efficiency is sought to reduce the size of the antennas, use batteries.... This leads to improvements in simpler equalization and therefore choose the best type of modulation.

In communication standards such as mobile calls, Time Division Multiple Access-based techniques (TDMA) were used, which split a single radio frequency channel into several time slots. With the advances mentioned above, the Frequency Division Multiple Access (FDMA) technique began to be exploited. These advances, whether in WIFI or in recent 5G communication schemes or NB-IoT, use multi-user Orthogonal Frequency Division Multiplexing (OFDM) and Single Carrier Frequency Domain Equalization (SC-FDE) techniques, which are modulations from several years ago, already used in the late 1990s in the case of SC-FDE. This is due to the use of different techniques applied in these modulations, improving their drawbacks, and not to the search for new ones.

Last research projects propose improvements as in [60] using new modulation technique to improve the performance of the conventional modulation that uses intensity modulation/direct detection (IM/DD) for On-Off Keying (OOK) modulation. But in fact, this modulation is not the most efficient one, and is not used in most modern systems and transmission schemes.

The paper [61] argues that OFDM is not able to meet the new challenges of future communications (latency, throughput, security...) and proposes to compare OFDM with cyclic prefix (CP) and FBMC with Offset Quadrature Amplitude Modulation (OQAM), in which the latter comes out as the winner.

In 2.4.3 we can see that almost all recent studies are based on 4G and 5G modulations and seek to get the most out of the transmission schemes by comparing new models. However, many of the proposed physical layers are still based on OFDM and/or its multiple user version. a more robust 5G communication using an OFDM modality with MIMO is proposed in [62] based on the following module design including improved modulation (OFDM-M), multiple antenna arrays and sub-band pre-distortion for average peak-to-power ratio (PAPR) reduction.

However, all these techniques are for technologies that use bandwidths greater than 20 MHz. Our system works at 3 kHz and the only thing that is comparable is the spectral efficiency (bps/Hz). In addition, the ionospheric channel is considered slow fading selective channel which is the same as the mobile technology. Therefore, we can rely on the techniques used to adapt them to HF communications.

2.4.1 OFDM

Multi-carrier techniques were discovered more than 50 years ago. One of the modulations using this technique is OFDM. OFDM is a modulation in which the symbols of a digital modulation (usually QAM or PSK) are placed in parallel on different small carriers (subcarriers). This relies on the orthogonality of the subcarriers created by the small spacing between them. Thus, the maximum of each of the subcarriers falls on the minimum of the adjacent one.

This modulation is still under research with some examples as: the study in [63] which proves that NVIS transmissions using OFDM between 2.5-7.6 MHz carriers are reliable when the SNR exceeds 14 dB and when the receive location is well characterized empirically prior to link deployment. Another example is the analysis of the principles of millimetre wave propagation from the study in [64] using the software defined radio (SDR) system, by varying OFDM design parameters such as modulations and number of subcarriers.

One of the advantages of subcarrier division is that its bandwidth is calculated with the coherence bandwidth, so each "packet" of symbols (or set of bits) suffers (or not) the same channel effects.

Another advantage of using this modulation that other digital modulations do not have is the use of mathematical expressions such as Fast Fourier Transform (FFT) and Inverse Fast Fourier Transform (IFFT) optimizing performance especially in the equalization that is performed in frequency in the receiving part. When the symbols are in the time domain once the IFFT is applied.

In summary, the composition of OFDM ensures data transmission in multiple parallel sub transmissions at lower speed, but in a robust way, which helps the stability of any communication system. Also, the use of a CP makes it highly resistant to multipath resulting in improved Intersymbolic Interference (ISI). Furthermore, another advantage is that the insertion of pilot symbols is easily comparable by the receiver, where Zero Forcing (ZF) equalization is mostly performed. These pilots can be followed where there are articles that demonstrate the best distribution as in the article [65], which argues that the hexagonal distribution always improves the horizontal distribution.

As a contrast, the fact of subdividing symbols into subcarriers causes the difference between the maximum point and the average value of the signal to be excessive. This effect is known as PAPR and induces the use of Class A amplifiers and the consumption of more power.

Several research studies on PAPR reduction are presented in: [66] which proposes an improved physical layer for new wireless systems by reducing the nonlinear effects introduced by the PAPR along with the linear areas of an amplifier. The combination of hybrid companding and pre-distorter offers better performance, it can reduce PAPR and compensating for nonlinear distortions caused by the PA.

Another study is the combination of M-QAM modulations, Low-Density Parity Check (LDPC) codes and Interleaved Frequency Division Multiple Access (IFDMA) multiaccess techniques is studied in [67] to increase system capacity, reduce the peak-to-average power ratio (PAPR), and improve Bit-Error Rate (BER) performance. Better performance results are achieved.

2.4.2 SC-FDE

In current communication standards, the need for a single transmitter for the user side (mobile terminal, or user equipment (UE)), forced to make changes in multicarrier techniques. SC-FDE was introduced in 1973 where some weaknesses of OFDM were improved (lower PAPR, lower sensitivity to carrier frequency offset, no need for linear amplifiers, robustness against spectral nulls).

The complete scheme of a SISO system with SC-FDE does not differ from that of OFDM except for where the Inverse Discrete Fourier Transform (IDFT) is implemented, keeping the Discrete Fourier Transform (DFT) in the receiver. The IDFT application is performed at the receiver, leaving the transmitter as simple as possible, having its waveform almost constant envelope characteristics, being considered a single carrier, and using a simple equalization as it is performed in the frequency domain.

In SC-FDE pilot schemes, values have a variation compared with other modulations. For example, OFDM can have a symbol full of pilots (all the subcarriers with the same value). In contrast, SC-FDE needs to have different pilot values due to the FFT, which converts these values to zero. Therefore, the root Zadoff-Chu sequence must be used, which is a sequence that presents different values, but in-module are the same value [37].

As a disadvantage, SC-FDE modulation is noise-sensitive, so the equalization method cannot be Zero Forcing (ZF) (as in OFDM) by taking noise into account, as well as the effects of the channel.

Fig. 5 shows the schematics of both modulations where the change in the position of the IFFT is clearly seen. Also, Table 1 summarizes the characteristics of both modulations.
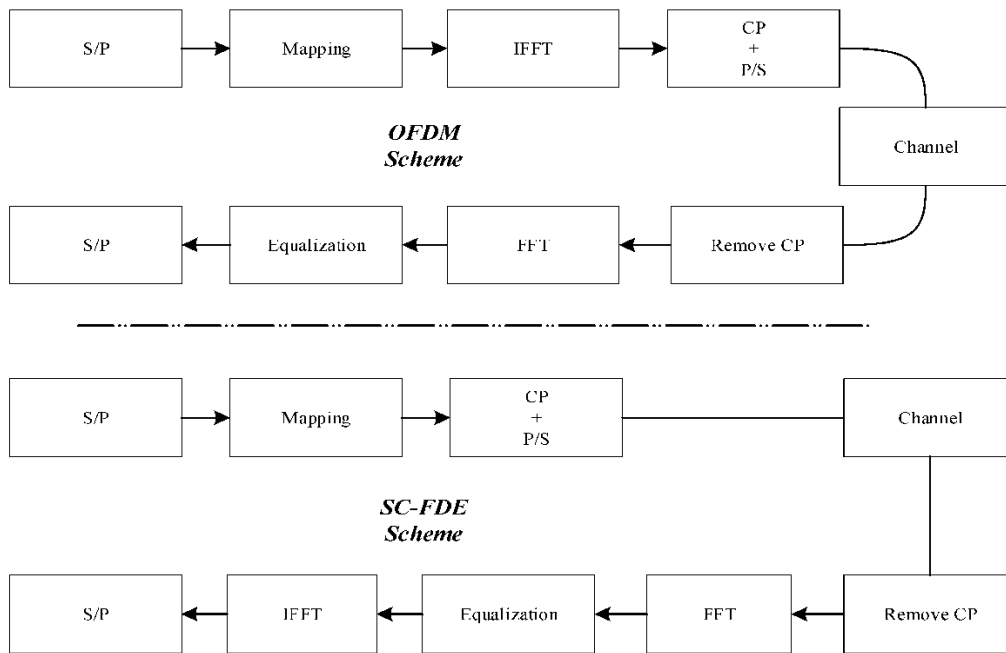
Fig. 5 OFDM and SC-FDE schemes. Note the change of IFFT position between OFDM and SC-FDE

Table 1. OFDM vs SC-FDE characteristic comparison

Parameters	OFDM	SC-FDE
Energy efficiency	Bad	Good
Robustness against ISI	Good	Bad
Robustness against Doppler Shift	Bad	Good
Robustness against CFO	Bad	Good
PAPR	Bad	Good
CCI	Bad	Good
Spectral Efficiency	Good	Bad
BER/Bitrate Efficiency	Good	Bad
Equalization complexity	Good	Bad

2.4.3   5G research

Since the implementation of 5G and its increasing use, all research is focused on the development of 5G. A evolution of mobile technologies from 2G to 5G in the physical layer [68]. Parameters such as spectrum, multiple user access, different types of channels, etc. are analysed. Equations are also formulated for the theoretical calculation of the speed offered by each technology.

- **Efficiency**: The efficiency of the 5G network was experimentally tested in [69] using MATLAB simulation for various modulation schemes. Quadrature phase shift keying (QPSK), 16QAM (quadrature amplitude modulation), 64QAM and 256QAM modulation schemes with signal to noise ratios (SNR) ranging from -10dB to 20dB in 5dB intervals were investigated.

- **Design:** Current design of 5G communications is not supported by the study of [70] arguing that is not as effective for future needs because there is already excess of user's demand. They propose procedures to overcome the current limitations of 5G. Different modulations for the OFDM scheme are compared in [71] and ranked according to efficiency and linked to 5G transmission schemes giving some design recommendations and future lines.
The study in [72] also proposes a new design by using a Filter Bank Multi Carrier (FBMC) for 5G against OFDM modulation in millimetre wave (MMW) transmissions, because it is much more robust against weather conditions that cause phase distortion.

- **Capacity Improvement:** In the pursuit of improving MU-MIMO systems in 5G, Per-user based Threshold Scheduling (PUTS) is proposed in [73] to solve BER performance allocation. The simulated results show that PUTS has improvement with the p level (p=0.442) in BER performance when compared to Fair Threshold Scheduling.

- **BER improvement:** Two new four-dimensional modulation schemes, 4DTCM-SP-128QAM and 4DTCM-SP-128TQAM, are proposed in [74] with lower BER. The simulation show that they can obtain 2.53dB and 1.33dB gain respectively with great potential used in long-haul optical transmission system.

- **IoT Application:** The work in [75] proposes a new receiver architecture appropriate for internet of things (IoT) and military applications. It has conventional power splitting under a linear model with a certain level of sensitivity together with modulation classification (SWPTMC) scheme.

- **Future:** [76] considers the implementation of a new waveform for the new 6G standards that are more spectrally efficient. An improvement in OFDM modulation called OFDM-HNIM is introduced as a hybrid modulation.
In this study [77], they deal with the potential and some implementation scenarios of spatial modulation (SM) techniques for the physical layer of 5G

wireless networks. The recent advances in SM technologies are reviewed and future research directions on the use of SM techniques towards high spectral and energy efficient 5G wireless communications networks are discussed.

2.5 Antennas

As mentioned before, communications systems are evolving day by day along with new technologies. The struggle to gain a couple of dBs of improvement is carried to all fields, and the antenna field is no exception.

If we take into account that HF communications are still widely used, for long distance communications and has been to date a very important communication tool used in disaster situations, the antennas for these communications are usually half-wave horizontal dipoles or half-wave V inverted dipoles, reaching sizes of 50 meters when talking about the 3 MHz frequency. This creates the need to minimize the size of the antennas to minimize the visual and aesthetic effect caused by having this type of communications active. One example would be the proposal of [78] which provides an example of shortwave active whip antenna design with working frequency range of 2MHz-30MHz. The designed active whip antenna has small size, light weight, wide frequency band and convenient disassembly, and can be widely used in some mobile occasions. This antenna aims to solve the difficulties of the current application of shortwave antenna.

2.5.1 Considerations

The power transmitted to the antenna is (partially) determined by the load at the input (input impedance). When the input impedance differs from that of the source (either because of the distance from the transmitter, and the connection is made by transmission lines or waveguide) an impedance mismatch occurs, measured by the reflection coefficient (ρ). Maximum power (maximum radiation efficiency = η_r) will only be transmitted to the antenna when impedance matching is present, i.e., when the antenna is matched (ρ=0). If this coefficient is related to radiation efficiency, we can get the concept of the total efficiency (η_t).

$$r = \frac{Z_L - Z_O}{Z_L + Z_O} , \eta_t = \eta_r (1 - |r^2|)$$

In order to be able to test a subway antenna we have to take all these factors into account in addition to defining certain objective parameters.

The size of an efficient antenna is proportional to the wavelength calculated from the frequency at which it is intended to operate. It can be concluded that NVIS antennas (taking into account that the operation band is between 3 and 10 MHZ) comprise a size between 15 and 50 meters using a λ /2 dipole (f<10 MHz and f>3 MHz respectively).

This leads to think about reducing the size of these antennas, so that they do not have a visual impact or at least reduce it, with the requirement to at least achieve a minimum gain of -20 dB.

2.6   Typical antennas

In order to minimize the large antennas that HF applications operate today, multiple antenna types and designs are discussed.

If we take a look at the latest research on antennas, we see only two types: (1) dual polarization and (2) vehicle antennas.

For dual polarization we can see that several systematic method for the design of dual-polarized HF antennas as proposed in [79] [80]. The first one is based on platforms for NVIS applications showing effective results. The second one is based on wireless communication systems, integrating a dual-linear to circular polarization converter (DLCPC) with a Ku-band linear polarization conversion metasurface (LPCM).

For vehicle antennas we can check the studies in [81][82] where an optimized antenna for NVIS when mounted on a typical "Land Rover" sized vehicle were presented. Or the project done in [83] alternative solutions to helicopter antennas for HF NVIS communications where proposed where was concluded that two towel-bar (loop) antennas, one on each side of the airframe and centred with respect to the hubs, can be used to reduce the severe drop in gain due to hub currents. At least, the project in [84], a low-profile triangular-shaped HF band receiver antenna is optimized for a long-distance communication system for NVIS, an alternative shaped antenna that is easy to fix on the vehicle with similar noise-related performance is optimized.

Dipole Antenna

As main characteristics, the $\lambda/2$ dipole has horizontal polarization, that is, parallel to the earth's surface, which is ideal for ionospheric reflection.
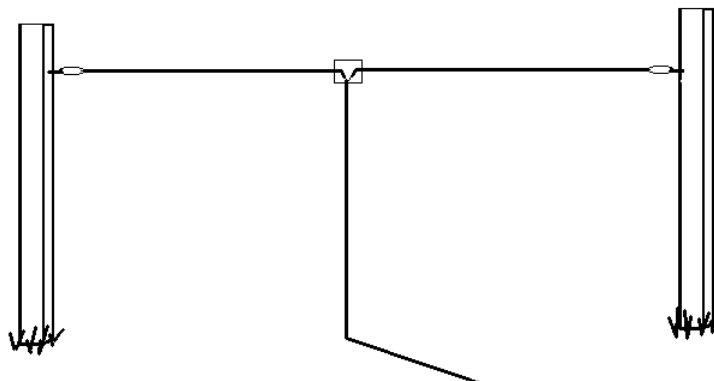
Fig. 6 *Dipole Antenna* [85]

Inverted-V Antenna

The V-inverted is a variant of the horizontal dipole, which is very attractive in amateur radio due to the lack of the need for two masts. The "feed" part becomes the maximum point of the antenna, and the arms hang at angles no greater than 120º. Thus, only one mast is needed. The gain of an inverted -V could achieve 6.8 dBi [86] and it has a radiation pattern nearly omni-directional.
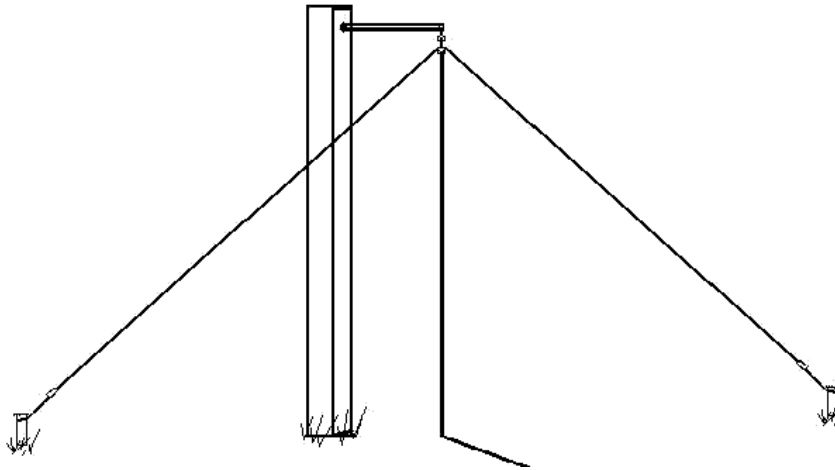
Fig. 7 *Inverted V Antenna* [85]

Loop Antenna

It is another variant of the dipole, where the arms form a circle. This type of antenna is very directive and very easy to install. On the other hand, its efficiency is rather poor, which is why it is used at such low frequencies. The gain of a loop is -2 dB y 3dB.
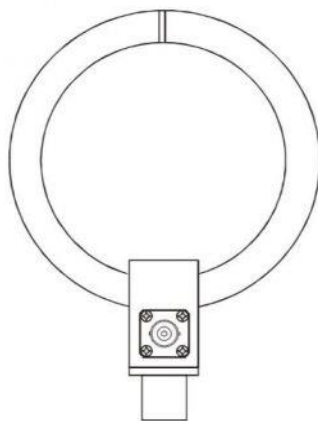
Fig. 8 *Small loop antenna* [87]

So far, several papers have simulated using different software different types of antennas in order to minimize the size. This is because, as mentioned before, the main application of this type of communications is in extreme situations of difficult access, where a military car transports the antenna.

2.7   Soil and its parameters

Once the design of the buried antenna is proposed, the properties of the soil that can influence the efficiency of the antenna are considered.

The composition of the soil is a mixture of air, water, organic and/or mineral materials. Based on these, various types of soil are distinguished, as well as their density. In studies such as [88][89][90] we see that depending on the amount of water in the soil and depending on the composition of its composition, the relative permittivity can vary between 5-6 times higher. In the table below, various values of the relative permittivity are shown for a particular soil only by changing the water content. This is due to the polarization capacity caused by the water molecules.

θ [cm³/cm³]	ε_r
0.10	5.343
0.15	7.451
0.20	10.116
0.25	13.281
0.30	16.889
0.35	20.881
0.40	25.201
0.45	29.791
0.50	34.592

Fig. 9 *relative permittivity increase (ε_r) and the water content in m³ compared to the volume of the soil (m³)* [90]

B. Contributions

This section will contain the development of the different objectives set out at the beginning of the thesis. During the development of the chapter, the conceptual and experimental contribution of each of the contributions is described.

In order to develop all the proposed objectives, the platform and hardware used are described below. Since the hardware was not developed solely by the author, who has only modified or added some components and is not part of his contribution, the most important parts are summarized below.

The hardware used in all studios is based on current SDR (Software Defined Radio) systems. SDR systems allow a wide range of possibilities due to their great versatility due to the possibility of designing components through software and not depending so much on the hardware. Specifically, our SDR system is composed of a primary element which is the FPGA "Red Pitaya STEMlab 125-14" [91] that has been used for signal processing thanks to its fast processing in the Digital Up Converter (DUC) and Digital Down Converter (DDC) stages thanks to DAC/ADC converters (Digital to analogue converter/ Analogue to Digital converter) which allow to digitize the analogue signal. A Raspberry Pi 3B+ [92] although this microprocessor is not strictly necessary (due to enough Central Processing Unit (CPU) of the Red Pitaya, but we use it for a future capacity requirement. So far, it manages all peripherals and the saving of frames received on a USB after being downlinked to baseband by the FPGA. A Teensy [93] (low-cost USB-based microcontroller) is used when the platform operates in Half-Duplex it switches between the transmit and receive modes of each node as well as the power management of the platform. A GPS [94] used as position sensor and used to synchronize transmitter and receiver. A Moteino M0 (low-power development board): used to implement the sensor's deployment. It is used together with Lora transceivers [95][96][97]. Finally, a BME280 [98], a low power weather sensor that integrates atmospheric pressure, temperature and relative humidity in a single device.

Apart from that, the typical radio communication hardware is detailed as follows:

- Amplifier:
  - Without power restriction and with the platform connected to the power supply, a Bonn 250 amplifier has been used with 48.5 dB gain, for example for ionosphere sounding tests.
  - For low-power applications a Minicircuits LZY-22+ was used with 30W typ. from 100 kHz to 200 MHz.
  - A Low Noise Amplifier (LNA) is placed after filtering the signal with a band pass filter (BPF) and before it enters the RF port of the Pitaya Network.

- Antennas:

    Horizontal and inverted-V dipole antennas have been used interchangeably. In the LaSalle façade there is a horizontal dipole acting as a transmitter, and in Cambrils (Tarragona) there is an inverted-V antenna, to which another one was added due to the study of the two propagation modes of the ionosphere. Both offer good performance (see 5.1), differing in the need for a single mast in the case of the V-inverted.

- Filters:

    A BPF have been designed by us giving an I.L of 0.6 dB in the 2-7 MHz range. However, sometimes we only wanted to filter AM signals in reception up to 2 MHz, so we used the Notch filter Flamingo AM for SDR applications [99].

Fig. 10 shows the different modules involved in the transmission and reception of NVIS communications. This diagram shows all the components of the platform throughout the SHETLAND-NET project.
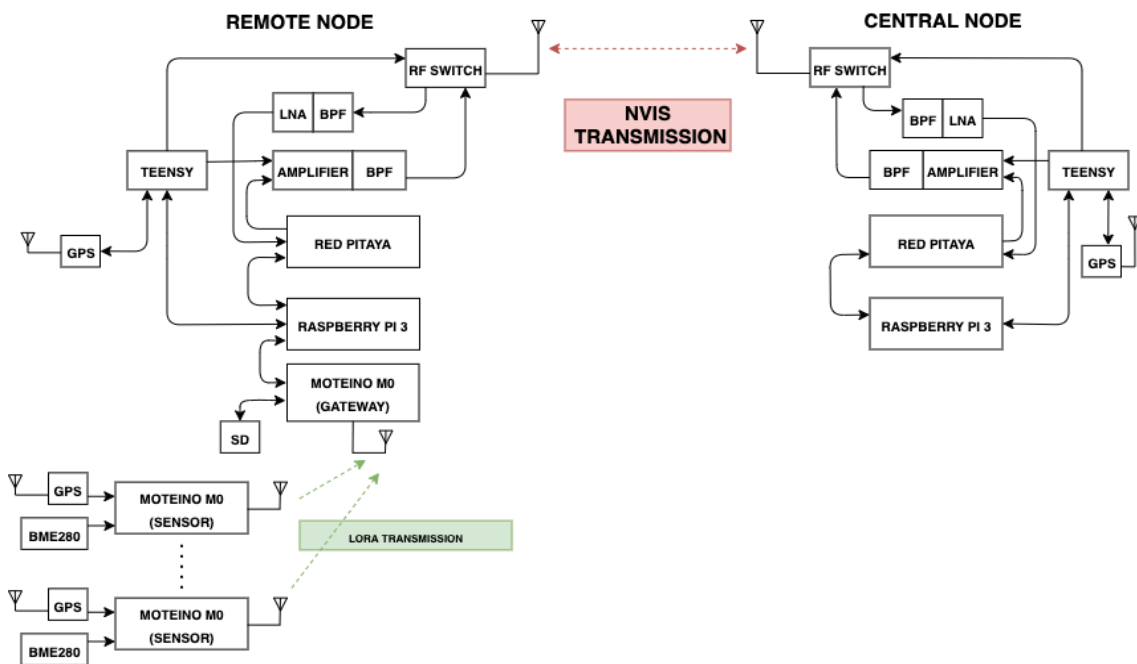
Fig. 10 *Current NVIS communication system.*

Fig. 11 *Researcher Tomás González installing the transmitter node at the Artigas Antarctic Research Base.*

3 Channel Sounding

3.1 Introduction

As mentioned in previous sections, the design of the physical layer of a telecommunications system is carried out based on the communications channel in order to estimate design parameters and subsequently correct the effects that this channel may have on signal reception. In the case of ionospheric communications, it becomes even more necessary because the state of the ionosphere depends on many factors (solar activity, frequency, among others) and it is difficult to predict the channel effects. Several conclusions can also be drawn, starting with the confirmation that the state of the ionosphere is not constant, but can also cause signals to be absorbed and therefore not to bounce back. This is why the motivation for this channel study arose.

To carry out this study, first a review of previous wells has been made, to know the values of the parameters to be studied. In this case, the most important parameters, apart from the channel availability, are the Delay Spread and the Doppler shift. Some sounding research are; (1) the study [100] of the influence of polarization interference on the frequency and impulse responses of a radio channel. (2) the study made in Wuhan transmission centre [101]. The maximum useful frequency (MUF) and frequency of optimum transmission (FOT) of NVIS communication at different times and stations are investigated using VOACAP shortwave communication frequency prediction software. (3) A wideband multi-carrier phase-coded signal (MCPC) and orthogonal subcarrier multiplexing is used on an SDR platform with the USRP-210 hardware for NVIS Sounding of HF Radio Channels [102].

Subsequently, a PN sequence has had to be designed, which is greater than the multipath expected for these channels, in addition to taking into account the Doppler Spread (see 3.4).

When performing the sounding and data analysis, it must be taken into account that there will be times when the ionosphere, due to solar activity and ionization, among other factors, will not allow the reflection of signals, so there will be no channel availability. For this reason, a night frequency and a day frequency are usually defined. However, for this study, the study will be carried out at a single frequency, due to the large volume of data.

Finally, a channel model is made, which will be used in the modulation methodology.

The dynamic behaviour of the ionosphere as a communication channel will be studied for both propagation modes that the ionosphere gives rise to. The ionosondes that provide ionograms, perform channel soundings with Vertical Incidence Skywave (VIS) and only collect values of availability of the ionosphere layers, without obtaining channel parameters. On the other hand, there are channel studies with the objective of performing the proposed study with one propagation mode (usually the ordinary wave) but they have always been performed with oblique transmissions.

Therefore, parameters such as channel availability, effects of this channel such as Ds, the different propagation modes of the ionosphere (Ordinary and Extraordinary) giving rise to two independent channels are then studied. This study is made with a system with an antenna adapted to 5.4 MHz. This frequency was chosen based on (1) several ionogram analyses provided by the Ionosonde from the Observatori de L'Ebre (Roquetes) and (2) the spectral behaviour of the receiver located in Cambrils will not present interference from other systems.

3.2 Polarization diversity

Polarization diversity consists of taking advantage of the orthogonality of two signals with a correlation coefficient close to zero. For this, two antennas need to be perpendicular located in the same frequency band in order to obtain the diversity gain. This concept is called Single Input Multiple Output (SIMO).

When sending a signal from the earth, it passes through the different layers of the ionosphere (E, F..). In the F2 which is the layer that this communication is centred, the electrons in this layer start an elliptical motion [38]. The polarization of the transmitted signal changes as a result of the movement. This fact causes the differentiation of two waves considered independent because despite having elliptical polarization, they have an opposite direction of rotation. These two waves called ordinary and extraordinary, being independent, have totally different properties.

For the Northern Hemisphere, the ordinary wave has the greater delay and left-hand circular polarization (LHCP), and the extraordinary wave presents the lesser delay and right-hand circular polarization (RHCP). The fact that there are two modes of propagation can be used to increase the capabilities of an NVIS communication channel using polarization diversity. Applying this technique the SNR and performance increases by combining both signals, due to the low cross-correlation factor between them [103].

This approach was deployed and tested between Barcelona and Cambrils where the link between the two cities is around 100 Km in direct line. This communication will have no LOS and has an elevation profile shown below.

Fig. 12. *Elevation profile between Barcelona and Cambrils for NVIS communication link.*

3.3 Hardware modifications

For this study some hardware changes had to be made because two different radio waves were received.

When receiving the ordinary and the extraordinary wave, two antennas perpendicular to each other are needed. Therefore, in the receiver located in Cambrils, two orthogonal antennas tuned to the same frequency were installed (see Fig. 13). In addition, when combining the two propagation modes, it must be taken into account that they have different polarization. Therefore, a phasing network is necessary. The phase shift of the received waves implies that the two can be constructively summed, since they are received at the same time. The phase shift is performed as follows: (1) with a splitter the signal received by one of the antennas is divided. (2) To one of the outputs is added the insertion of a cable with length $\lambda/4$ that will be the phase shift of 90º and (3) the direct signal received by the other antenna is joined with another splitter. (4) The same scheme is followed for the other antenna that is perpendicular. In **Fig. 14**, a block diagram of the phasing network is shown.
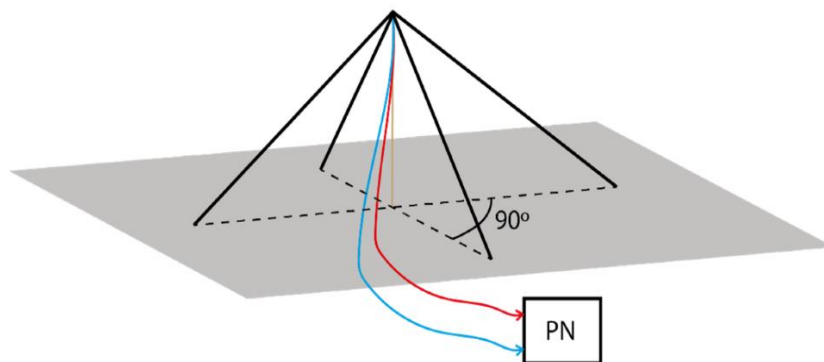
Fig. 13 *Diagram of the orthogonal inverted vee antennas in the receiver*
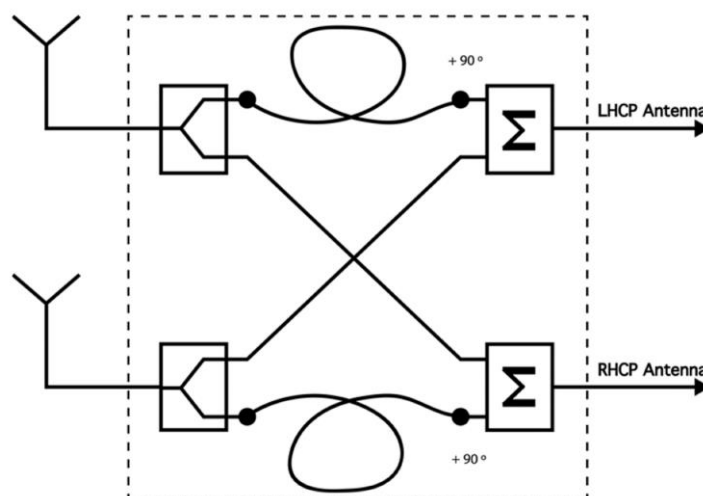
Fig. 14 *Block diagram of the phasing network*

The phasing network explained above is valid for a single frequency. In the case that the sounding would be done for the entire band, all the phasing network offsets would have to be recalculated.

On the other hand, ideally and in further studies, this implementation will be done internally in the FPGA so that all these phase shifts will be automated, and any frequency can be used.

3.4 Data frame design

In order to carry out this study, a physical layer is defined in which the following parameters are established despite being a basic frame.

The definition of the frame has been based on other studies done in [104]. This frame is part of level one of the Open Systems Interconnection model (OSI model). The design of this frame uses a Pseudo-noise (PN) sequence of 5.12 ms with a bandwidth of 12 KHz, which was defined as being greater than the multipath spread which is less than 1 ms. The correlation between the transmitted and received PN sequence at the transmitter results in a peak on which the synchronization between transmitter and receiver will be based. Generally, a 600 Hz tone with a duration of 60 ms is used after the PN for doppler shift correction. This results in 6000 samples where it is intended to correct the error generated by the internal clocks of the Pitaya Network. This parameter was defined by the correction of a maximum of 50 Hz with respect to 600 Hz.

For the Ds study, the tone had to be replaced by a null signal, in order to differentiate the correlation peaks of the PN sequences. When we detect several peaks, we can calculate the Ds value, being the later path.

Fig. 15 shows the data frame used for the Ds measurement. In this figure, we can see that the design of this frame uses a PN sequence.
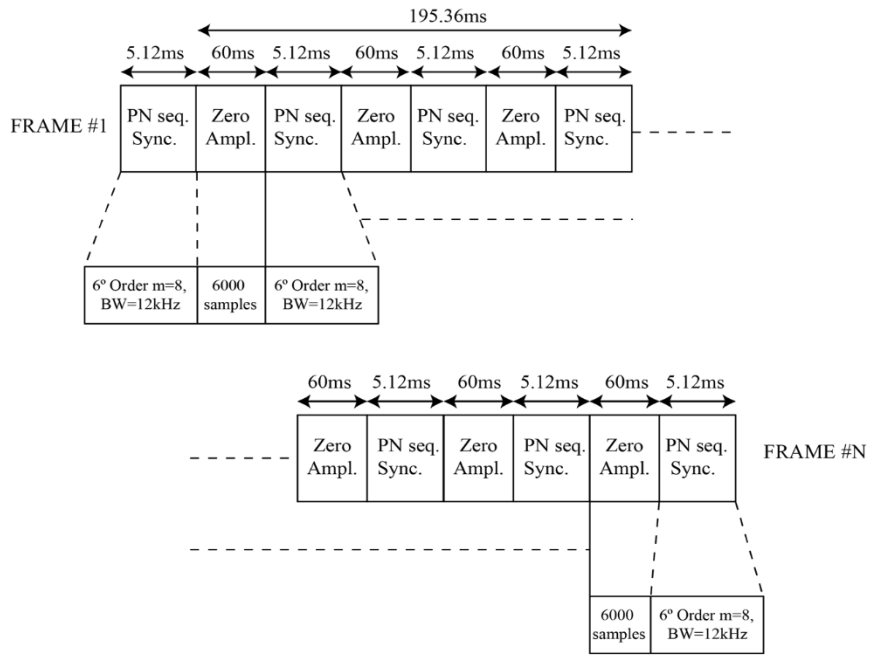
Fig. 15 *Data frame for Delay Spread measurement*

Normally, for channel availability studies, ionosondes use very high powers (>100W). With these powers we will find more multipaths and a higher Ds, however, as the system to be studied is low-energy, a transmission power of 50W will be used, which is much higher than the powers we use when transmitting data.

3.5 Results

This section presents the detailed results obtained from the channel survey. First, the channel availability is discussed, then the correlation of the two propagation modes is discussed, followed by the channel effects study and finally, the Energy per bit to Noise power spectral density ratio (EbNo) improvement.

3.5.1 Channel availability

For channel availability, we used the frame explained in the previous section, transmitting 5 transmissions every 10 minutes (to avoid overheating the amplifier) at 50W for several months.

The results of the availability study for the two propagation modes have been calculated from the correlations of the PN sequences as shown in Fig. 16. This figure shows the percentage of detected packets (Y-axis) as a function of an hourly distribution (X-axis). The calculation was defined as follows: the total number of data frames received with respect to the total number of data frames transmitted.
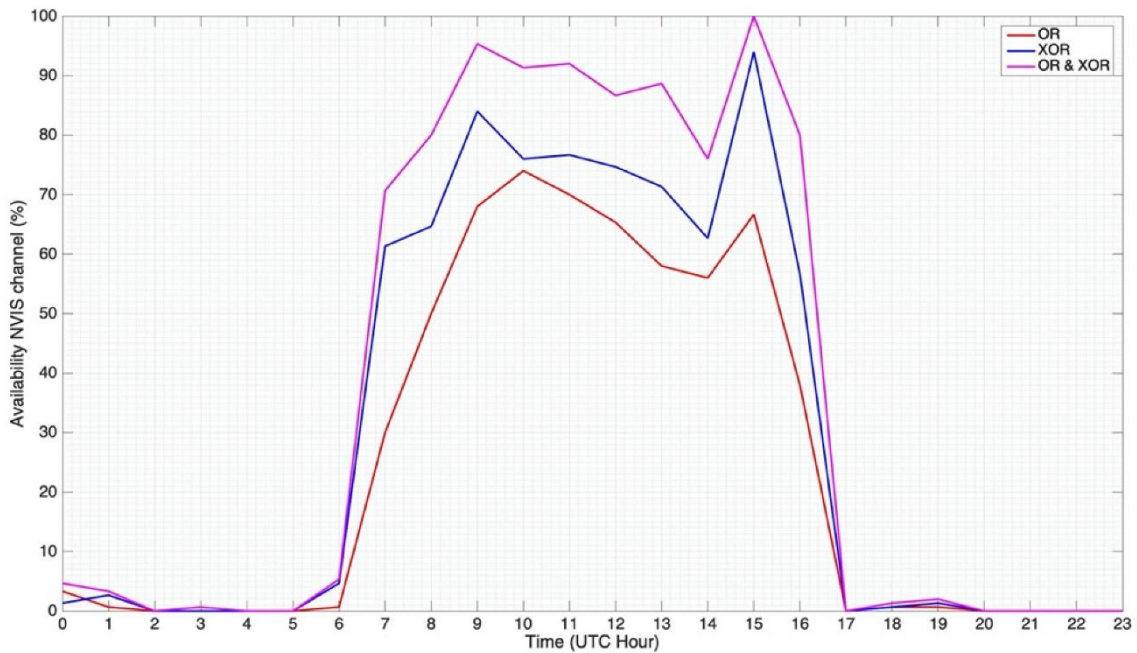
Fig. 16 Percentage of demodulated packets for the two ionosphere propagation modes.

As a first observation, we can see how the ordinary wave (OR) starts to be available from 7 a.m., as well as the extraordinary wave (XOR). We see that the OR has much less availability than the XOR. This casuistry can be observed until 17 p.m., when both are no longer available. It should be noted that these tests were conducted between November and December, so the hours of availability are similar to sunrise and sunset.

These reflections occur in the F2 layer where the electron density determines whether the wave is able to bounce or pass through the ionosphere. In Ben Witvliet's thesis it is proved that there is an interval of hours where there is always propagation through the ionosphere, which is called "Happy Hour".

It can also be verified that there was no reflection around 6 a.m. and it was from 6.30 a.m. when ionospheric reflection began to exist for the XOR wave. In our study, having made the study by hours and not 30-minute periods, this result may have been rounded, however, it follows the same behaviour as their study. On the other hand, in Ben's study, the "Happy Hour" interval was much longer, extending up to 9 p.m. In our case, it only extended until 5 pm. This may be due to the lower electron density in November and December.

The figure also shows the sum of the two propagation waves, where the improvement is relevant. This calculation can be done as long as the two signals coming from the two propagation modes have a cross-correlation coefficient lower than 0.7 (decorrelated signals) [105] and thus the SNR can be increased. To calculate the correlation, both signals must be synchronized, and the correlation percentage must be determined. In **Fig. 16**, the probability of cross-correlation with factor below 0.7 is shown (only the hours with more sun).
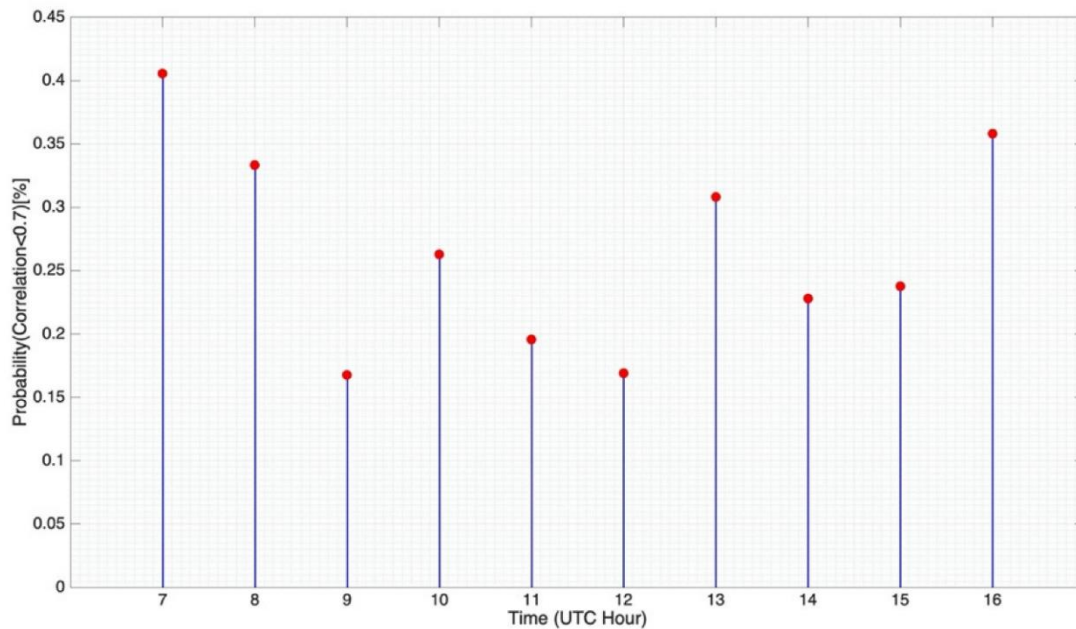
Fig. 17 Percentage of cross-correlation with coefficient factor below 0.7 between both propagation channels

In the next figure, the Ds of the both signals are calculated. This study is performed by sending a PN sequence in order to synchronize the reception of the signal, and by checking how long the last late path takes. Looking at the results, we can conclude that the Delay Spread on average are not that large. However, if we look at the peak points, we see that the average is affected by a factor of ~6 in the worst case. This peak is from the XOR wave, with a value of 2.89 ms giving a coherence bandwidth of 346 Hz. In the case of the OR, the coherence bandwidth is increased to 369 Hz since it has 2.71 ms of Ds. Comparing these results with the STANAG and MIL-STD standards with bandwidths 2.38 kHz, it implies a strong ISI effect since the symbol time is 0.42 ms.

In other studies as in [106] focused on the study of the HF ionospheric channel on high latitude paths. This study took place 20 years ago between Svalbard (Norway), Oslo and Kiruna (Sweden) and concluded that at frequencies between 2.8 MHz and 21.9 MHz: the multipath spread at a bandwidth of 3 kHz ranged between 1 ms to 11 ms.
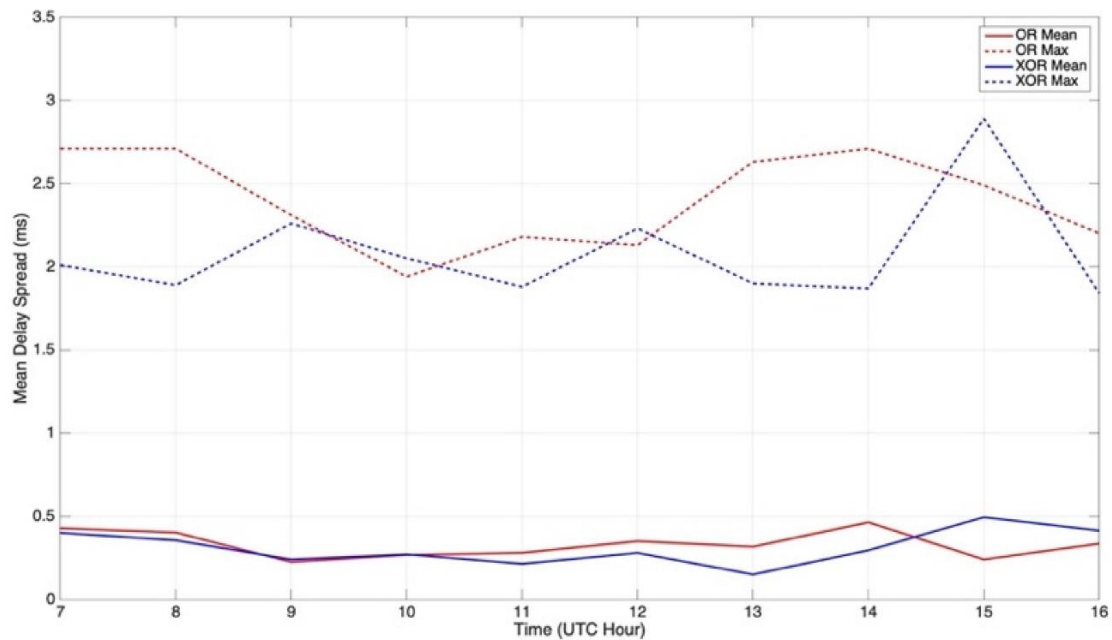
Fig. 18 *Delay spread distribution in hours with maximum sun.*

The Doppler shift parameter was also studied. In [107] we can see that the Doppler for this type of communications is around 4 Hz. This frequency difference is not much when compared to the errors that are capable of causing low-cost boards that usually have low stability clocks. The figure below shows a Doppler shift that is dulled by the low accuracy of the Pitaya Network of ± 50 ppm. Due to the temperature variation, added to the Doppler shift effect that the signal undergoes in transmission, it can take errors since -14.5 Hz until -19.5 Hz. Also, for comparison, [108]presents the signal characteristics associated with ionospheric propagation for a 1400 km link oriented along the mid-latitude trough between Sweden and the UK. It is concluded that the observed delay and Doppler spread characteristics are strongly dependent on time of day and season.
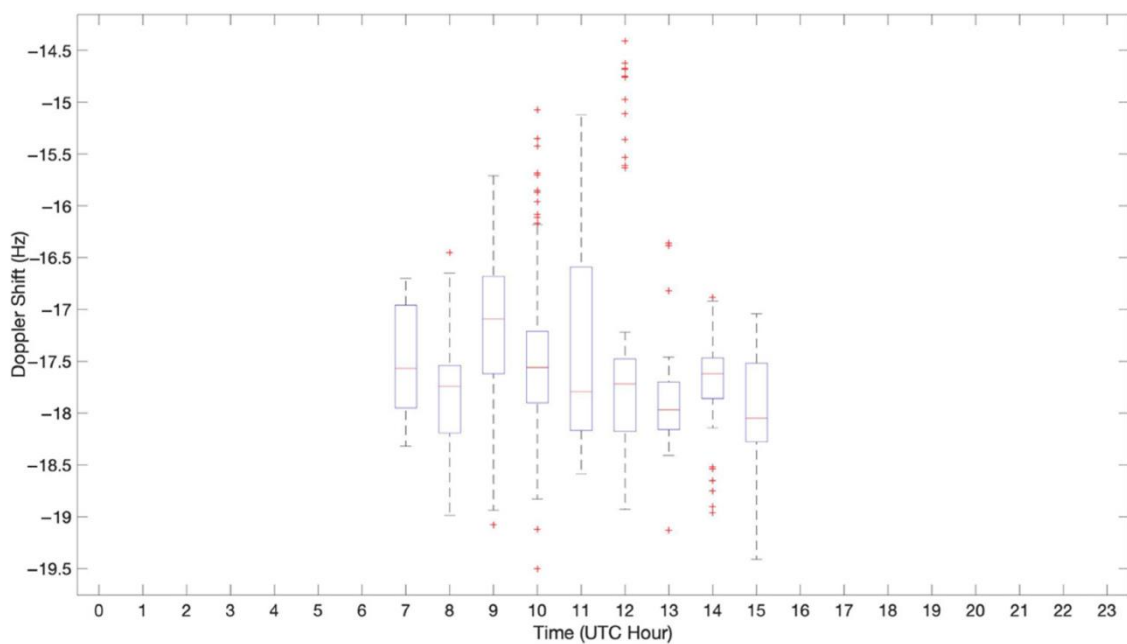
Fig. 19 *Doppler shift (Hz)*

Finally, a calculation is made of the increase in EbNo that an NVIS communication could have by combining the two propagation modes. The **Fig. 20** shows the EbNo received by each wave, and also the combination of the two waves with two different diversity techniques (selection combination and equal gain combination). We can see that the increment is 4 dB at 12 p.m using the selection combining technique. Another point to highlight is that the Selection Combining technique improves in all hours and the Equal-gain combining improves almost always but in smaller quantities. Possibly, if the EbNo were higher, and the propagation modes were even more independent with even lower cross-correlation, both results would improve, especially Equal-Gain Combining.
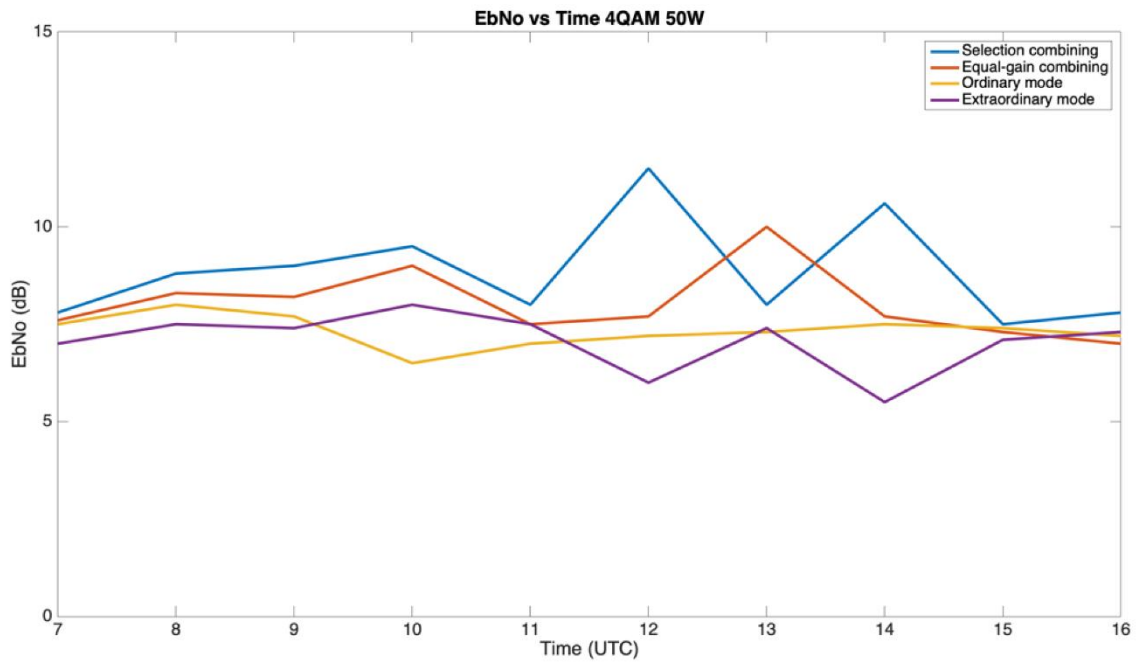
Fig. 20 *EbNo comparison between both propagation modes and two diversity techniques applied.*

4 Modulations and Multiple Access

4.1 Introduction

Normally HF Communications comply with transmission schemes already established by well-known standards such as MIL-STD or STANAG. These schemes are made with very small bandwidths to ensure that the little information that is sent, arrives as reliable as possible. NVIS compared to oblique transmission has many variations, starting with the nature of the bounces. In the case of NVIS this is due to the multiple ionosphere-earth hops. This fact makes the Ds different. On the other hand, the application on which this study is focused is for an IoT sensor network, so we are looking for schemes, where the equalization is as simple as possible. In a previous study we evaluated OFDM technology, which is typically used with higher bandwidths and ensures high multipath protection and frequency equalization.

With the results of the channel model, the SC-FDE modulation was designed and subsequently, it was tested under simulation with the parameters of the channel study, simulating the multipath and varying noise values. Subsequently, a test bench was designed to know the real power threshold at which it could demodulate correctly. Finally, all these tests were contrasted with real tests.

The following is a summary of the characteristics of OFDM and SC-FDE that are proposed to be compared.

4.2 OFDM

As a first premise, OFDM modulation was considered since these modulations have become widespread thanks to the use of spectral bandwidth and the use of mathematical expressions such as the Fast Fourier Transform and the Inverse Fast Fourier Transform (FFT and IFFT) that optimize performance for real-time applications.

The design of the OFDM done in [86] was based to the most similar as the HF standards. The proposed physical layer was based on OFDM modulation with modulation order 4 (QPSK) and it had good results for a specific EbNo. The configuration parameters were also based on channel sounding done in [109] configurating values of for example Delay Spread, number of subcarriers, numbers of pilots... In summary, the main characteristics are shown in the following table.

Table 2. OFDM design parameters

Parameters	OFDM
Bandwidth	3 kHz
Useful symbol length	T_S = 9.33 ms
Prefix cyclic length	T_{CP} = 3 ms
Number of subcarriers	N_{SC} = 28
Number of pilot subcarriers	N_P = 10
Number of data subcarriers	N_D = 17
Number of subcarriers DC NULL	N_{DC} = 1
Number of symbols OFDM	N_{SOFDM} = 7
Time duration of OFDM packet	N_{PT} = 86.31 ms
Bits in packet	Bits = 238 bits
Frequency pilot separation	NF = 3
Time pilot separation	-
IBO	3 dB
Modulation	QPSK
Equalization	Zero Forcing
Bitrate of signal frame	1.741 Kbps

Some parameters, such as the bandwidth value, are defined by HF standards. On the other hand, some parameters as for example, the definition of the cyclic prefix length or OFDM symbol time is based on the study of the channel using the ordinary layer. Of course, a small oversize is made between the value obtained by the channel sounding, as a precaution. In the case of the CP a value of 2.75 ms was measured but in the frame, we have defined the value of 3 ms.

For channel equalization, the ZF technique was used, since applying the inverse of the estimated channel, which is calculated with the pilot symbols, results in a simple equation to calculate in the frequency domain. The received pilot is compared with the transmitted one to take a value of how the channel changes, and the OFDM symbols are multiplied by the inverse of the received channel response.

4.3 SC-FDE design

In other NVIS studies, such as [110][111][112] narrowband modulations have proven that communications are quite reliable in a wide range of scenarios. So far, HF standards (military or otherwise) have used 3 kHz channels with single-carrier modulations such as PSK and QAM with low modulation orders (2-4).

Once the study of OFDM for NVIS systems was carried out, it was proposed to solve the drawbacks of using this modulation, it was proposed to solve the drawbacks of using this modulation. The nature of the OFDM waveform induces a high PAPR, and consequently is intolerant to amplifier nonlinearities (it is advisable to use class A amplifiers) and is sensitive to carrier frequency offsets (CFOs) [24].

Until now we have mentioned that NVIS transmissions are low power. On the other hand, from the point of view of a remote node (the one closest to the sensor), battery usage is a critical limitation. It is true that OFDM has worked well for some scenarios, this is why both 4G, 5G, or the new generations of WiFi schemes use this modulation with multiuser variation (OFDMA). It is worth mentioning that these technologies use these modulations in the downlink channel where power consumption is not an issue since they are usually connected to the power. If we consider the Uplink channels of these technologies or some IoT technologies such as NB-IoT, they use SC-FDE. Therefore, it is proposed to use Single Carrier modulation with frequency domain equalization (SC-FDE), which maintains many of the properties of OFDM and solves the major drawbacks.

In order to compare OFDM and SC-FDE as closely as possible, most of the design parameters were maintained. It should be noted that SC-FDE symbols have a much longer lifetime than OFDM symbols due to the distribution. Consequently, the symbols are shorter in the frequency domain. At the conceptual level, the SC-FDE is assigned subcarriers (like OFDM) that are calculated from the coherence bandwidth. Dividing the OFDM symbol time by the theoretical number of subcarriers of the SC-FDE gives the symbol duration as shown in Table 3.

The value of the Delay Spread defines the Cyclic Prefix (CP) to be used. Since the channel is the same, and it is a parameter that is applied in the transmission scheme in the same way in OFDM as in SC-FDE, this value is maintained. In [113] the Ds had it maximum value in 2.7 ms, so 3 ms must be enough. However, this value is very pessimistic, since the average does not exceed 0.5, so that in a future design, a CP could be implemented dynamically.

For equalization, SC-FDE is more sensitive to noise than OFDM, so we proceed to use MMSE equalization, which for low SNR is the best option, thus correcting Intersymbol Interference (ISI) and noise. For this, an SC-FDE symbol of known values (pilots) is also transmitted (same design of the OFDM).

The improvements in throughput (2%) can be seen in the table below, which summarizes the main design parameters. Additionally, they are compared to the OFDM design proposed in [86] since they have a similar configuration.

Table 3. SC-FDE vs OFDM parameters

Parameters	SC-FDE Values	OFDM Values
Bandwidth	3 kHz	3 kHz
Useful symbol length (TS)	0.33 ms	9.33 ms
Prefix cyclic length (TCP)	3 ms	3 ms
Number of subcarriers (NSC)	28	28
Number of symbols (Nsymbol)	7	7
Number of pilot/symbol	1	1
Number of data symbol	6	6
Packet duration	87.64 ms	86.31 ms
Bits in packet	336 bits	324 bits
Modulation	QPSK	QPSK
Equalization	MMSE	ZF
Bitrate of signal frame	3.833 kbps	3.753 kbps

4.3.1 SC-FDE Implementation

For the SC-FDE study, a new protocol was defined following the same structure as in [86], adding the SC-FDE and then comparing the PSK, QAM, OFDM and SC-FDE modulations [114].

We start from a system already established between Barcelona and Cambrils, with a distance between cities of 100 km in a straight line. This system (described in 3) uses $\lambda/2$ dipole antennas fixed at 5.4 MHz.

The transmitted frame is composed of 4 packets (1 for each modulation) with specific headers as follows: (1) For the mere fact of synchronizing the frames received at the receiver, a Pseudorandom Noise (PN) sequence with resampling of 8 and having a length of 5 ms is used; (2) To correct the doppler shift effect introduced by the FPGA used (see 3) which is of the order of 20 Hz adding the two sides; (3) Finally, to identify each modulation the same PN sequence as before is sent.

As the NVIS communication to be enhanced is for IoT environments that are in remote areas, low power consumption systems are needed. Putting in context that the OFDM study was concluded for a power of 12 W, we will test the same threshold by raising and lowering this power by a factor 2 (6, 12 and 25 W).

After the first approach, a second test bed was designed to perform consumption optimization. Since OFDM used a Clipping Ratio (CR) for PAPR reduction, a sweep of clipping values from 3 dB to 8 dB is performed. It is true that SC-FDE has much lower PAPRs, but the introduction of this clipping can improve efficiency.

4.3.2 Results

BER vs Eb/No

One of the most commonly used options for comparing modulations is the BER ratio EbNo. It indicates the normalized signal to noise ratio (SNR).

Fig. 21 shows the behaviour of BER EbNo of the SC-FDE with 2 bits per symbol along with the FSK, QAM, and OFDM studied in [20]. FSK and QAM need higher EbNo than the OFDM and SC-FDE, which show very similar results. For BER of 10^{-3}, the SC-FDE needs 1 dB less than the OFDM, but for BER 10^{-4}, the OFDM needs 17.5 dB and the SC-FDE needs more than 18 dB.
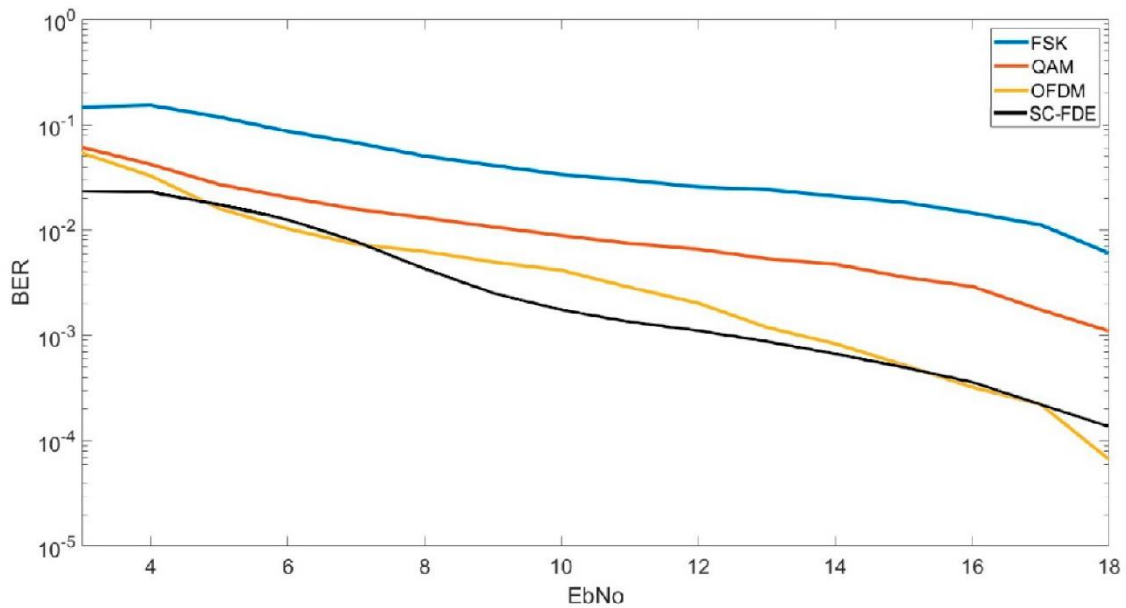
Fig. 21. BER vs. EbNo comparison between FSK, QAM, OFDM, and SC-FDE

BER CDF

A quick and reliable way to show the behaviour of a modulation is the Cumulative Distribution Function (CDF) plot where the probability of occurrence of a particular value is shown. In the X-plot, the different BER values are distributed on the x-axis (Xo in the figure) and the probabilities of occurrence are shown on the y-axis with the connotation P(BER<Xo).

Fig. 22 shows the CDF of the SC-FDE with the 3 transmission powers separately. As expected, the evolution for each power is noticeable in the smaller BERs, since the error resolution is sharper. On the other hand, we see that all the powers for a BER 10-2 (1 error per 100) has more than 90% probability, which is almost an ideal transmission. It should also be noted that the transmission schemes used do not use corrector codes (FEC). On the other hand, as previously anticipated, the clipping technique will be studied after this study, so these probabilities would improve, in any case. With 6W we obtain probabilities greater than 70% for BER 10-3, with 12W we obtain probabilities of approximately 80% for the same BER, and with 25W we obtain probabilities of approximately almost 90%. As a first conclusion, it can be stated that the SC-FDE provides high performances for low powers, having a good trade-off around 12W.
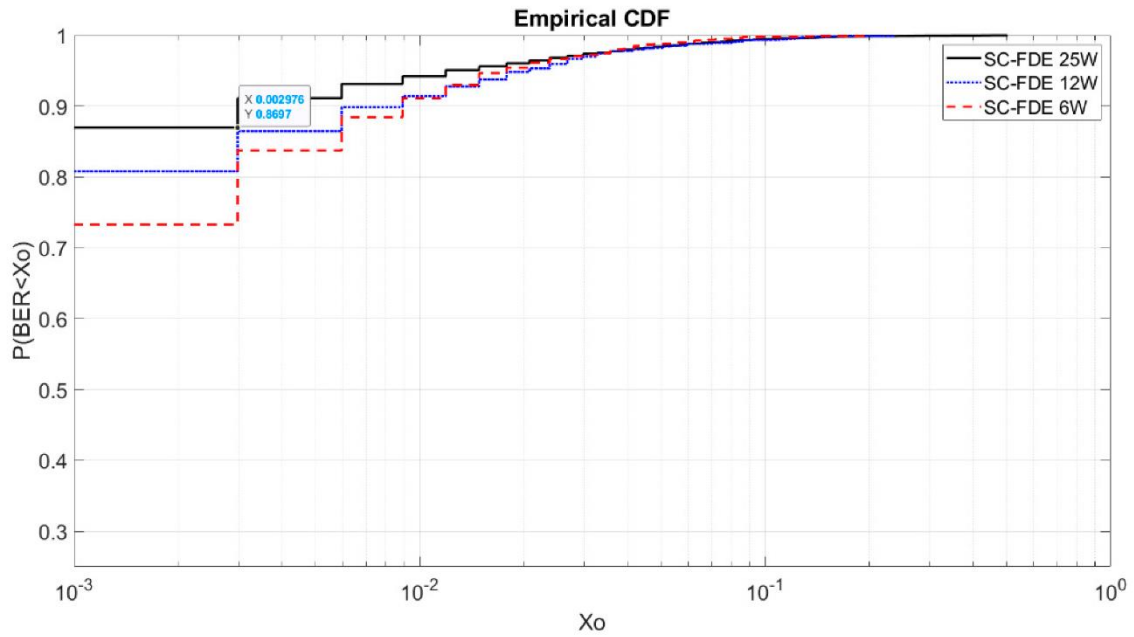
Fig. 22 *CDF plot of SC-FDE modulation with 6 W, 12 W, and 25 W of peak power*

OFDM vs SC-FDE in terms of power

Fig. 23 shows the CDF of the SC-FDE and OFDM with 12 W which was the trade-off between the transmitted power and the BER obtained.

As a first analysis, it can be seen that there is a large difference, which must be caused by the high noise levels that are very detrimental to OFDM. The SC-FDE with 12 W, is able to demodulate with more than 80% probability to have a BER of 10-3, while the OFDM only achieves a 50% probability.

It should be noted that the biggest problem is the high PAPR that makes the average power of both signals not so comparable. In the following subchapter the technique used to combat PAPR (including SC-FDE) is mentioned for further analysis.
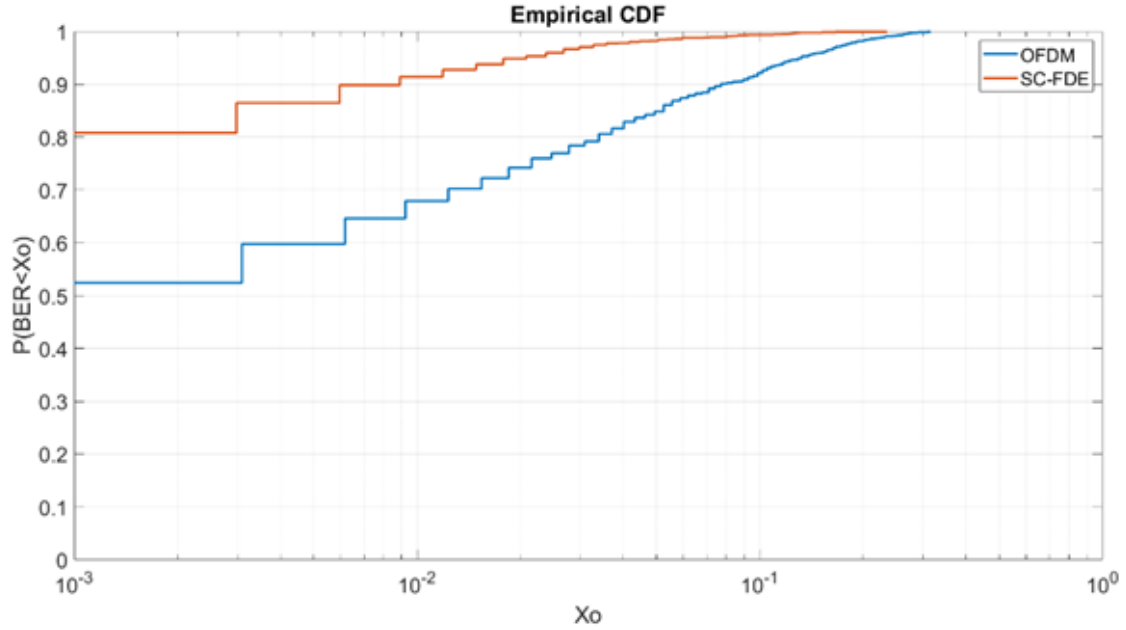
Fig. 23 *Comparison of CDF plot of SC-FDE and OFDM with 12 W of peak power*

CR Sweep

Based on the first conclusions of the previous graph, we proceed to try to increase the average power by reducing the PAPR. The clipping technique was used for this purpose.

There are multiple techniques that seek to reduce PAPR. One of the most widely used is Crest Factor Reduction (CFR). This technique can use several methods (Clipping and Filtering, Peak Windowing, Peak Cancellation...). Thanks to its low computational cost and high performance as can be seen in [115][116], this method is used in this study. The objective of this method is to saturate the signal from a fixed threshold by limiting the peaks of the signal. This causes out-of-band emissions and interference due to the introduction of nonlinearities. Fig. 24 shows an example of the clipping technique application along with its formula.

The signal x(n) keeps its value as long as it does not exceed the threshold. If x(n) overcomes the threshold the signal values automatically become the CR value.

$$y(n) \begin{cases} x(n), & \max(|x(n)| < CR \\ CR, & \max(|x(n)| \geq CR \end{cases} \qquad (3)$$
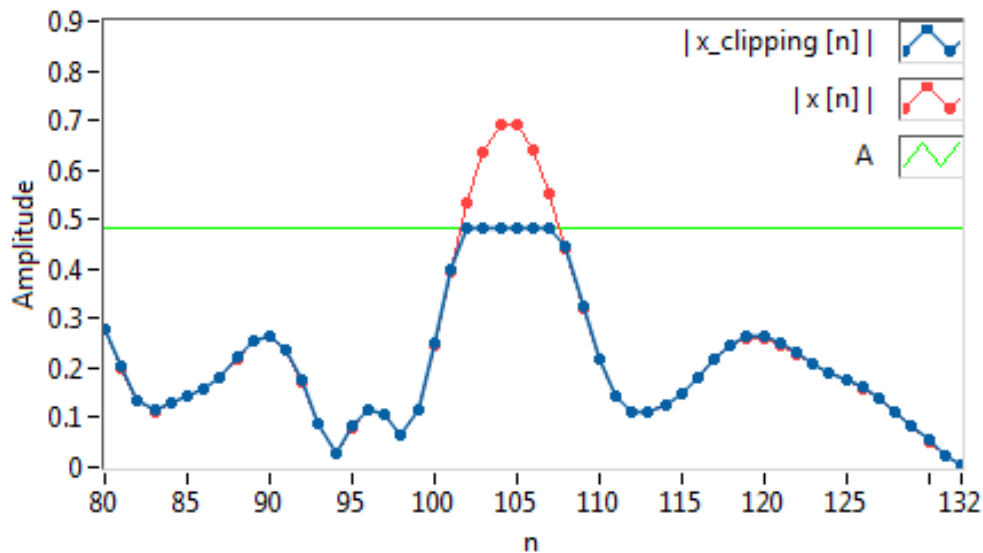
Fig. 24 *Clipping technique. The red line shows the original signal, and the blue line shows the clipped signal due to the threshold drawn in green (CR)* [117]

A CR sweep was studied, with values starting at 3 dB with 1 dB steps up to 8 dBs. For our study, the CR value is calculated from the peak value of our signal (peak value - CR). It must be taken into account that as the CR value increases, the error vector magnitude (EVM) increases due to the saturation produced by the signal limitations (in short, we are eliminating part of the useful signal). Despite having a higher EVM, the BER could be better due to the increase of the average power. The trade-off between power consumption and BER results must be taken into account.

Fig. 22 shows the results of this study for the 6W power. If we compare the results with Fig. 25, we see that a minimum and a small CR value already has a considerable BER increase. We start from a 70% probability for a BER of 10^{-3}, applying 3 dB of CR, we obtain more than 80% probability. If a CR of 6 dB was applied, a probability of more than 85% for a BER of 10^{-3} could be attained. On the other hand, we see that for a CR of more than 6 dB, the BER is again lower. This is because the signal clipping is so abrupt that too much useful signal is lost, resulting in more errors no matter how much the average power has been increased. This is the point where the EVM was large enough, and the increase of average power did not help due to the large in-band distortion.

Fig. 26 shows the results of this study for the 12W power. The results are better but following the trend seen with the 6W power. For a CR of 6 dB, it gives a probability between 90 and 95% for a BER of 10^{-3} and almost 100% for a BER of 10^{-2}.

Fig. 27 shows the results of this study for the 25W power. The results show a better probability/BER for other values of CR. The value of 6 dB is still the best, and this must be because all these transmissions are made without the typical error correction

schemes such as coding and interleaving. Thus "residual" errors are seen, because the probability of that BER has not changed.
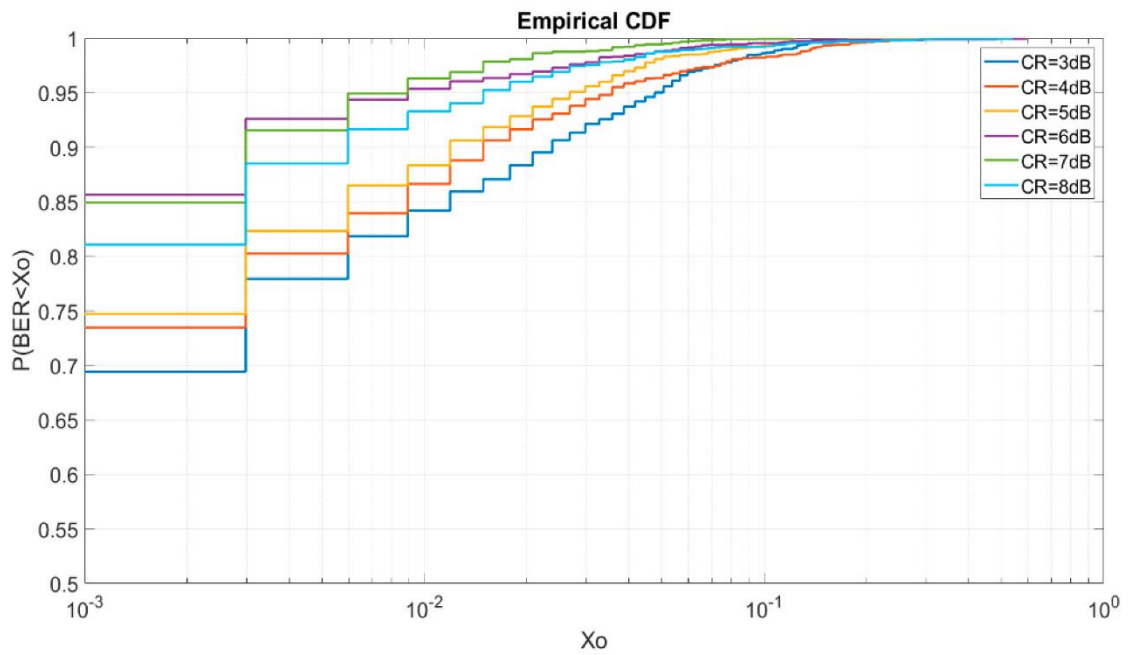
Fig. 25 *6 W SC-FDE CR sweep CDF.*
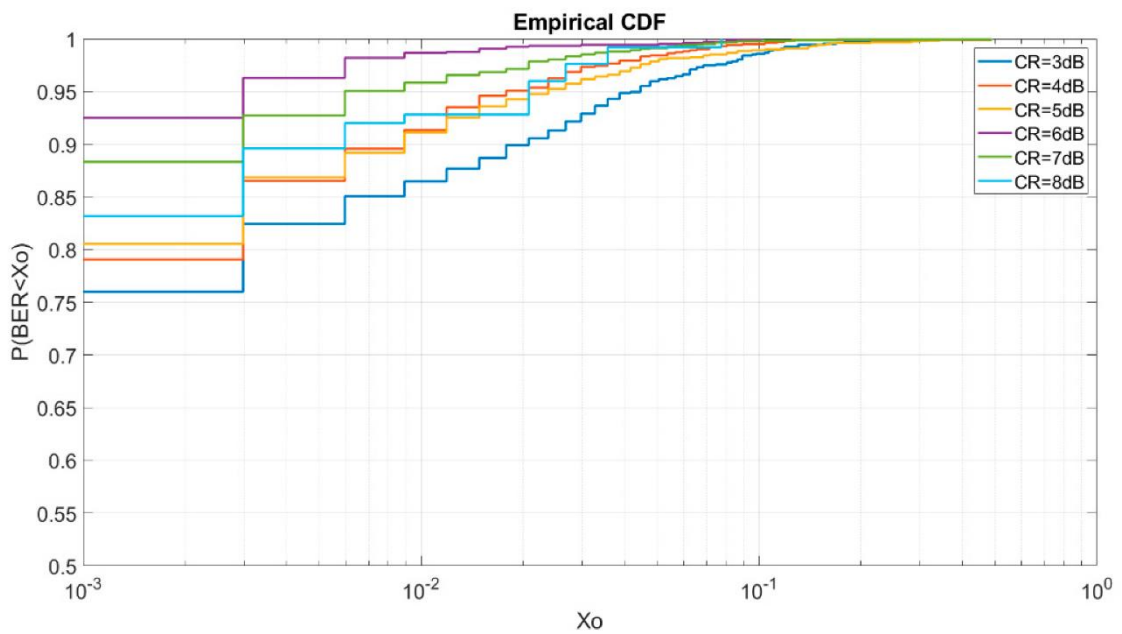
Fig. 26 *12 W SC-FDE CR sweep CDF*
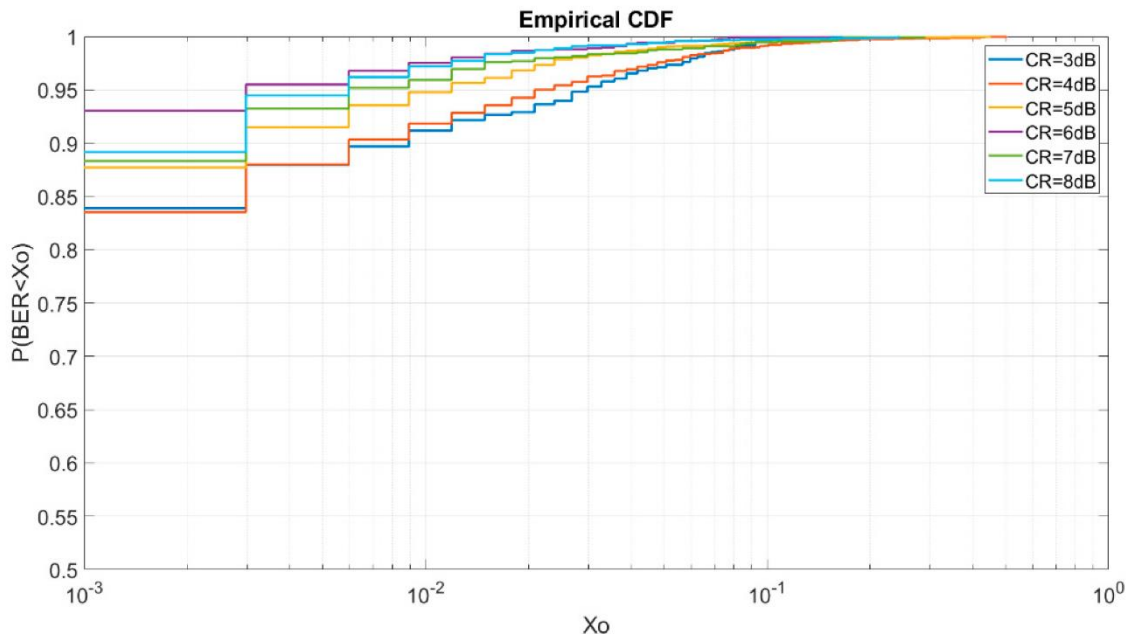
Fig. 27 *25 W SC-FDE CR sweep CDF.*

When choosing the transmit power (peak power), the 6W power is discarded (although it could be used for smaller modulation orders or more ideal channels) and we proceed to use 12W with a CR of 6 dB. The 25W power is unnecessary because it does not provide much improvement compared to 12W and spends twice as much energy.

OFDM vs SC-FDE in terms of CR sweep

At this point, we compare the best results of the OFDM modulations from the study in [86] and the results of SC-FDE calculated previously. As a first observation, we note that the CR of SC-FDE is much lower than that of OFDM. This is due to the fact that the carrier division causes a high PAPR as mentioned above. On the other hand, the SC-FDE, although it is also treated as if it had subcarriers, is actually a single carrier. Fig. 28 shows that the best result obtained for OFDM is for a BER $3 \cdot 10^{-3}$ with a probability of 80% using an IBO of 9 dB (IBO=CR), giving an average power of 4.6W. If we compare these results for the 6W SC-FDE and a 6 dB CR which should give a similar average power, it shows 85% for BER 10^{-3} and between 90 and 95% for BER $3 \cdot 10^{-3}$.
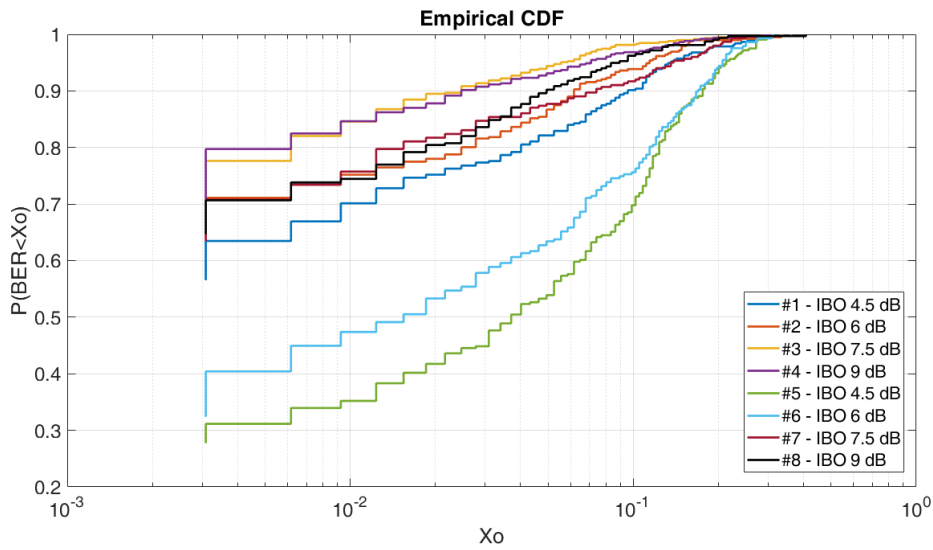
Fig. 28 *Results of an IBO sweep for OFDM* [86]

4.4   Field tests in Antarctica

The Antarctic continent is a continent dedicated to science, with many scientific projects, in which many sensors are deployed, in order to obtain data, which is then processed by scientists. Normally, this data is stored locally in the sensor itself, or the person who owns the sensor goes to the location of this sensor, to download this data. This situation is not possible many times, due to: (1) The weather, which restricts the ability to leave the station. Permission for these "excursions" is given by the station manager. (2) Many scientists take samples for a year, so the sensor is collecting data for the entire year. Often, harsh weather conditions severely damage the sensor, in the worst case rendering it totally unusable.

For this reason, one of the motivations of this project is to facilitate life in these environments and that scientists can easily access these data. In the case of transmitting these data, the use of traditional radios limits the sending of data due to distance and the

use of satellite, apart from the cost mentioned in previous points, the vision that one has with the satellite is often limited.

Once the SC-FDE studies for NVIS communication between Barcelona and Cambrils had been carried out, we tried to apply this communication in a remote location that could have a real application.

One of the most remote places in the world is the Antarctic continent and more specifically the islands. Artigas Station located in the King George island aims to become a robust communication station in the coming years [118][119], for this reason, we have considered it interesting to test NVIS links considering the Artigas base as a node that will be connected to the power grid and will be the receiver, so that when it receives data from sensors it can upload this data to an online platform or a cloud.

As a result of a collaboration with the Uruguayan Antarctic Institute (IAU), which through its Head of the Science Department, the Uruguayan base Artigas gave us all kinds of facilities to be able to install a communications node at the base on King George Island. As a project funded by the Spanish government, there was no impediment to the installation of an NVIS node at the Juan Carlos I Base on Livingston Island.

Finally, it was decided to test this previously tested link between Barcelona and Cambrils, between the above mentioned Antarctic stations located in the South Shetland Islands, King George (Artigas Uruguayan Antarctic Station), and Livingston Island (Juan Carlos I Spanish Station) where the link between the two islands is almost 94 km apart. This communication will not have LOS and has an elevation profile with many high peaks, the highest being at 82.7 km from the Artigas Base where there is a peak of 507 meters. The following two figures show the location and elevation profile of the radio link.

Fig. 29 *Test Area. Juan Carlos I (Spanish Station) is located in the Livingston Island and the Artigas (Uruguayan Station) is located in King George Island. Both Island are part of South Shetland Islands*
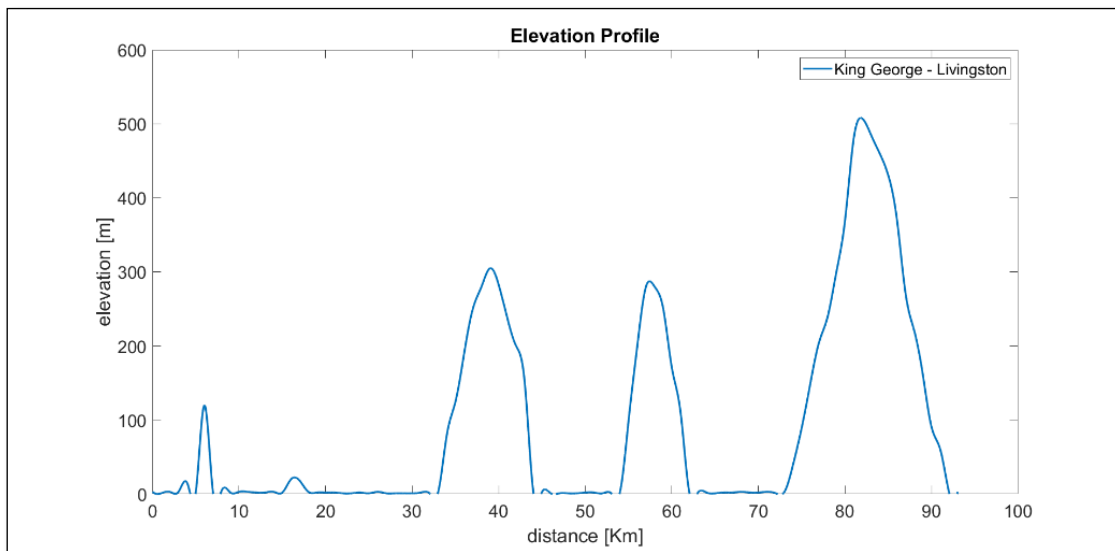
Fig. 30 *Elevation profile between both Antarctic Stations. The highest peak is more than 500 meters therefore, there is no LOS*

The following figure shows the installation of the NVIS antenna mast that the author will install at the Artigas Antarctic Research Base.

Fig. 31 *Researcher Tomás González installing the antenna at the Artigas Antarctic Research Base.*

4.4.1 Design

As described in previous points, for any type of transmission, it is recommended to make a channel sounding to know the behaviour of the channel. In this case, we cannot use the same one that we have done in this study, because the view of the ionosphere is different in this location. From the point of view of electromagnetic noise, it is lower than in a large city like Barcelona, but it is necessary to do a previous radio electrical spectrum analysis. The Observatori de l'Ebre [120], which attended the same Antarctic campaign, carried out this study in Juan Carlos I Station using the VIS version (totally vertical transmission). Thanks to their collaboration, at least we could see the channel availability. In spite of the strict regulations in place on the Antarctic continent, we found that the spectrum was full of communications (or interference), so despite seeing the ionograms provided, we had to tune the antenna to a less than ideal frequency. Globally, all telecommunications guidelines are set by the International Telecommunications Union (ITU), which is an international telecommunications regulatory body. In the ionograms, the frequency with best availability was placed at 4.1 MHz. This frequency does not interfere with the communications of the Uruguayan base nor with the JCI. An important fact is that the noise level in the Antarctic bases is lower compared to the big cities. This is relevant due to the need for low power systems. In several studies between similar distances in Barcelona, the peak power used in the link was around 12W. For the Antarctic link study, a power sweep was made be-tween 4 W and 16 W as well as out of standard bandwidth and modulation order as follows:

Table 4 *Tests of: power, modulation order and modulations*

Channel Bandwidth	Power	Modulation Order	Modulations
3 kHz	4, 6, 8 W	M=4	QAM, SC-FDE
6 kHZ	6, 8, 16 W	M=4	QAM, SC-FDE
3 kHZ	8 W	M=8	PSK, SC-FDE

4.4.2   Results

As it is a completely different channel to the one between the Barcelona-Cambrils link and we did not have time to make a proper channel survey, we defined the same frame design. Following the same structure as in the previous tests, we proceed to find the power threshold that gives us the best compromise between BER and power consumption. Different scenarios are presented below in order to have a fast vision of channel behaviour and design parameters such as transmit power and modulation orders.

Study of 3 kHz bandwidth and modulation order M=4
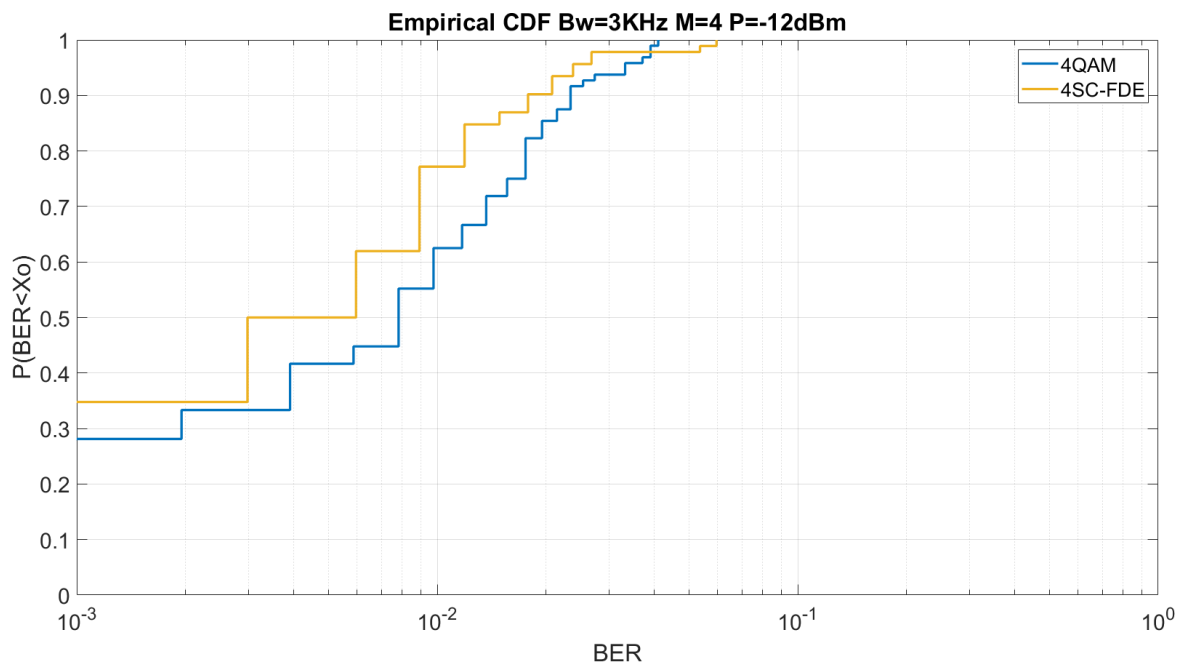
Fig. 32 *CDF of 3 kHz transmissions with power 4W and modulation order 4.*

The results show that powers of -12 dBm FPGA output power (4W) are not enough to our applications having BER of 10^{-2} with less than 80 % and 40% for BER of 10^{-3}. It could be a transmission power for modulation order 2, which, having to distinguish only 2 symbols, the receiver would be fully capable of doing so with very high probabilities.
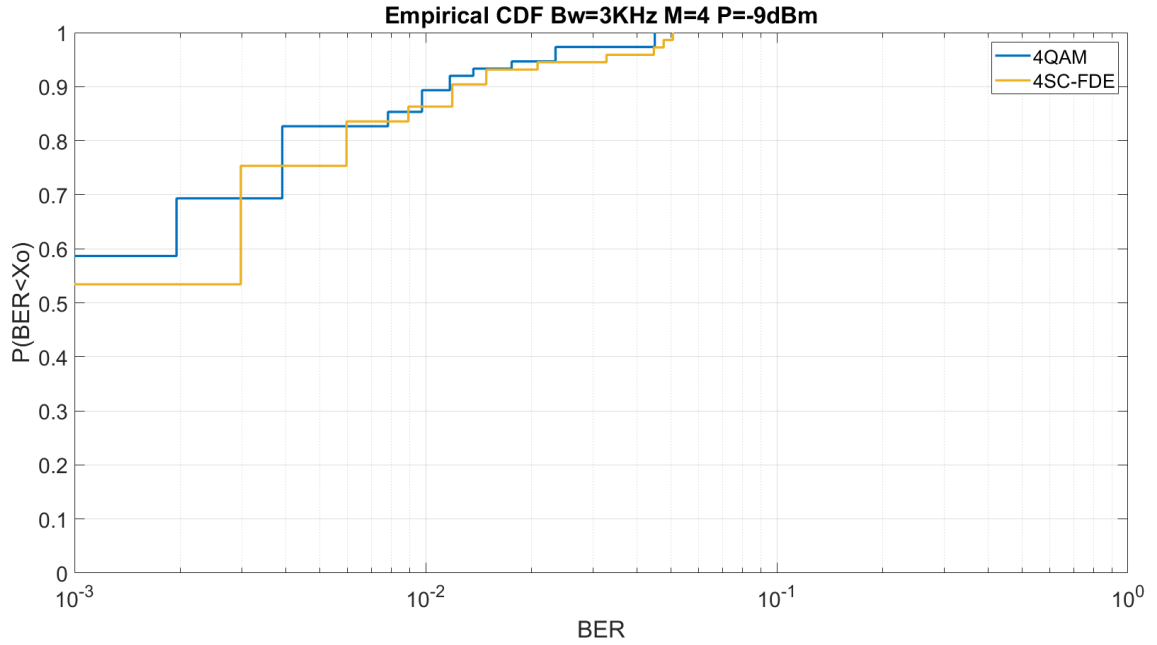
Fig. 33 *CDF of 3 kHz transmissions with power 6W and modulation order 4.*

The results show that the -9 dBm FPGA output power (6W) are little better than the previous one having BER of 10^{-2} between 80% and 90%. Following the line of the previous case, with a modulation order M=2 for very simple applications would be enough, but if we look for an order M=4 it is still not enough.
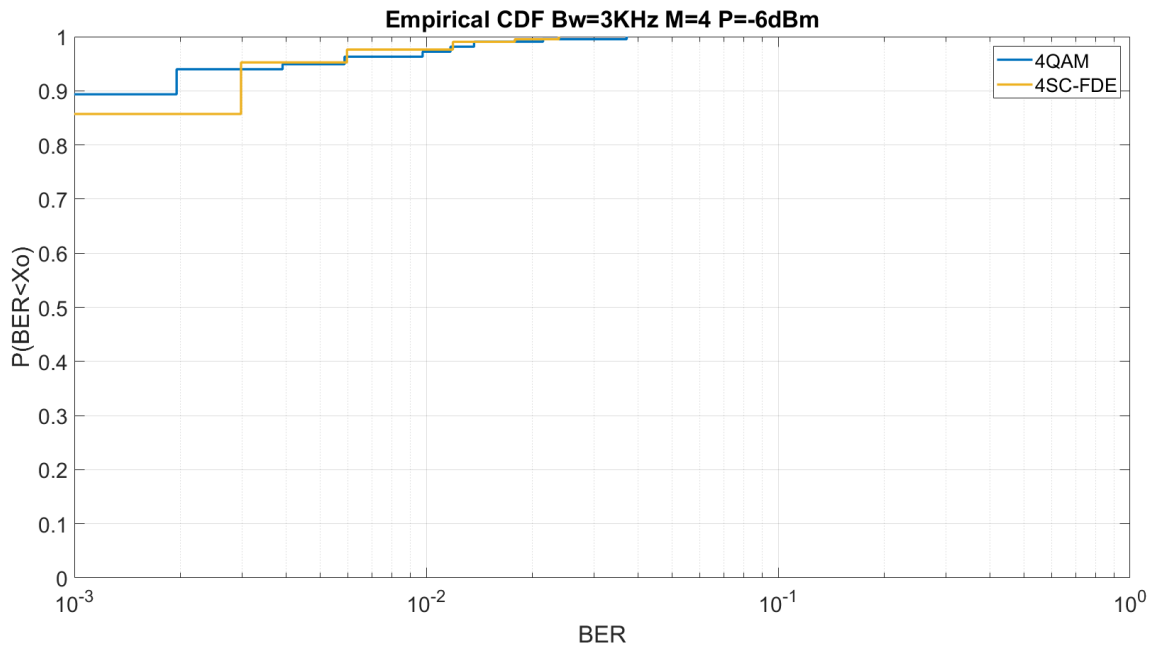
Fig. 34 *CDF of 3 kHz transmissions with 8W and modulation order 4.*

The results show that 8W powers are almost ideal. It presents a BER of 10-2 almost 100% and a BER of 10^{-3} around 90%. This would be the threshold we are looking for reliable communication.

Study of 6 kHz bandwidth and modulation order M=4

Once the threshold has been found for communications with a bandwidth of 3 kHz and modulation order 4, a study is carried out for higher bandwidths in order to improve throughput with a slight increase in power.

We have tested bandwidths of twice the standard size to test the channel degradation that would result if we wanted to have twice the bit rate. The following figures show the same tests as above by increasing the bandwidth. To make the comparisons fairer we have also adjusted the powers to double by adding 3 db.
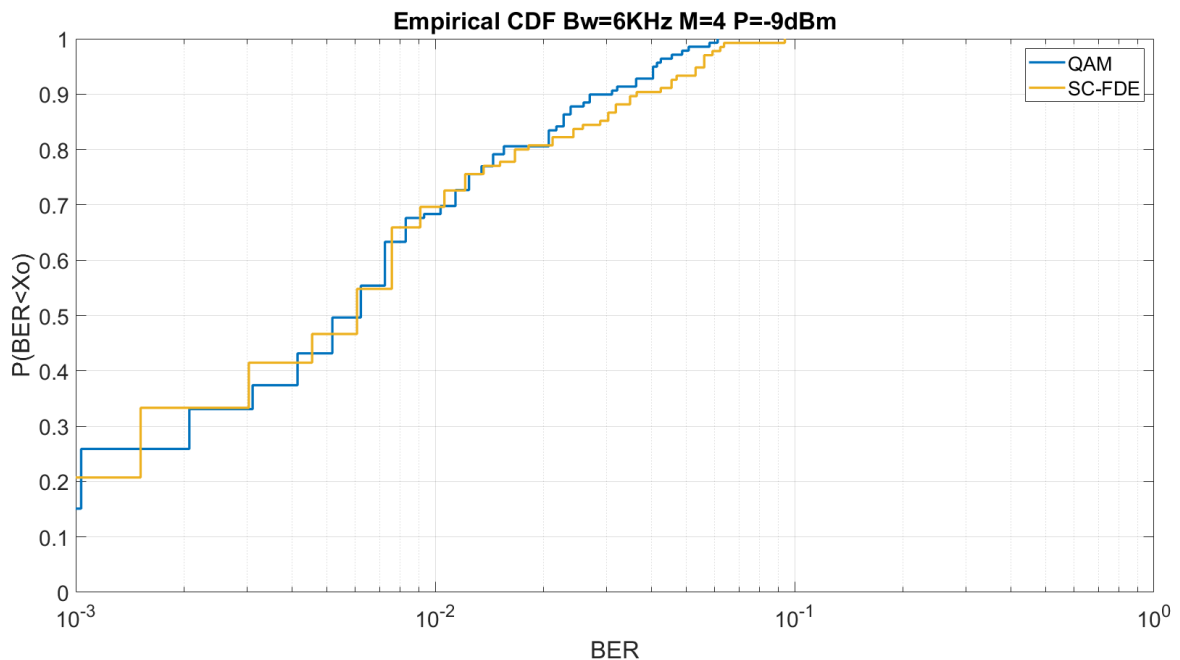
Fig. 35. *CDF of 6 kHz transmissions with power 6W and modulation order 4.*

The results show that powers -9 dBm FPGA output power (6W) with 6 kHz are quite similar to the 4W with 3 kHz (see Fig. 32) taking into account that the higher bandwidths are more difficult to demodulate. It behaves with BER of 10^{-2} between 70 % and very poor behaviour with BER 10^{-3}.

The power is increased by a factor of 2, although it is felt that the increase should be a factor of 4.
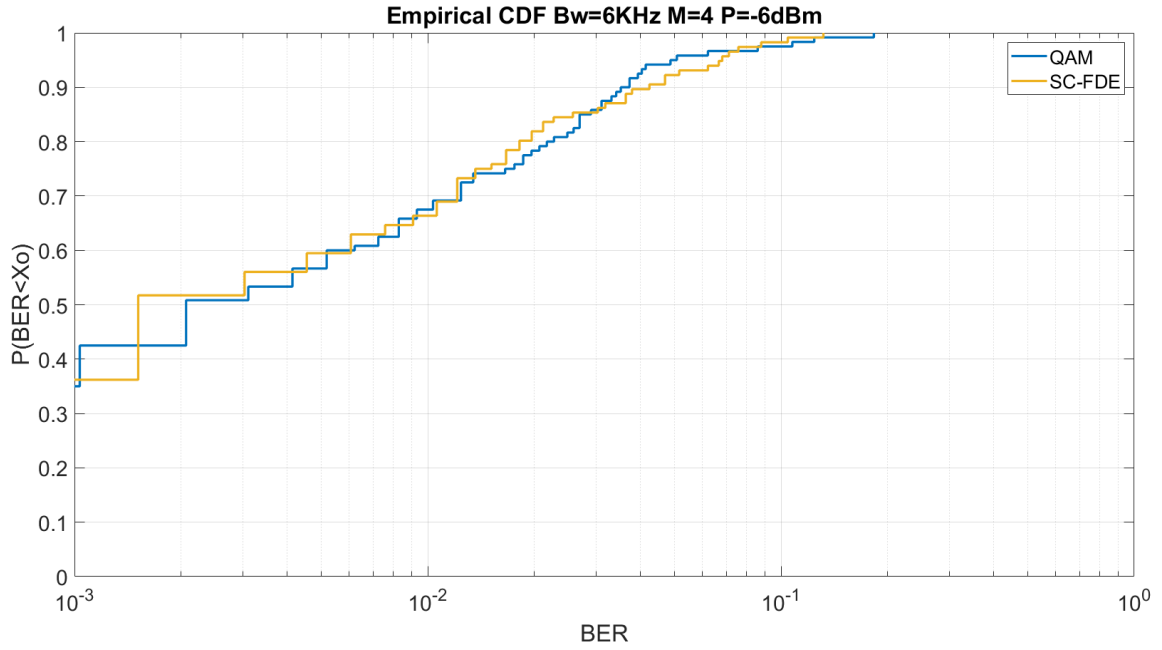
Fig. 36. *CDF of 6 kHz transmissions with power 8W and modulation order 4.*

Despite the factor 2 power increase and having reached the "ideal" power for 3 kHz bandwidths, the demodulation of 6 kHz bandwidths is very detrimental to the results, making this power increase almost unnoticeable. Only an increase in probability is seen for BER 10^{-3}, which rises to just over 40%.
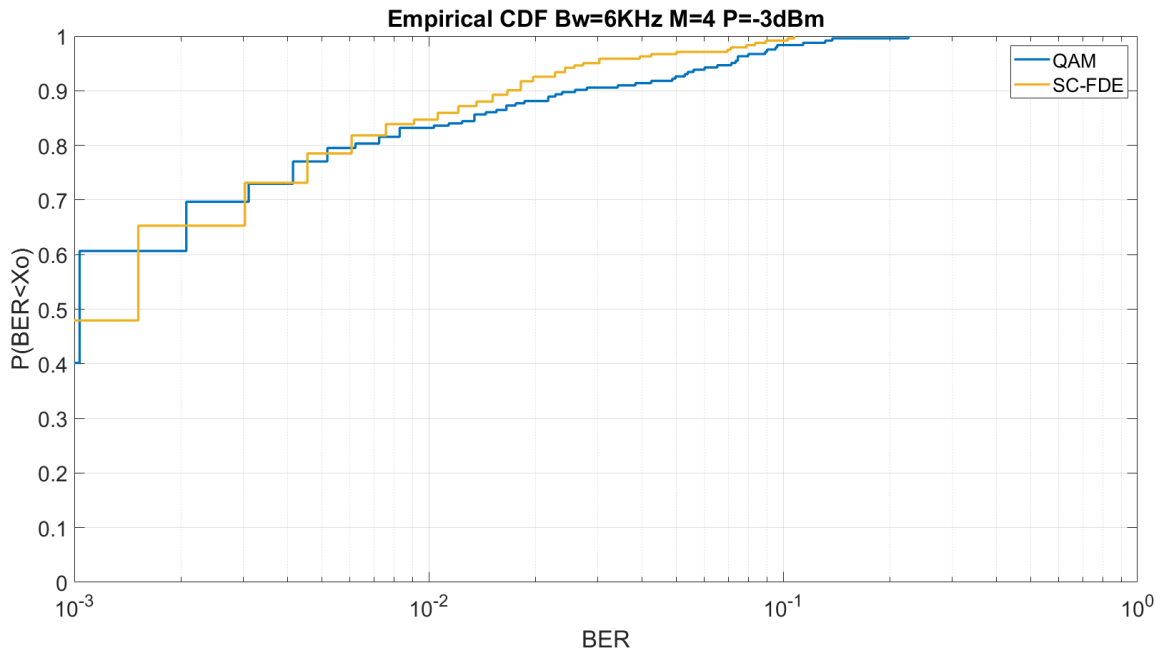
Fig. 37 *CDF of 6 kHz transmissions with power 16W and modulation order 4.*

These results show similar results for 3 kHz and 6W (see Fig. 35). With this output power from the FPGA, our amplifier enters the maximum power zone. The results do improve, however we thought about not implementing it because we would have to change some part in the design and the demodulation part. The results are BER of 10^{-2} between 80 % and 90 % and BER of 10^{-3} around 55%.

Not having much success with bandwidths above 3 kHz and in search of using increased throughput, the modulation order is increased to M=8. This would mean an increase of 1.5 times the communication rate. As with the increase in bandwidth, going up one order of modulation leads to an increase in power, so we raise the results of Bw=3 kHz and M=4 by 3 dB. 16W is the maximum output power of the amplifier.

Study of 3 kHz bandwidth and modulation order M=8
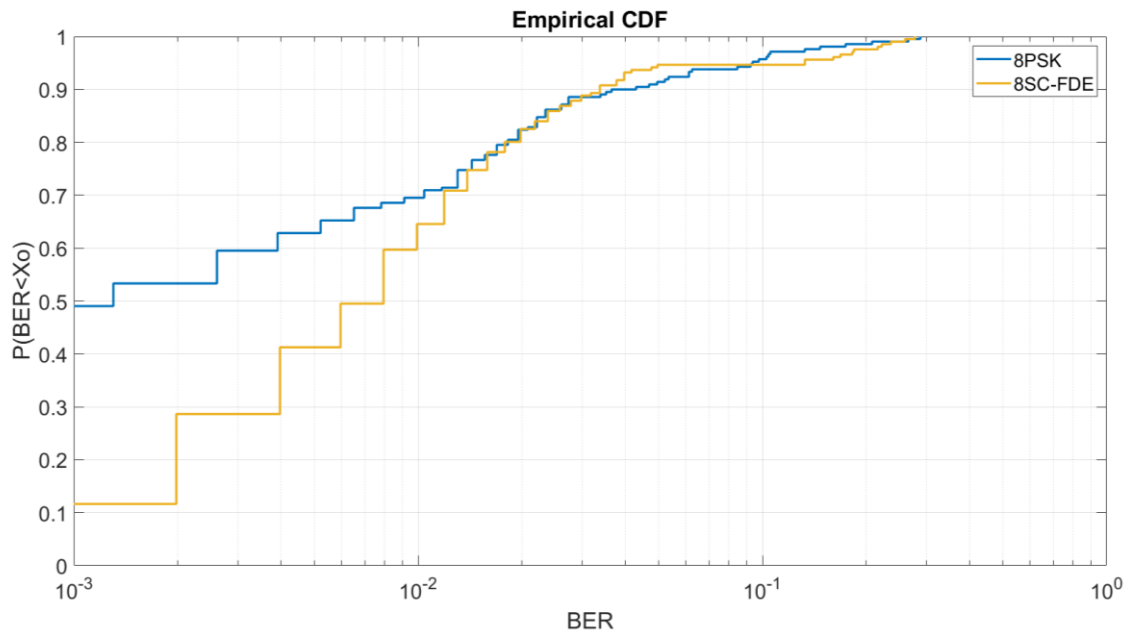
Fig. 38 *CDF of 3 kHz transmissions with power 8W and modulation order 8.*

The results we see are neither good nor sufficient. It seems that the 8PSK time equalisation has better but insufficient results. If we look at the theoretical BER/EbNo graph, maintaining a BER of 10-3 for order 4 results in an EbNo of 7 dB and for modulation order 8 this EbNo becomes 10 dB. These results are made from one channel without taking into account channel effects such as multipath.
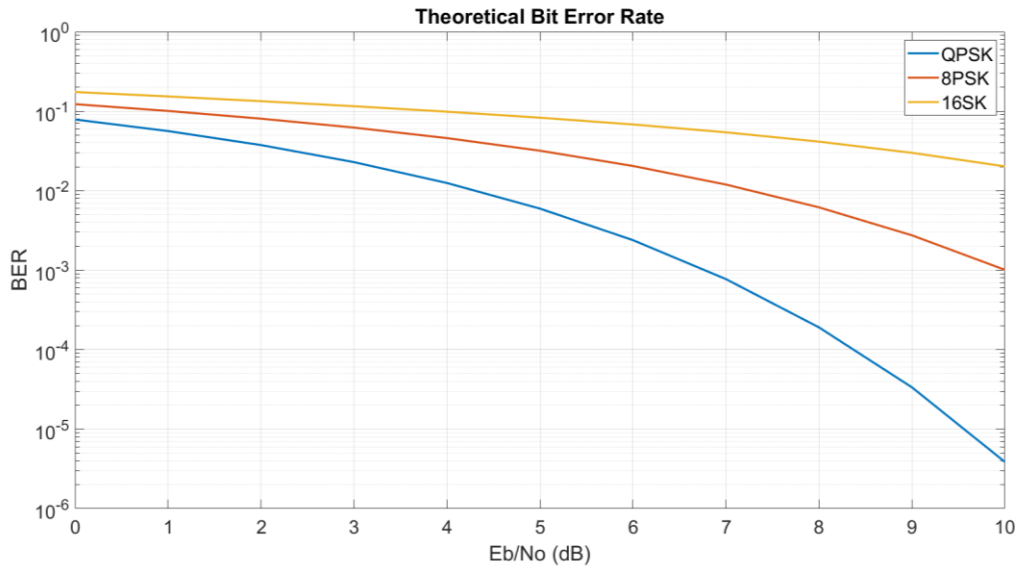
Fig. 39 *Theoretical BER/EbNo graph*

4.4.3 Results Discussion

We can state that the results obtained are good considering the following points:

- The traditional HF communications that currently exist in the Antarctic bases that use powers higher than 100W, sometimes even reaching 500W are difficult to compare, since they use between 5 and 25 times the power that we are using for the tested NVIS link considering 20W.

- We could also compare them with VHF communications which are the most used in Antarctica. They use the same power as ionospheric communications (< 20W), reaching distances around 20-30 Km due to two heights; (1) the height of the transmitting and receiving antenna. The higher the antenna the greater the distance due to the possibility of LOS. (2) Due to the terrain orography (high mountains) resulting in no LOS.

- Our tests show that using 9-10 W and without the use of an operator they can be used as a backup for a satellite and/or as the gateway to an IoT ecosystem.

- The presence of the E Layer results in very high multipath effect.

The next table summarize the best design for our proposed physical layer.

Table 5. Physical layer proposal

Power	Modulation	Bitrate	Motivation
9-10 W	4-SC-FDE	~3 Kbps	Easy equalization in frequency-domain
9-10 W	4-QAM	~3 Kbps	Complex equalization in time-domain but better robustness

5 Compact antenna

The NVIS platform developed in this thesis has been improved in all fields (physical layer from a sounding study and implementation of a second antenna to take advantage of the polarization diversity and thus gain in robustness), and also takes into account the hardware through which the signals are transferred, which is the antenna.

As this is a system in which the uplink layer is studied where low consumption by the sensor is a priority, reducing the size of the antenna and losing efficiency would be very detrimental. However, for the study of the miniaturization of the antenna to avoid visual pollution and reduce the area where the antenna is positioned, it has been proposed to study this antenna and see how it impacts our system in reference to the transmission power.

The influence of soil types and soil depth is summarized below, and the different antenna parameters at different heights are simulated for a buried antenna. Finally, an experimental test of this antenna is performed in Cambrils as a receiving antenna compared to a horizontal dipole.

5.1 Introduction

Commonly HF communications use linear antennas formed by electrically thin conductor wires. This fact makes the length much greater than the diameter of the conductor, causing the currents to move longitudinally over the conductor surface. The most commonly used linear antenna is the $\lambda/2$ dipole, which despite not having much directivity or gain (D=2.15 dB and G=1.76 dBi) is very simple to implement and has good performance.

With the motivation to reduce the size and visual impact, as mentioned in section 2.4, many antennas used in HF were analysed (Horizontal Dipole, V-Inverted and Small loop). The Small loop is discarded for efficiency and gain comparison with dipole type antennas. Finally, the V-inverted is discarded due to the tilt angles. Finally, a buried antenna was designed to maintain the properties of the dipole (large antenna) but without visual impact. The minimum requirements and the first simulation of these parameters are detailed below.

5.2 Buried Antenna design

In response to the hypothesis of whether it was feasible to bury an antenna and that the radiation is sufficient for NVIS communication, the following parameters were

defined (assuming the possible losses or compensating them through other elements of the system).

- Dipole antenna
    - Considering the frequency at which we work, the wavelengths and types of antennas for NVIS communications, the study focuses on dipole antennas (the most commonly used antenna is the horizontal dipole which is the most efficient for NVIS applications).
- Reconfigurable antennas:
    - The variability of the behaviour of the ionosphere has already been seen. Therefore, the antennas should be easily adaptable to other frequencies within the NVIS operating range.
- -20 dB gain [3-7 MHz]
    - The antenna gain should be at least -20 dBi within the range [3-7 MHz] which is the range where one frequency could be defined for daytime and another for nighttime.
- Vertical radiation pattern
    - The radiation pattern has to have its maximum in the direction normal to the ground in order to make the NVIS application.

When choosing the best configuration for the simulations, the most important parameters are radiation efficiency, gain, bandwidth, and transmission impedance mismatch coefficient. These will be affected by the ground where the antenna is buried.

The soil is a conductive element according to its composition. Obviously, it also depends on the level of water it has, since it is one of the most conductive elements [88][89][121]. In addition to water, the soil is composed of organic elements that modify the electrical properties as explained in section 2.7. In our simulation we have defined the parameters explained below distinguishing between a wet and a dry soil.

- dry soil: presents a conductivity of 0.0001 S/m and a relative permittivity of ε_r= 2.5.
- wet soil: presents a conductivity of 0.01 S/m and a relative permittivity of ε_r=35. In this case, the radiation efficiency was so small that this option was directly discarded for this study. However, this does not mean that it cannot be used, it will simply entail the use of higher power to achieve the same communication.
- Permafrost: presents a conductivity higher than 0.0001 S/m and a relative permittivity range between ε=4-8 [122] [123]. Permafrost, although it is out of study, possibly in the future in the context of Antarctica, the feasibility of installing this type of antennas there on these soils could be studied.

The following table shows the results of the radiation efficiency of the buried antenna, according to the simulation of the different types of dry and wet soils based on their parameters that influence their behaviour, dielectric constant and conductivity. IE3D software was used for these simulations. The simulation results are performed for a

frequency of 5 MHz and a copper tube thickness of 10 mm, which is the most common value.

Table 6. Simulation of different soils and burial depths of a horizontal dipole

Size (m)	Soil	Height (cm)	Radiation Eficciency
15	Dry	100	9.84 %
15	Dry	50	8.15 %
15	Dry	25	6.95 %
15	Dry	10	5.81 %
15	Dry	0	3.32 %
15	Wet	0	0.5 %
15	Dry	-10	3.41 %

As previously mentioned, the radiation efficiency value for the antennas for wet soil is much lower, so the study will focus on dry soil. This is due to the high conductivity of this type of soil, causing the radiation to propagate more at ground level and not suffer a rebound as it happens with dry soil.

Therefore, depending on how much we bury this antenna will be reflected in the properties of the antenna. As a first study, simulations were made of a 15-meter copper pipe buried in the ground and obtaining results with different depths. The diameter of the copper pipe was initially 10 mm due to the most usual value. In the Fig. 40 we can see the variation of the realizable gain for different depths.
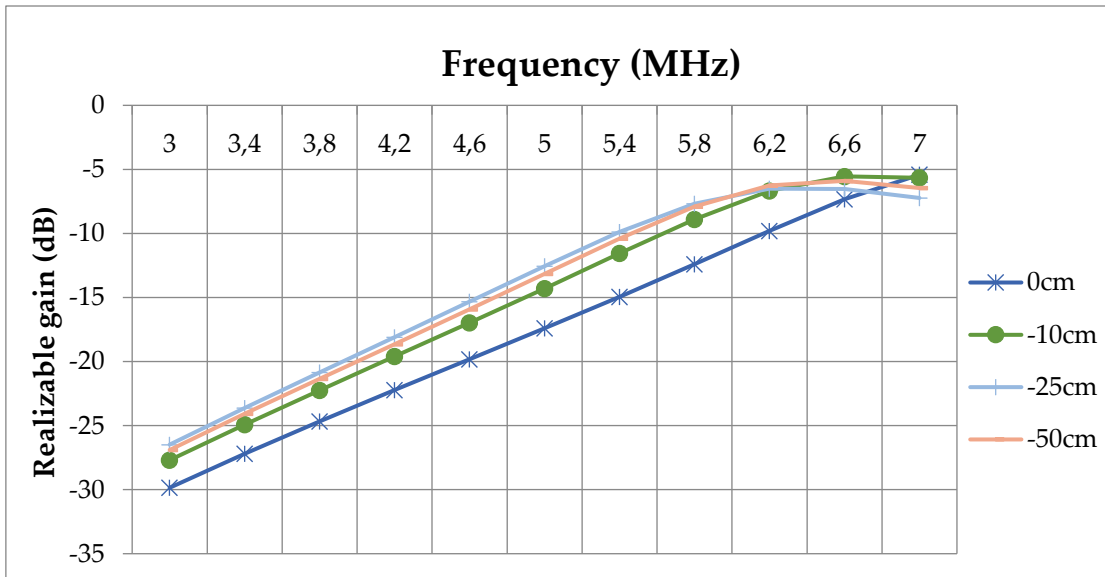
Fig. 40 *realizable gain for different depths*

Our system has adapted antennas at 5.4 MHz. The graph shows that by burying 10 centimetres we can have an achievable gain of around -11 dB. It is true that burying the antenna deeper also increases the gain, but the trade-off with the effort is not profitable.

Once, having studied the behaviour of different depths, we proceed to find a matching network to achieve better transmission parameters (antenna efficiency and achievable gain). The matching process is performed with the AWR Microwave Office software.

The matching network for the 15m antenna buried 10cm is shown below.
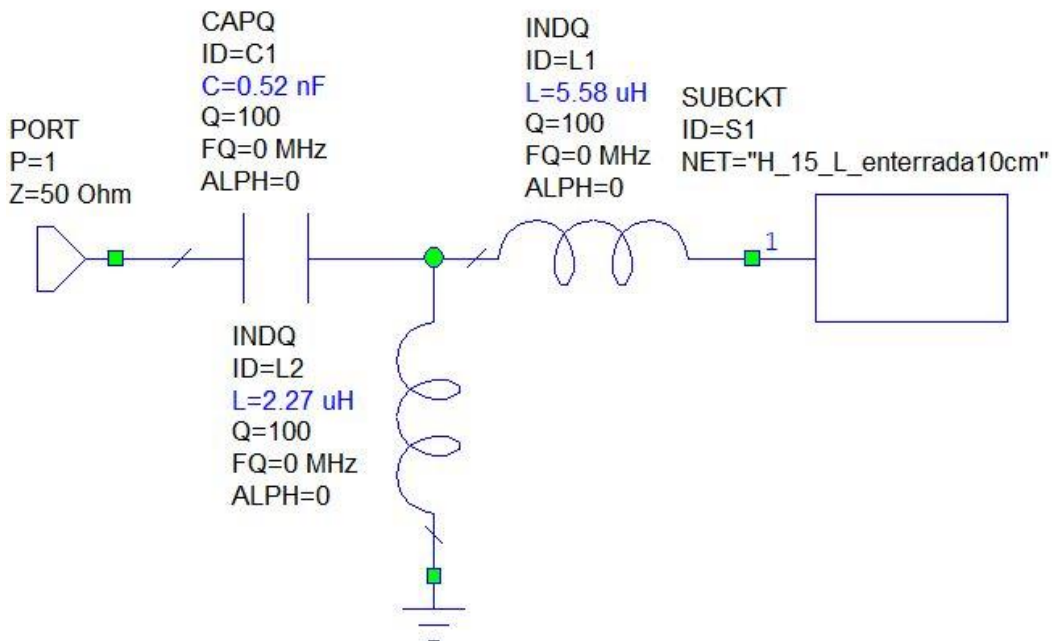
Fig. 41 *Adaptation network for antenna of 15m and depth 10cm*

This matching requires 3 matching elements, a series coil, a parallel coil and a series capacitor. With these elements and a quality factor of 100, 5 MHz matching is achieved. The following figure shows the reflection coefficient S11.
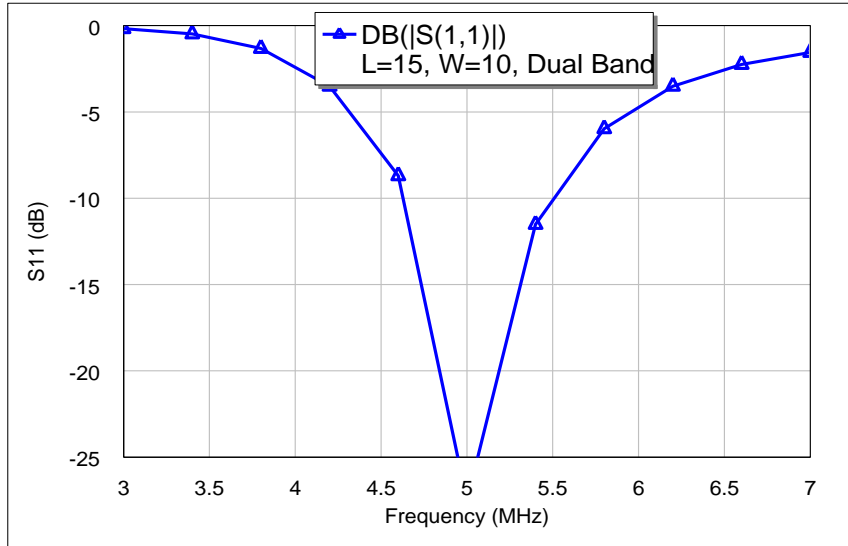
Fig. 42. *Reflection coefficient S11 at 5 MHz*

From the inclusion of this adaptive network, we can see the difference between putting it in or not. It can be seen that the difference is remarkable especially in the frequencies in which we are going to work. The difference in efficiency is almost 4 times and the gain shown in the figure is almost 7 dB.
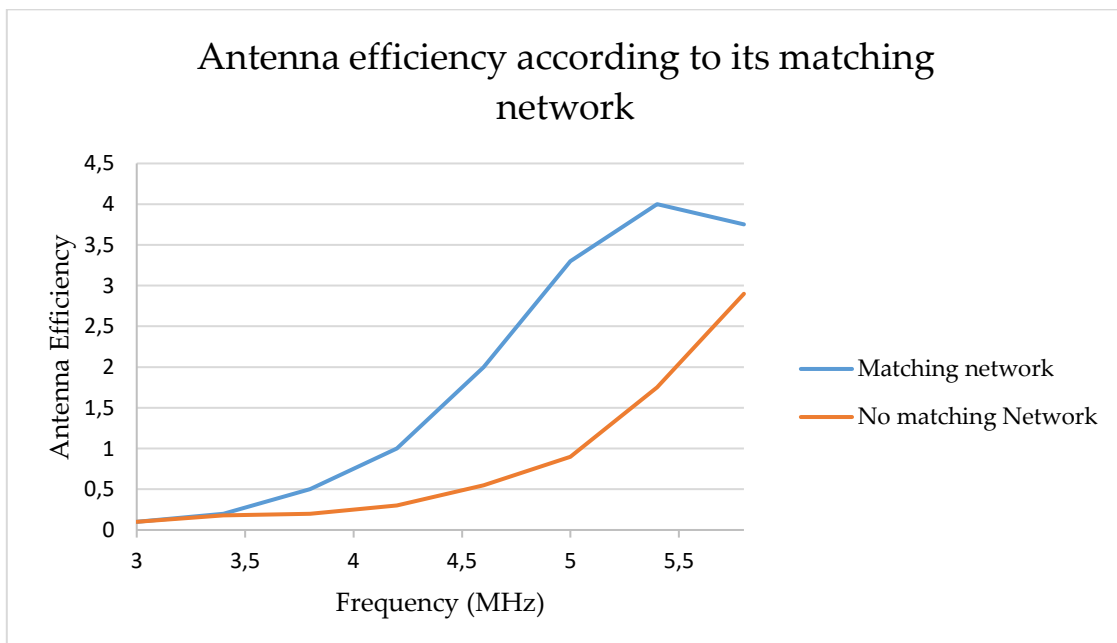
Fig. 43 *Improvement of antenna efficiency with matching network*
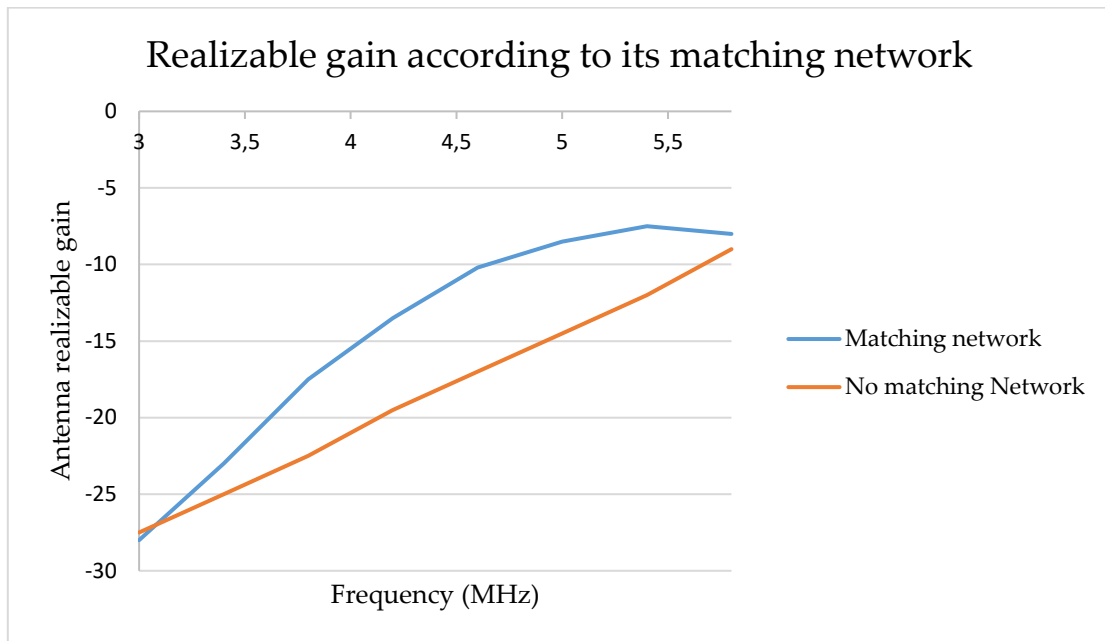
Fig. 44 *Improvement of antenna realizable gain with matching network*

Following the above matching network, we can, by changing the values, make this antenna dual band. So far, the antennas used for these nodes are single frequency. Using the same scheme with two coils and a capacitor, we achieve these two bands, 3 MHz and 6.2 MHz. According to the following graph, the gain would be a little more than -12 dB, compared to -25 dB for a single frequency.
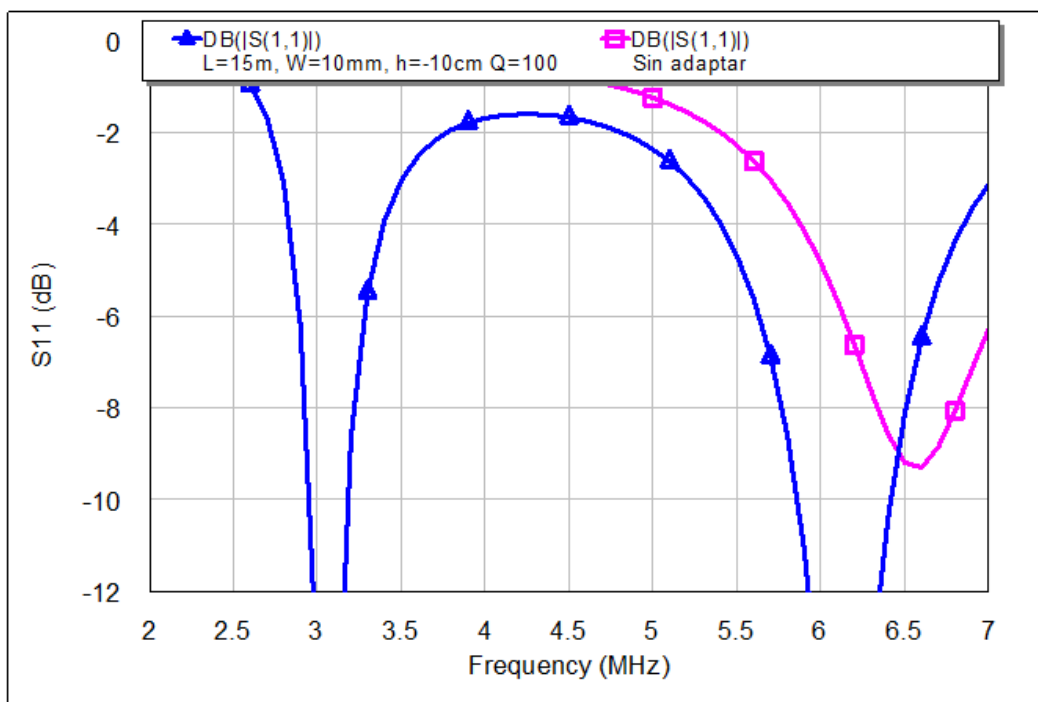
Fig. 45 *S11 coefficient with matching network for dual band antenna*

5.3 Buried Antenna implementation

Based on the above simulation, we proceeded to carry out the study in a practical way. The only change made was the change of diameter to 18 mm. In practice, A 15-meter horizontal dipole was built with 18 mm radius copper tubes, together with a balun that balanced the signals to reduce the effect of interference. In order to reduce the effects of the soil when burying the antenna, a plastic corrugated pipe has been used to isolate the copper pipe from the soil. Finally, a 10 cm diameter PVC pipe is used to provide sufficient space between the first protection of the corrugated pipe and the soil. The cooper tube is located in a concentric way to have same distance to the surface and the deepest part of soil, for that reason a dielectric has been put around the cooper tube each 2 meters.
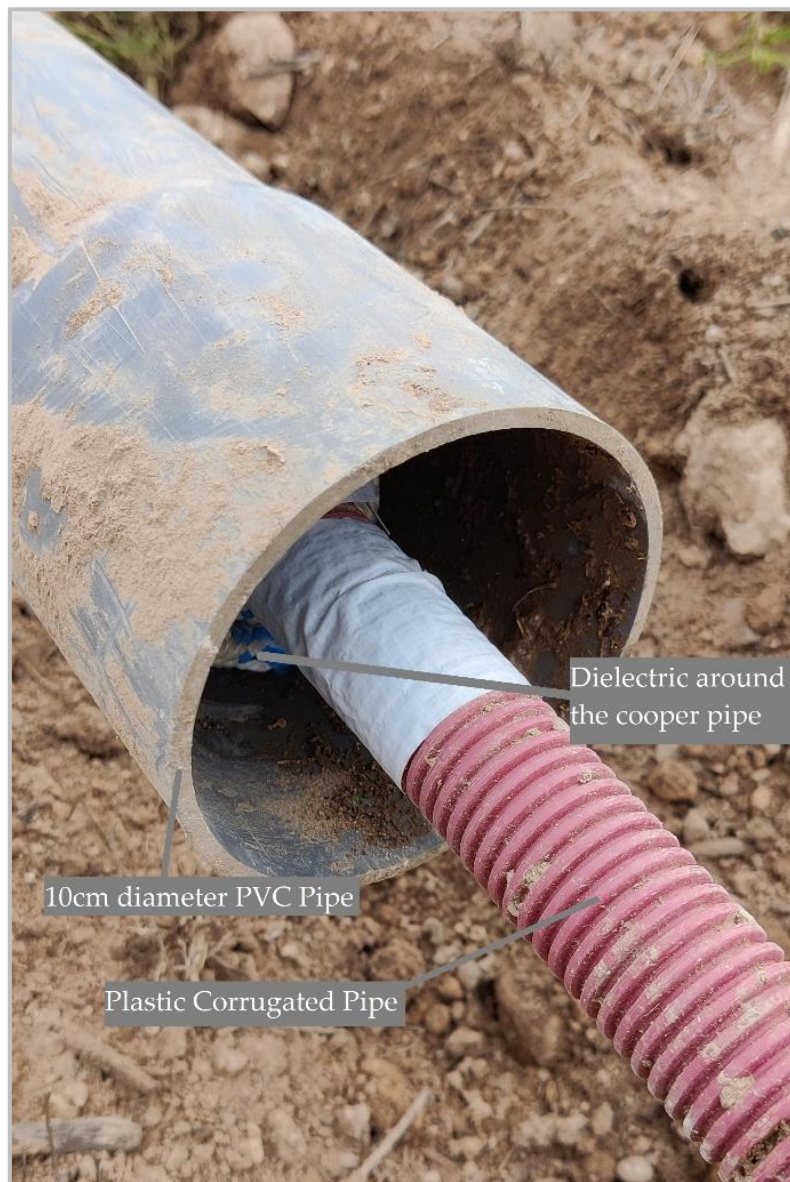
Fig. 46 *18 mm diameter copper pipe with all its elements to be buried.*

The installation was made at the Cambrils receiver node where the antenna was buried with the help of other members of the research group. In the next figure we can see the antenna burial process.

Fig. 47 *Buried Horizontal dipole*

5.4 Antenna matching

The first test that was done was the antenna adaptation. First, we looked at the horizontal dipole of our system and subsequently, we looked at the adaptations of the antenna to be buried, first resting on the ground and secondly buried 10 centimetres. The first thing we see is that our antenna has an S11 of S11 of -18.67 dB and the antenna just supported gives us an S11 of -13.26 dB at the frequency of 6.02 MHz. By burying it the matching value is reduced by about 1 dB and it shifts almost 800 kHz down. This is due to the conductivity created by the ground.

To compare both antennas, the second marker shows that for 5.4 MHz S11=-11.71 dB, which is still sufficient. Compared to the horizontal dipole (S11= -18.67 dB for 5.4 MHz), there is 7 dB of matching difference, so this value should be considered.
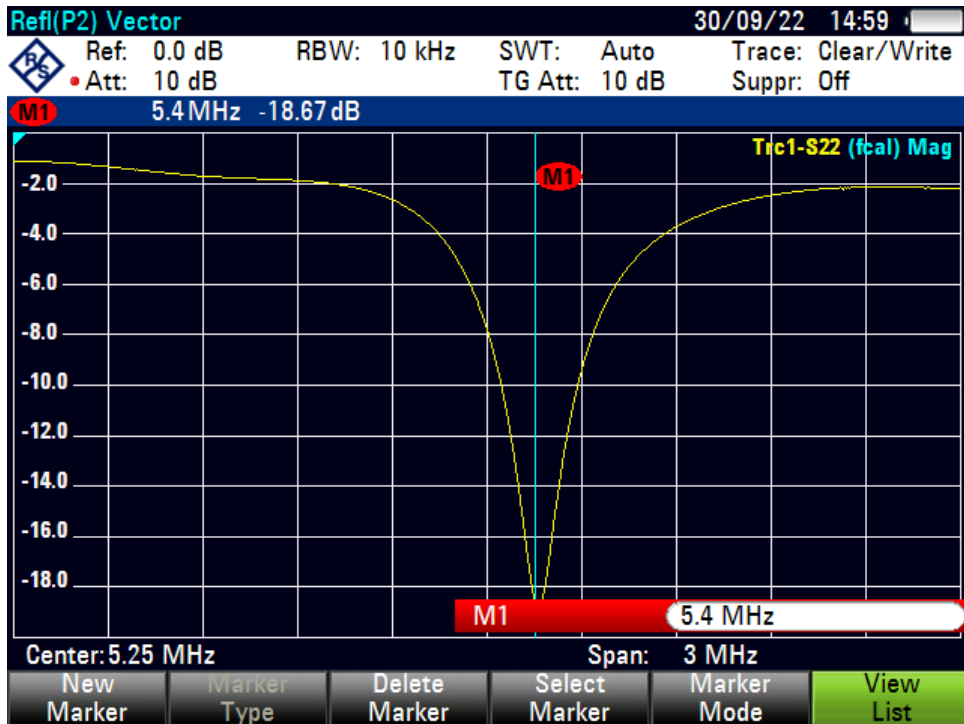
Fig. 48 Horizontal dipole Adaptation
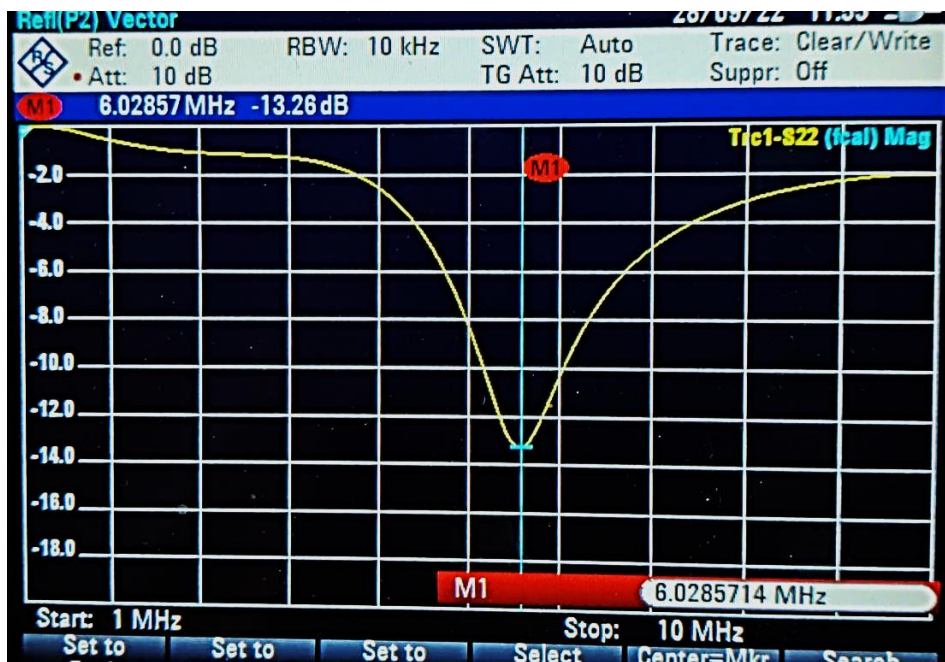
Fig. 49 Horizontal dipole Adaptation (resting on the soil ground)
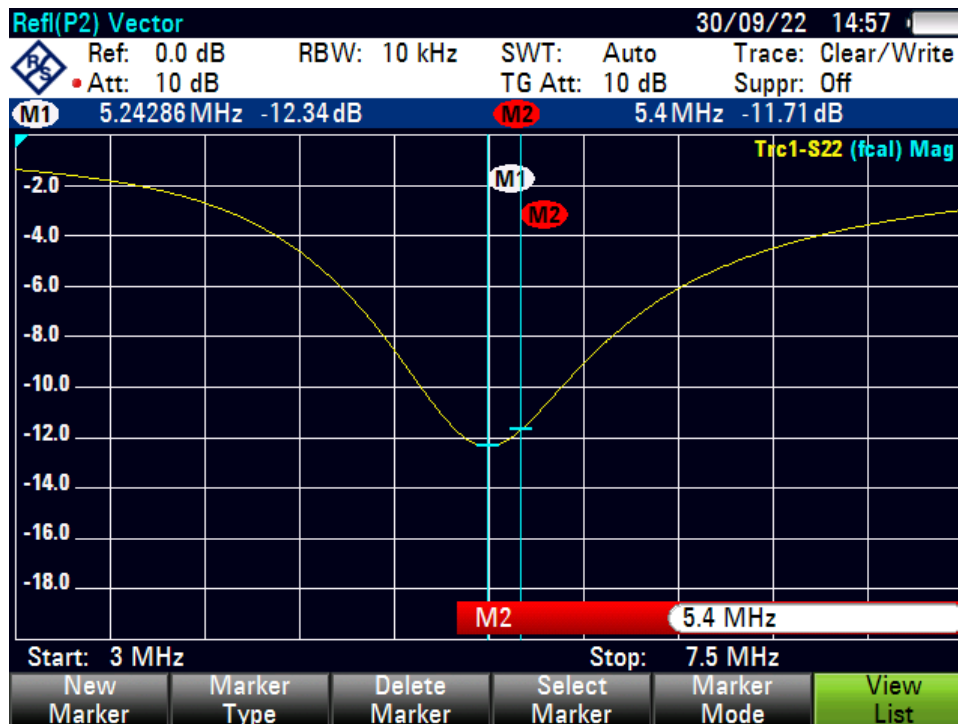
Fig. 50 *Buried Antenna adaptation (Buried)*

5.5 Gain measurement

Many factors such as the dimensions of the antenna and the fact that it radiates upwards, make the gain difficult to measure. However, we can compare it to a horizontal dipole at 13 meters height. This height is due to soil type which makes the height lower when the permittivity and conductivity are high [124].

For this reason, the first sounding is performed with a Kenwood radio station capable of transmitting at 49-50 dBm only by sending a FM signal (with no modulation on it) through a horizontal dipole tuned to 5.4 MHz. This fact allows us to check the signal received with the buried antenna and then compare it with the same horizontal dipole as the transmitter.

These measurements were done with a Max Hold option and the resolution bandwidth the most accurate as possible. We took 1 minute for each measurement because we wanted to consider the multiple behaviour changes of the ionosphere. For this test, the difference is 19.6 dB. If we do the Link Budget calculation, the radio propagation loss amounts to -104.1 dB. Seeing that the gain of the horizontal dipole is 4 dBi, we can deduce that the gain of the buried antenna is -15.6 dBi.
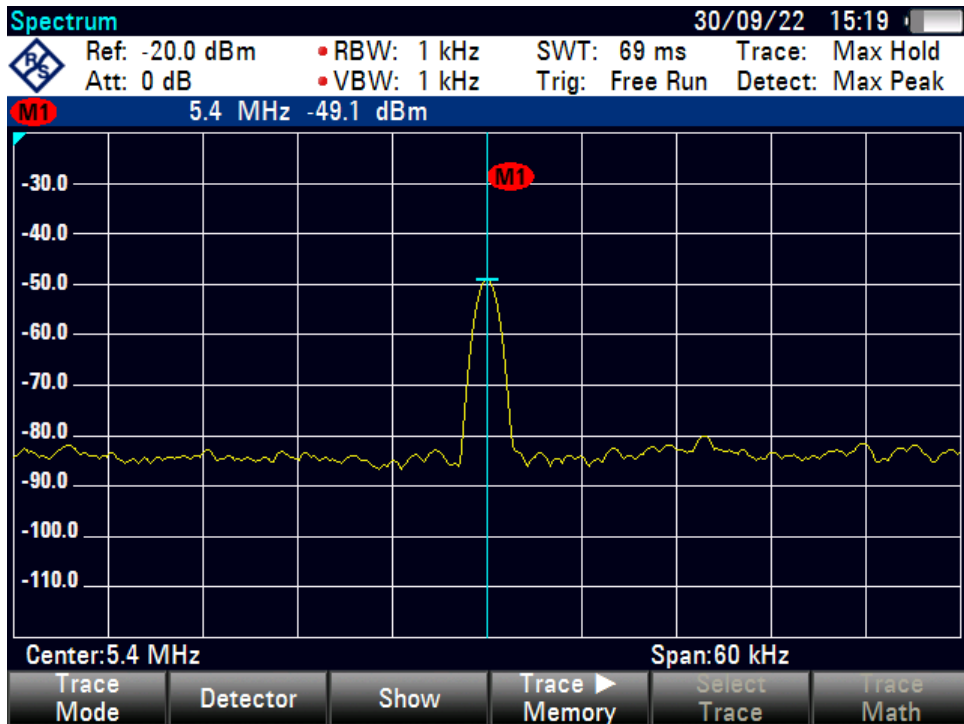
Fig. 51 _Horizontal Dipole received power_
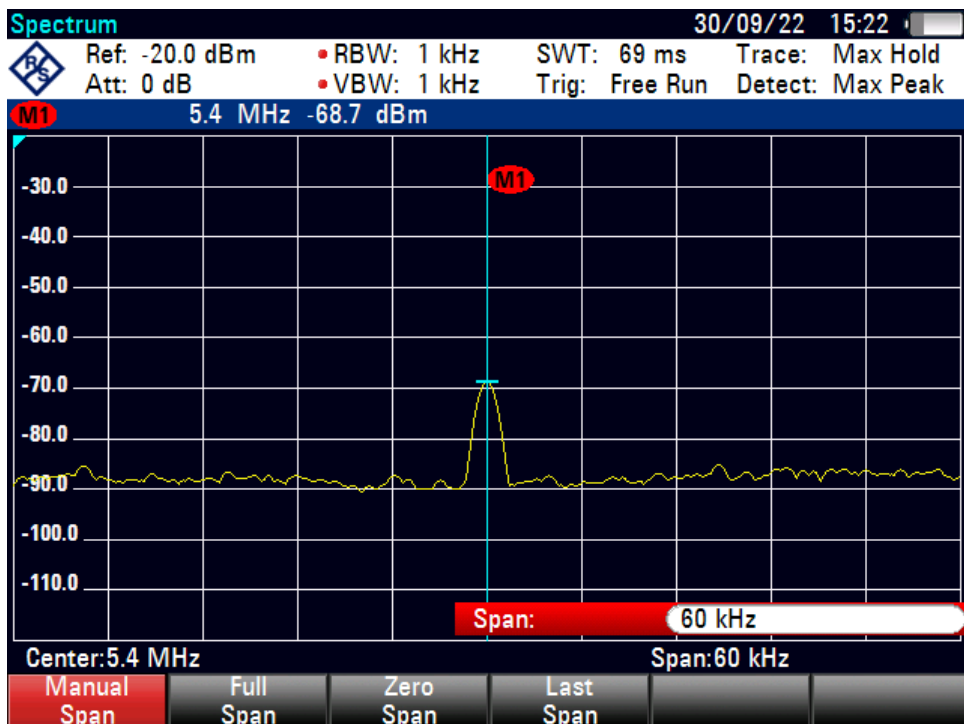
Fig. 52 _Buried Dipole received power_

5.6   Results discussion

The results achieved for this antenna are obviously not ideal, but this could already be sensed. The gain in simulations was already low, and in practice it can be seen that in the best case the received power compared to a horizontal dipole is at least 10 dB difference. These tests are made with a Balun, and the most convenient would be to make a matching network achieving better efficiency and also would achieve the adaptation of two frequencies. The increase in the diameter of the copper tube could also be studied.

If we compare the controlled loses measure, we can see that this is the value of a Broadband Folded antenna loses. This type of antennas are designed to cover a wide range of frequencies (in this case between 1.8 and 30 MHz) so their losses are high.
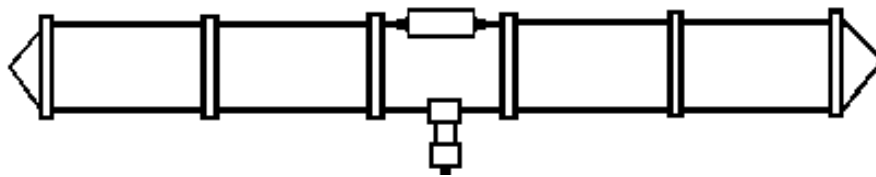
Fig. 53 *Broadband Folded Dipole Antenna* [125]

If we compare these results with other research studies for example the proposal of [126] which introduces a new ship-integrated HF antenna due to the requirements of the most modern high-speed vessels. The antenna adopts an array of slot antennas excited by a contact line, which can be matched to an existing superstructure of the ship. It has good horizontal omnidirectivity and the horizontal directivity coefficient is higher than -4dB. Directivity is related to gain and we can conclude has controlled loses.

Another study would be a lightweight broadband HF antenna design for vehicular OTM NVIS applications by [127]. It was demonstrated that a multi-arm half-loop performs as well as dipole when the antenna configuration is properly chosen. The same authors proposed in [128] the design of a low-profile electrical moving HF antenna with an instantaneous impedance bandwidth of 24 kHz and a gain better than -25 dBi for NVIS. It is a rectangular two-arm half-loop operating from 2 to 10 MHz.

6 Conclusions

6.1 Summary

In this thesis, we have studied multiple ways to improve an NVIS system that works with a physical layer based on STANAG and MIL-STD standards. This system had to be as robust as possible since it will be installed in remote areas in order to be used as a hub node for IoT sensors.

Three important points of a telecommunication system have been studied: (1) A study of the ionosphere as a communication channel for a single frequency, together with the two propagation modes, concluding that taking advantage of the two propagation modes there is an improvement in the total robustness of 4 dB. (2) The physical layer, despite following the same scheme of the data frame, a modulation that improves the simplicity of the equalization (equalization in the frequency domain) for real-time applications has been investigated and compared with the previous proposal with this same type of equalization (OFDM). (3) Finally, one of the most problematic aspects of the systems operating in the HF bands, are the large size of the antennas, which hinder their placement, as well as the visual pollution they cause. It has been proposed an antenna that is buried 10 centimetres under an earth ground that in spite of presenting relevant losses (<20 dB), are able to be used with these systems.

6.2 Achieved goals for each hypothesis

To conclude this thesis, we will start from the hypotheses formulated. Each one of the hypotheses has been studied and has been developed during the thesis with a conclusion for each one of them. This chapter will summarize the objectives set and how they have been achieved.

> ❖ **Hypothesis 1:** *Ionosphere sounding over two propagation modes (Ordinary and Extraordinary)*

Due to the rapid changes in the ionosphere, which are difficult to predict, a study of the ionosphere as a communication channel was proposed. As explained in point 2, the ionosphere has an almost cyclic behaviour every 10 years. However, when defining the physical layer of a communications system where the channel is so hostile, it should be as close as possible to the characteristics of that channel, so the channel study is necessary to be able to update the design parameters. In this context, it was proposed to perform a channel study for a single frequency, for the two propagation modes of the ionosphere (Ordinary and Extraordinary). These two propagation modes have been treated as independent channels in order to use the polarization diversity in reception SIMO technique.

For the development of this objective, a physical layer was defined to study the behaviour of the ionosphere as a communication channel. Subsequently, the system

was adapted for a frequency of 5.4 MHz, which is the frequency where the ionosphere was most available and without having any interfering system.

With these configurations, a sounding was carried out between Barcelona (transmitter) and Cambrils (receiver), where the two propagation modes, both ordinary and extraordinary, were studied for several months. As a conclusion, by using the SIMO technique, the robustness significantly increases the communication channel.

❖ **Hypothesis 2:** *SC-FDE will overcome OFDM for these kinds of communications.*

Previously, the OFDM multicarrier technique was considered to replace the NVIS physical layer available to the research group. Up to that time, discrete modulations had been studied and tested (FSK, PSK and QAM), but time equalization made real-time applications difficult. For some specific scenarios, OFDM obtained results comparable to those obtained with QAM modulation. On the other hand, since a system was needed where power consumption was as low-power as possible, it was proposed to find a solution to the high PAPR presented by OFDM due to frequency division. It was proposed to study the SC-FDE modulation that many current standards use on the device side (uplink channel) since battery consumption is critical as opposed to a base station. Although SC-FDE does not correct for channel effects as well as OFDM does, it does correct for noise.

For the study of this modulation, we needed the channel study done in objective 1, to then make a design with the parameters obtained. With the system configured, studies were made for several months, and from the CDF plots we could see the behaviour of this modulation. We also used the clipping technique to be able to trim the main peaks to increase the average power of the signal and obtain better results in robustness. As results, we see that the results of this modulation are comparable in all situations to the QAM modulation but with the advantage that the equalization is in frequency.

Finally, this study was extrapolated for the communication of the Antarctic Base Artigas (Uruguay) and Juan Carlos I (Spain) in the 2021-2022 campaign. This study was done without a previous channel study due to the time we had available. On the other hand, they showed better results than in the channel made between Barcelona and Cambrils since in Antarctica there is much less electromagnetic noise. On the other hand, it can be seen in the graphs that by increasing both the modulation order and the channel bandwidth, the results do not agree with the theory. This is due to the proposed physical layer parameters that do not hold elsewhere on earth.

❖ **Hypothesis 3:** *Invisible antennas could be used for NVIS IoT communications.*

We are not aware, but nowadays anyone who pays attention to infrastructure installations in any city, can notice the multitude of antennas (and other elements) that

are seen. Surely, we have become accustomed to this fact, but visual pollution is starting to be no less of a problem. Put in context, HF communications, more specifically with NVIS technology (3-10 MHz), use antennas with sizes ranging from 50 to 15 meters. A scenario is proposed in which the antenna is completely buried and is able to radiate enough to be used as an NVIS antenna.

Based on simulations of buried antennas at different heights and also simulating their matching network, the deployment of a 15 meter dipole antenna buried underground was implemented. Using an HF radio with a transmit power of 100 W, transmissions were made at the same time instants in order to compare the results under the same ionospheric reflection conditions.

As a conclusion to the study, the received power of a 30 meter horizontal dipole adapted to 5.4 MHz had a reception almost 20 dB higher, taking into account the size (twice the size).

6.3   Global view

Nowadays, there are still remote places without access to communication. Possibly, places like Antarctica, being a continent dedicated to science, the need for a minimally decent communication is essential. In other places, perhaps they do not need these communications (or they do, but not at such a high cost).

If we talk about the commercialization of this type of communications, it is difficult to analyse the viability of NVIS communications. To close this thesis, it is inevitable to talk about the inclusion of the technology developed by SpaceX (Starlink). This proposal to launch thousands of satellites to provide broadband communication, low latency, and low cost to even the most remote locations. Possibly the study or application of NVIS worldwide is becoming less and less meaningful, although it can still be seen as a communication alternative, especially for natural disasters, due to its rapid deployment and low cost of installation alone, without the need to pay a service fee. On the other hand, when a standard is implemented, be it for communication or whatever, there is always the option of complementing the other technology (in this case).

Let's remember that this is a technology with its maximum use in emergency communications. So far it has been possible to provide a communication service with a platform at a cost almost insignificant at the level of what a government could pay. It is true that the evolution of telecommunication systems is advancing at a very fast pace. 5G systems have not yet been implemented in many cities, but 6G communications are already being tested. It remains to be seen where these developments will lead.

6.4   Future Work

The following are improvements that should be investigated and implemented to take full advantage of this technology.

- Bitrate improvement:

    Although the bitrate is sufficient for most sensors, there are some that need to store more data. Bitrates can even be improved by using higher bandwidths with techniques such as Carrier Aggregation (introduced in 3G standards), using higher modulations orders or making the frame design more efficient. As for the frame design, SC-FDE and QAM show very similar behaviour in most scenarios, but in a future line, SC-FDE configuration can be improved by changing the number of subcarriers, carrier spacing or even making the CP adaptive. The channel estimation can also be extrapolated by the CP itself or even with the PN sequence that we use to identify the modulation. Furthermore, we should keep in mind that frequency domain equalization is always preferable and, in this scenario, the SC-FDE will always be preferable.

- Robustness improvement:

    Robustness in this type of communications is crucial. In this thesis, we have made a study of polarization diversity, but there are several types of techniques that can improve robustness and even bitrate. On the other hand, we have used the SIMO technique, but it would be necessary to implement the MIMO technique that many standards currently use (such as WIFI). This would require the installation of at least two antennas in transmission, thus increasing spectral efficiency. For this, it is necessary to develop the phasing network digitally with the FPGA to be able to use it at any frequency.

- Antenna size reduction:

    Antennas are possibly a pending issue in HF communications due to their large size. Compact antennas, even transparent, are already being investigated to avoid visual contamination of the environments where they could be installed in these systems. However, as in all communication systems are based on trade-offs, when reducing the antenna size, you usually lose efficiency, so it is difficult to find that balance.

- Channel availability improvement:

    Finally, the problem of intermittent communication due to the behaviour of the ionosphere could be solved with the Delay Tolerant Networking (DTN) protocol. The DTN protocol was introduced in [129] [130] used in the central nodes that act as a gateway to avoid losing sensor data. When the ionosphere becomes available again, the central node will send the data through NVIS [131]. This protocol could be adapted to our platform to solve the connection loss. In [132] different transport protocols were compared simulating scenarios similar to Antarctica with good results reducing packets lost due to the ionosphere. Next steps are to acquire this protocol to our system for then be a complete IoT solution.

- Antarctica:

  In the near future, all the studies that have been done on NVIS should have an impact on Antarctica. It has been approximately 20 years in which the School of Engineering of La Salle (Ramon Llull University) has been trying to study and improve all the capabilities of ionospheric communications. Several studies have been carried out in Antarctica in order to solve the high cost of satellite communications. Perhaps with a little more work, it will finally be possible to leave a permanent NVIS node installed to test the platform for years and really see the results in a non-extrapolated and purely experimental way. I would like to take this opportunity to thank my colleagues Josep Mª Masó and Adrià Mallorquí for their experiences in Antarctica and to encourage them to continue with their respective research.

Fig. 54 On the left, Josep Mº Masó is with the author at the Artigas Antarctic Research Station. At right, Adrià Mallorquí is with the author at the Juan Carlos I Antarctic Station.

6.5 Contributions

As a final point of conclusion, the author will list and summarize the publications in indexed scientific journals that have been made from the studies presented throughout the thesis.

- NVIS Multicarrier Modulations for Remote-Sensor Applications

  Maso JM, Gonzalez T, Male J, Porte J, Pijoan JL, Badia D. NVIS Multicarrier Modulations for Remote-Sensor Applications. Sensors. 2020; 20(21):6232. https://doi.org/10.3390/s20216232

  This publication was the author's first contribution. This publication arose from the author's master's thesis, which was supervised by his colleague Josep Masó and his research group. In this paper, they proposed a physical layer with the frequency multiplexing technique (OFDM), in which they sought a modulation with frequency equalization as the main objective and that could also be robust enough for hostile channels such as NVIS. A sounding study was made between Barcelona and Cambrils finding the power threshold for these communications as well as varying the modulation order. The author contributed in research, software development, writing and editing. The entire study methodology was coordinated with Josep Masó, designing the different test benches, as well as the design of simulations and verifications.

- Analysis of the Ordinary and Extraordinary Ionospheric Modes for NVIS Digital Communications Channels.

  Male J, Porte J, Gonzalez T, Maso JM, Pijoan JL, Badia D. Analysis of the Ordinary and Extraordinary Ionospheric Modes for NVIS Digital Communications Channels. Sensors. 2021; 21(6):2210. https://doi.org/10.3390/s21062210

  This publication was the second contribution of the author together with his colleague Jordi Malé and his research group. In this paper, a single frequency channel study was made for the two propagation modes of the ionosphere using NVIS transmissions between Barcelona and Cambrils. For this study, a phasing network antenna had to be added in order to treat the signals with the same polarization. For the study of some parameters such as the Delay Spread, the physical layer of the system had to be modified. The author contributed in research, software development, writing and editing. The entire study methodology was coordinated with Jordi Male and Joaquim Porte. In this paper, the most important contribution was in the verification of results and in the implementation and not so much in the design of tests.

- SC-FDE Layer for Sensor Networks in Remote Areas Using NVIS Communications

  Gonzalez T, Porte J, Male J, Navarro J, Maso JM, Zaballos A, Pijoan JL, Badia D. SC-FDE Layer for Sensor Networks in Remote Areas Using NVIS Communications. Electronics. 2021; 10(14):1636. https://doi.org/10.3390/electronics10141636

  This publication was the third contribution of the author, who had the opportunity to lead the whole research process together with the rest of the team. In this article, the alternative to OFDM proposed in the first article was proposed. In this study, the starting point was the same physical layer structure, but the parameters were adapted to the SC-FDE, in which energy consumption was greatly improved by not having so much PAPR. A sounding study was made between Barcelona and Cambrils finding the power threshold for these communications as well as varying the modulation order. The author contributed in research, software development, writing and editing. In this paper, it was the first article in which the author led the entire study from start to finish, from test design to verification of results. The implementation was also part of his work together with the rest of the team.

- Simulated Multiuser Modulations for Remote Sensing Applications under NVIS
  (Under review by the research team)

  This publication, which is currently under review, was based on the final thesis of the student Miquel Martínez, which the same author supervised. In this article, OFDM modulation and its multiuser version OFDMA were compared in order to give priority to the endpoint that needed to transmit more data by distributing the subcarriers more efficiently. On the other hand, a mixed modulation combining both techniques is proposed, since OFDMA in such a small channel loses a lot of efficiency due to the identification used for the subcarriers. The author contributed to the research, writing, editing, methodology, supervision and validation.

- Horizontal Buried Dipole for NVIS communications
  (Under review by the research team)

  This publication, currently under review, is the result of a collaboration with the prestigious Dr. Jaume Anguera and Mr. Eric Morcillo who was in charge of the first studies of a buried antenna. The author was responsible for carrying out the implementation of this antenna, obtaining much more accurate experimental results and seeing behaviors in the adaptation that could not be seen in the simulations, such as, for example, the mismatch of the antenna by not using insulating materials when depositing the antenna in the soil.

- Low-Cost IoT Sensor Network for remote sensing communication in South Shetland Islands (Under review by the research team)

This publication, which is still under review, is perhaps the most rewarding of the whole thesis. As a first point, the author was able to live the experience of spending 4 months in the Antarctic research bases with his two colleagues Josep Masó and Adrià Mallorquí. On the other hand, the contribution of the article, tells how the Antarctic Bases are in terms of infrastructure, what it costs to maintain a satellite connection in these territories and finally, how NVIS communications could contribute in remote areas.

7 Referencias

[1]   J. Andujar Marquez, Jose & Pijoan, "Design and Construction of an Advanced Digital HF Communications System," *Física de la Tierra*, 2000.

[2]   J. L. Pijoan, J. C. Socoro, J. A. Moran, and F. Tarres, "DSP-based ionospheric radio-link using DS-CDMA and on-line channel estimation," *Proceedings of the Mediterranean Electrotechnical Conference - MELECON*, vol. 2, pp. 860–863, 2000, doi: 10.1109/MELCON.2000.880069.

[3]   J. C. Socoro, J. L. Pijoan, J. A. Moran, and F. Tarres, "New receivers for DS-SS in time variant multipath channels based on the PN alignment concept," *IEEE International Symposium on Spread Spectrum Techniques and Applications*, vol. 2, pp. 647–651, 2000, doi: 10.1109/ISSSTA.2000.876513.

[4]   C. Vilella, D. Miralles, and J. L. Pijoan, "An Antarctica-to-Spain HF ionospheric radio link: Sounding results," *Radio Sci*, vol. 43, no. 4, Aug. 2008, doi: 10.1029/2007RS003812.

[5]   C. Vilella Parra, "Comunicacions avançades d'HF entre la Base Antàrtica Espanyola i l'Observatori de l'Ebre: caracterització de canal i transmissió de dades," *TDX (Tesis Doctorals en Xarxa)*, May 2009.

[6]   M. Deumal, C. Vilella, J. L. Pijoan, and P. Bergadà, "Partially clipping (PC) method for the peak-to-average power ratio (PAPR) reduction in OFDM," *IEEE International Symposium on Personal, Indoor and Mobile Radio Communications, PIMRC*, vol. 1, pp. 464–468, 2004, doi: 10.1109/PIMRC.2004.1370914.

[7]   M. Deumal, J. L. Pijoan, I. Gutierrez, and A. Behravan, "Peak reduction of multi-carrier systems by controlled spectral outgrowth," *ICASSP, IEEE International Conference on Acoustics, Speech and Signal Processing - Proceedings*, vol. 4, 2006, doi: 10.1109/ICASSP.2006.1660969.

[8]   M. Deumal, C. Vilella, J. C. Socoro, R. M. Alsina, and J. L. Pijoan, "A DS-SS signaling based system proposal for low SNR HF digital communications," Oct. 2006, pp. 128–132. doi: 10.1049/CP:20060251.

[9]   M. Deumal Herraiz Enginyeria Arquitectura La Salle, "Multicarrier communication systems with low sensibility to nonlinear amplification," *TDX (Tesis Doctorals en Xarxa)*, Jul. 2008.

[10]   R. Aquilue, P. Bergada, I. Gutierrez, and J. L. Pijoan, "Channel estimation for long distance HF communications on OFDM pilot symbols," Oct. 2006, pp. 110–114. doi: 10.1049/CP:20060246.

[11]   R. Aquilué, P. Bergadà, M. Deumal, and J. L. Pijoan, "Multicarrier symbol design for HF transmissions from the antarctica based on real channel measurements,"

Proceedings - IEEE Military Communications Conference MILCOM, 2006, doi: 10.1109/MILCOM.2006.302451.

[12]   P. Bergada, M. Deumal, R. M. Alsina, and J. L. Pijoan, "Time interleaving study for an OFDM long-haul HF radio link," *IET Conference Publications*, vol. 2009, no. 549 CP, pp. 264–267, 2009, doi: 10.1049/CP.2009.0076/CITE/REFWORKS.

[13]   A. G. Ads *et al.*, "A comprehensive sounding of the ionospheric HF radio link from Antarctica to Spain," *Radio Sci*, vol. 48, no. 1, pp. 1–12, 2013, doi: 10.1029/2012RS005074.

[14]   P. Bergada *et al.*, "Digital transmission techniques for a long haul HF link: DSSS versus OFDM," *Radio Sci*, vol. 49, 2014, doi: 10.1002/2013RS005203.

[15]   M. Hervás, J. L. Pijoan, E. M. Alsina-Pagès, M. Salvador, and D. Badia, "Single-carrier frequency domain equalisation proposal for very long haul HF radio links," *Electron Lett*, vol. 50, no. 17, pp. 1252–1254, Aug. 2014, doi: 10.1049/el.2014.1184.

[16]   M. Hervás, R. Ma Alsina-Pagès, F. Orga, D. Altadill, J. L. Pijoan, and D. Badia, "Narrowband and Wideband Channel Sounding of an Antarctica to Spain Ionospheric Radio Link," *Remote Sensing 2015, Vol. 7, Pages 11712-11730*, vol. 7, no. 9, pp. 11712–11730, Sep. 2015, doi: 10.3390/RS70911712.

[17]   A. G. Ads *et al.*, "Vertical and oblique ionospheric soundings over the long haul HF link between Antarctica and Spain," *Radio Sci*, vol. 50, no. 9, pp. 916–930, Sep. 2015, doi: 10.1002/2015RS005773.

[18]   M. Hervás, R. M. Alsina-Pagès, J. L. Pijoan, M. Salvador, and D. Badia, "Advanced modulation schemes for an Antarctic Long Haul HF Link: Performance comparison between SC-FDE, OFDMA and SC-FDMA in a hostile environment," *Telecommun Syst*, vol. 62, no. 4, pp. 757–770, Aug. 2016, doi: 10.1007/s11235-015-0110-x.

[19]   R. M. Alsina-Pagès, M. Hervás, F. Orga, J. L. Pijoan, D. Badia, and D. Altadill, "Physical Layer Definition for a Long-Haul HF Antarctica to Spain Radio Link," *Remote Sensing 2016, Vol. 8, Page 380*, vol. 8, no. 5, p. 380, May 2016, doi: 10.3390/RS8050380.

[20]   B. W. Reinisch *et al.*, "New Digisonde for research and monitoring applications," *Radio Sci*, vol. 44, no. 1, p. n/a-n/a, Feb. 2009, doi: 10.1029/2008RS004115.

[21]   J. Porte, J. Maso, J. L. Pijoan, M. Miret, D. Badia, and J. Jayasinghe, "Education and e-health for developing countries using NVIS communications," *IEEE Region 10 Humanitarian Technology Conference, R10-HTC*, vol. 2018-December, Jan. 2019, doi: 10.1109/R10-HTC.2018.8629842.

[22] J. M. Maso, T. Gonzalez, J. Male, J. Porte, J. L. Pijoan, and D. Badia, "NVIS Multicarrier Modulations for Remote-Sensor Applications," *Sensors 2020, Vol. 20, Page 6232*, vol. 20, no. 21, p. 6232, Oct. 2020, doi: 10.3390/S20216232.

[23] T. Dutono, "An Ethical Review of Operating Procedures Concerning the Current Condition of 7 MHz Amateur Band Usage in Indonesia," *IES 2019 - International Electronics Symposium: The Role of Techno-Intelligence in Creating an Open Energy System Towards Energy Democracy, Proceedings*, pp. 49–52, Sep. 2019, doi: 10.1109/ELECSYM.2019.8901586.

[24] "La tendencia es que la Alta Frecuencia (HF) se convierta en una alternativa a la comunicación por satélite (SATCOM)," 2021. https://www.defensa.com/america-latina/tendencia-alta-frecuencia-hf-convierta-alternativa-comunicacion

[25] J. Wang, G. Ding, and H. Wang, "HF communications: Past, present, and future," *China Communications*, vol. 15, no. 9, pp. 1–9, Sep. 2018, doi: 10.1109/CC.2018.8456447.

[26] J. Wang, G. Ding, and H. Wang, "HF communications: Past, present, and future," *China Communications*, vol. 15, no. 9, pp. 1–9, Sep. 2018, doi: 10.1109/CC.2018.8456447.

[27] E. E. Johnson, *Third-generation and Wideband HF Radio Communications*. Norwood, M.A. : Artech House, 2013.

[28] B. T. Hunt, D. B. Haab, T. C. Sego, T. V. Holschuh, H. Moradi, and B. Farhang-Boroujeny, "Examining the Performance of MIL-STD-188-110D Waveform 0 Against FBMC-SS Over Skywave HF Channels," *IEEE Trans Veh Technol*, pp. 1–12, 2022, doi: 10.1109/TVT.2022.3189762.

[29] J. Zander, "Greedy Channel allocation in Meshed Wideband HF Radio Networks with Channel Aggregation," *2022 16th European Conference on Antennas and Propagation, EuCAP 2022*, 2022, doi: 10.23919/EUCAP53622.2022.9769257.

[30] H. Saarnisaari, V. Hovinen, H. Tuomivaara, and J. Yli-Kaakinen, "Short range HF radio channel measurements: Search for one path channels," *2016 International Conference on Military Communications and Information Systems, ICMCIS 2016*, Jun. 2016, doi: 10.1109/ICMCIS.2016.7496559.

[31] F. Orga, M. Hervas, and R. M. Alsina-Pages, "Flexible Low-Cost SDR Platform for HF Communications: Near vertical incidence skywave preliminary results.," *IEEE Antennas Propag Mag*, vol. 58, no. 6, pp. 49–56, Dec. 2016, doi: 10.1109/MAP.2016.2609800.

[32] R. W. Nelson, B. G. Butikofer, J. A. Lahart, and D. H. Church, "Wideband HF and 4G ALE Near Vertical Incidence Skywave test results," *Proceedings - IEEE*

Military Communications Conference MILCOM, vol. 2015-December, pp. 1439–1444, Dec. 2015, doi: 10.1109/MILCOM.2015.7357647.

[33]   W. Li, K. Wang, L. You, and Z. Huang, "A New Deep Learning Framework for HF Signal Detection in Wideband Spectrogram," *IEEE Signal Process Lett*, 2022, doi: 10.1109/LSP.2022.3179958.

[34]   Y. Li, G. Ding, H. Wang, L. You, and X. Yu, "Cooperative Multistation Secure Transmission in HF Skywave Massive MIMO Communications for Wide-Area IoT Applications," *IEEE Trans Reliab*, pp. 1–13, 2022, doi: 10.1109/TR.2022.3182665.

[35]   R. R. A. Syms, A. Voronov, and O. Sydoruk, "HF RFID Tag Location Using Magneto-inductive waves," *IEEE Journal of Radio Frequency Identification*, 2022, doi: 10.1109/JRFID.2022.3182894.

[36]   M. C. Walden, "High-Frequency Near Vertical Incidence Skywave Propagation: Findings associated with the 5 MHz Experiment.," *IEEE Antennas Propag Mag*, vol. 58, no. 6, pp. 16–28, Dec. 2016, doi: 10.1109/MAP.2016.2609798.

[37]   "HF Communications are making a comeback, and here's why you need to get in on it! - Base Camp Connect." https://www.basecampconnect.com/hf-communications-making-a-comeback/ (accessed Oct. 05, 2022).

[38]   K. Davies, "Ionospheric Radio," *Ionospheric Radio*, Jan. 1990, doi: 10.1049/PBEW031E.

[39]   I. Perez-Alvarez, I. Raos, S. Zazo, E. Mendieta-Otero, H. Santana-Sosa, and J. M. Paez Borrallo, "Interactive digital voice over HF," pp. 31–36, Nov. 2005, doi: 10.1049/CP:20030424.

[40]   J. Nieto, "Performance comparison of uncoded and coded OFDM and OFDM-CDMA waveforms on HF multipath/fading channels," *https://doi.org/10.1117/12.604570*, vol. 5819, pp. 77–88, Jun. 2005, doi: 10.1117/12.604570.

[41]   E. G. Thomas and S. G. Shepherd, "Virtual Height Characteristics of Ionospheric and Ground Scatter Observed by Mid-Latitude SuperDARN HF Radars," *Radio Sci*, vol. 57, no. 6, Jun. 2022, doi: 10.1029/2022RS007429.

[42]   W. Yan, L. Xue, Y. Junbo, and L. Peng, "Transmitter Elevation Angle Prediction of near Vertical Incidence Skywave Communication Link," *International Conference on Communication Technology Proceedings, ICCT*, vol. 2020-October, pp. 384–389, Oct. 2020, doi: 10.1109/ICCT50939.2020.9295795.

[43]   P. J. Coetzee and W. P. Du Plessis, "Performance Limiters of Near-Vertical-Incidence Skywave Propagation: A Scientific Approach," *IEEE Antennas Propag Mag*, vol. 62, no. 3, pp. 39–44, Jun. 2020, doi: 10.1109/MAP.2019.2943313.

[44]   T. Dutono, Z. Zakariyah, and T. B. Santoso, "A Report of C-class Solar Flare Affecting NVIS Link at 5 MHz Band (∗)," *IES 2019 - International Electronics Symposium: The Role of Techno-Intelligence in Creating an Open Energy System Towards Energy Democracy, Proceedings*, pp. 105–109, Sep. 2019, doi: 10.1109/ELECSYM.2019.8901653.

[45]   U. Gil *et al.*, "Analysis of the NVIS channel availability in the medium wave band," *IEEE International Symposium on Broadband Multimedia Systems and Broadcasting, BMSB*, 2012, doi: 10.1109/BMSB.2012.6264276.

[46]   V. Dear, A. Kurniawan, Iskandar, P. Abadi, and R. Pradipta, "A Simple Method for Visualizing the NVIS Open Channel Based on Ionogram," *2021 IEEE USNC-URSI Radio Science Meeting (Joint with AP-S Symposium), USNC-URSI 2021 - Proceedings*, pp. 96–97, 2021, doi: 10.23919/USNC-URSI51813.2021.9703504.

[47]   A. A. Elsukov, D. V. Ivanov, V. V. Ovchinnikov, N. A. Konkin, and M. I. Ryabova, "BPSK Ionosonde Based on SDR Platform to Support NVIS Communication," *2018 Systems of Signal Synchronization, Generating and Processing in Telecommunications, SYNCHROINFO 2018*, Sep. 2018, doi: 10.1109/SYNCHROINFO.2018.8457027.

[48]   X. Li *et al.*, "Forecasting Ionospheric foF2 Based on Deep Learning Method," *Remote Sensing 2021, Vol. 13, Page 3849*, vol. 13, no. 19, p. 3849, Sep. 2021, doi: 10.3390/RS13193849.

[49]   M. Rajabi, A. Amiri-Simkooei, H. Nahavandchi, and V. Nafisi, "Modeling and Prediction of Regular Ionospheric Variations and Deterministic Anomalies," *Remote Sensing 2020, Vol. 12, Page 936*, vol. 12, no. 6, p. 936, Mar. 2020, doi: 10.3390/RS12060936.

[50]   J. Tang, Y. Li, M. Ding, H. Liu, D. Yang, and X. Wu, "An Ionospheric TEC Forecasting Model Based on a CNN-LSTM-Attention Mechanism Neural Network," *Remote Sensing 2022, Vol. 14, Page 2433*, vol. 14, no. 10, p. 2433, May 2022, doi: 10.3390/RS14102433.

[51]   "ESA - Solar cycle 25 prediction, NOAA." https://www.esa.int/ESA_Multimedia/Images/2020/10/Solar_cycle_25_prediction_NOAA (accessed Oct. 05, 2022).

[52]   "File:SolarCycle25 Prediction Bhowmik Nandy 2018.jpg - Wikimedia Commons." https://commons.wikimedia.org/wiki/File:SolarCycle25_Prediction_Bhowmik_Nandy_2018.jpg (accessed Feb. 20, 2023).

[53]   S. González-Aurioles Fernández, J. Francisco, and V. Valdés, "Análisis de Sistemas MIMO para comunicaciones inalámbricas de 4 Generación," 2014.

[54] "What is MIMO? - Grandmetric."
https://www.grandmetric.com/2018/02/07/what-is-mimo/ (accessed Nov. 28, 2022).

[55] U. Umaisaroh, G. Hendrantoro, A. Mauludiyanto, and T. Fukusako, "Capacity of 2 2 MIMO HF NVIS Channels with Linearly Polarized Horizontal Antennas," *IEEE Wireless Communications Letters*, vol. 8, no. 4, pp. 1120–1123, Aug. 2019, doi: 10.1109/LWC.2019.2908648.

[56] S. L. Manalu, G. Hendrantoro, and A. Mauludiyanto, "Design of measurement system for HF MIMO NVIS channel," *Proceedings - 2017 4th International Conference on Information Technology, Computer, and Electrical Engineering, ICITACEE 2017*, vol. 2018-January, pp. 300–305, Jul. 2017, doi: 10.1109/ICITACEE.2017.8257722.

[57] X. Yu, A. A. Lu, X. Gao, G. Y. Li, G. Ding, and C. X. Wang, "HF Skywave Massive MIMO Communication," *IEEE Trans Wirel Commun*, vol. 21, no. 4, pp. 2769–2785, Apr. 2022, doi: 10.1109/TWC.2021.3115820.

[58] X. Yu, A. A. Lu, X. Gao, G. Y. Li, G. Ding, and C. X. Wang, "Massive MIMO Communication over HF Skywave Channels," *2021 IEEE Global Communications Conference, GLOBECOM 2021 - Proceedings*, 2021, doi: 10.1109/GLOBECOM46510.2021.9686031.

[59] S. Zazo, I. Raos, I. Perez-Alvarez, H. Santana-Sosa, E. Mendieta-Otero, and J. Lopez-Perez, "MIMO transmission in the frequency domain over the HF channel," pp. 202–206, Oct. 2006, doi: 10.1049/CP:20060267.

[60] X. Wang *et al.*, "A New Modulation Technique to Improve Received Power Under Turbulence Effects For Free Space Optical Communication," *IOP Conf Ser Mater Sci Eng*, vol. 767, no. 1, p. 012035, Feb. 2020, doi: 10.1088/1757-899X/767/1/012035.

[61] J. K. Arthur, T. B. T. C. Aka, and A. Acakpovi, "Comparative Analysis of Orthogonal Frequency Division Modulation and Filter Bank-Based Multicarrier Modulation," *2019 International Conference on Communications, Signal Processing and Networks, ICCSPN 2019*, May 2019, doi: 10.1109/ICCSPN46366.2019.9150197.

[62] A. Vora and K. D. Kang, "Index Modulation with PAPR and Beamforming for 5G MIMO-OFDM," *IEEE 5G World Forum, 5GWF 2018 - Conference Proceedings*, pp. 389–394, Oct. 2018, doi: 10.1109/5GWF.2018.8516925.

[63] P. Bechet, S. Miclaus, A. Miclaus, and C. Balint, "Experimental analysis of noise level and channels availability for high frequency OFDM data transmission in NVIS propagation conditions," *IEEE International Symposium on Electromagnetic Compatibility*, vol. 2016-November, pp. 844–849, Nov. 2016, doi: 10.1109/EMCEUROPE.2016.7739206.

[64] M. Aivazyan, H. Avetisyan, L. Grigoryan, and A. Babayan, "Waveform modulation for the 5G mobile telecommunication systems," *Proceedings of 2016 IEEE East-West Design and Test Symposium, EWDTS 2016*, 2016, doi: 10.1109/EWDTS.2016.7807714.

[65] M. J. Fernandez-Getino Garcia, S. Zazo, and J. M. Paez-Borrallo, "Pilot patterns for channel estimation in OFDM," *Electron Lett*, vol. 36, no. 12, pp. 1049–1050, 2000, doi: 10.1049/EL:20000714.

[66] A. M. K. Bebyrahma, T. Suryani, and Suwadi, "Analysis of Combined PAPR Reduction Technique with Predistorter for OFDM System in 5G," pp. 478–483, Aug. 2022, doi: 10.1109/ISITIA56226.2022.9855274.

[67] A. L. Ortega-Ortega and J. F. Bravo-Torres, "Combining LDPC codes, M-QAM modulations, and IFDMA multiple-access to achieve 5G requirements," *2017 International Conference on Electronics, Communications and Computers (CONIELECOMP)*, pp. 1–5, 2017, doi: 10.1109/CONIELECOMP.2017.7891828.

[68] J. M. Sanchez, "Mobile revolution: From 2G to 5G," *2021 IEEE Colombian Conference on Communications and Computing, COLCOM 2021*, May 2021, doi: 10.1109/COLCOM52710.2021.9486300.

[69] S. Thangamayan, M. D. Walunjkar, D. Kumar Ray, M. Venkatesan, A. Banik, and K. P. Amrutkar, "5G Modulation Technique Comparisons Using Simulation Approach," pp. 848–856, Aug. 2022, doi: 10.1109/ICIEM54221.2022.9853137.

[70] V. Chauhan and Srinivasans, "A Review on 5G Network System with its limitation and different Approaches to build strong 5G Network System," pp. 403–410, Aug. 2022, doi: 10.1109/ICIEM54221.2022.9853134.

[71] A. M. Jaradat, J. M. Hamamreh, and H. Arslan, "Modulation Options for OFDM-Based Waveforms: Classification, Comparison, and Future Directions," *IEEE Access*, vol. 7, pp. 17263–17278, 2019, doi: 10.1109/ACCESS.2019.2895958.

[72] Y. Golovachev, A. Mazor, G. A. Pinhasi, and Y. Pinhasi, "Effectiveness of Various 5G Modulation Techniques in Different Weather Conditions," *2019 IEEE International Conference on Microwaves, Antennas, Communications and Electronic Systems, COMCAS 2019*, Nov. 2019, doi: 10.1109/COMCAS44984.2019.8958042.

[73] S. Balaji and K. Chanthirasekaran, "Per user based Threshold Scheduling to improve Bit Error Rate performance for Multi User MIMO Networks compared to Fair Threshold Scheduling," pp. 528–532, Aug. 2022, doi: 10.1109/ICIEM54221.2022.9853013.

[74] Y. Zhang, D. Guo, H. Chang, F. Wang, and Z. Li, "New Efficient Four-Dimensional Trellis Coded Modulation Format," *2021 19th International Conference on Optical Communications and Networks, ICOCN 2021*, 2021, doi: 10.1109/ICOCN53177.2021.9563823.

[75]   R. Gupta and I. Krikidis, "A new receiver design: Simultaneous wireless power transfer with modulation classification," *2020 IEEE Wireless Power Transfer Conference, WPTC 2020*, pp. 331–333, Nov. 2020, doi: 10.1109/WPTC48563.2020.9295579.

[76]   M. T. Mahmud and H. G. Ryu, "Performance Evaluation of OFDM Hybrid Number and Index Modulation for 6G Mobile System," *International Conference on ICT Convergence*, vol. 2021-October, pp. 39–42, 2021, doi: 10.1109/ICTC52510.2021.9621057.

[77]   E. Başar, "5G Telsiz Ağlari için Uzaysal Modülasyon Teknikleri," *2016 24th Signal Processing and Communication Application Conference, SIU 2016 - Proceedings*, pp. 777–780, Jun. 2016, doi: 10.1109/SIU.2016.7495855.

[78]   Y. Ma, Z. Jin, and L. Luo, "Analysis and Design of an Electrically Small Broadband Whip Antenna," *13th International Symposium on Antennas, Propagation and EM Theory, ISAPE 2021 - Proceedings*, 2021, doi: 10.1109/ISAPE54070.2021.9753633.

[79]   K. Ren, M. Ranjbar Nikkhah, and N. Behdad, "Design of Dual-Polarized, Platform-Based HF Antennas Using the Characteristic Mode Theory," *IEEE Trans Antennas Propag*, vol. 68, no. 7, pp. 5130–5141, Jul. 2020, doi: 10.1109/TAP.2020.2975547.

[80]   P. Yang, R. Dang, and L. Li, "Dual-Linear-to-Circular Polarization Converter Based Polarization-Twisting Metasurface Antenna for Generating Dual Band Dual Circularly Polarized Radiation in Ku-band," *IEEE Trans Antennas Propag*, 2022, doi: 10.1109/TAP.2022.3178803.

[81]   B. A. Austin, "An optimised vehicular loop antenna for NVIS applications," pp. 43–47, Nov. 2005, doi: 10.1049/CP:20000146.

[82]   B. A. Austin and W. C. Liu, "Assessment of vehicle-mounted antennas for NVIS applications," *IEE Proceedings: Microwaves, Antennas and Propagation*, vol. 149, no. 3, pp. 147–152, Jun. 2002, doi: 10.1049/IP-MAP:20020393.

[83]   J. E. Richie and T. Joda, "HF antennas for NVIS applications mounted to helicopters with tandem main rotor blades," *IEEE Trans Electromagn Compat*, vol. 45, no. 2, pp. 444–448, May 2003, doi: 10.1109/TEMC.2003.811317.

[84]   S. N. Jha, R. Lamey, and J. Y. Bernier, "Small Footprint Triangular Shaped HF band NVIS Antenna based on Noise related Parametric Studies," *2021 IEEE International Symposium on Antennas and Propagation and North American Radio Science Meeting, APS/URSI 2021 - Proceedings*, pp. 1958–1959, 2021, doi: 10.1109/APS/URSI47566.2021.9704321.

[85]   "The Dipole Antenna - What is a dipole Antenna?" https://www.hamuniverse.com/dipoleantenna.html (accessed Oct. 10, 2022).

[86]   J. M. Maso, T. Gonzalez, J. Male, J. Porte, J. L. Pijoan, and D. Badia, "NVIS multicarrier modulations for remote-sensor applications," *Sensors (Switzerland)*, vol. 20, no. 21, pp. 1–19, Sep. 2020, doi: 10.3390/s20216232.

[87]   "HFRA 5154- 0.1 - 30 MHZ TRANSMITTING LOOP ANTENNA." https://absolute-emc.com/product/hfra-5154-01-30-mhz-transmitting-loop-antenna

[88]   L. M. Thring, D. Boddice, N. Metje, G. Curioni, D. N. Chapman, and L. Pring, "Factors affecting soil permittivity and proposals to obtain gravimetric water content from time domain reflectometry measurements," *Canadian Geotechnical Journal*, vol. 51, no. 11, pp. 1303–1317, Nov. 2014, doi: 10.1139/CGJ-2013-0313/ASSET/IMAGES/CGJ-2013-0313TAB8.GIF.

[89]   J. B. Rhebergen, H. A. Lensen, P. B. W. Schwering, G. R. Marin, and J. M. H. Hendrickx, "Soil moisture distribution around land mines and the effect on relative permittivity," *https://doi.org/10.1117/12.479098*, vol. 4742, pp. 269–280, Aug. 2002, doi: 10.1117/12.479098.

[90]   R. Porretta and F. Bianchi, "Profiles of relative permittivity and electrical conductivity from unsaturated soil water content models," *Annals of Geophysics*, vol. 59, no. 3, p. G0320, Jul. 2016, doi: 10.4401/ag-6990.

[91]   "STEMlab 125-14 - Red Pitaya." https://redpitaya.com/stemlab-125-14/ (accessed May 04, 2022).

[92]   "Buy a Raspberry Pi 3 Model B+ – Raspberry Pi." https://www.raspberrypi.com/products/raspberry-pi-3-model-b-plus/ (accessed May 04, 2022).

[93]   "Teensy USB Development Board." https://www.pjrc.com/teensy/ (accessed May 04, 2022).

[94]   "TANGO 20 Antennas - Siretta - Enabling Industrial IoT." https://www.siretta.com/products/antennas/tango-20/ (accessed May 04, 2022).

[95]   "Moteino M0." https://lowpowerlab.com/shop/product/184 (accessed May 04, 2022).

[96]   "RFM95 LoRa transceiver." https://lowpowerlab.com/shop/product/143 (accessed May 04, 2022).

[97]   K. Cengiz, "216196-0001 | Antena de telemetría 868MHZ - 915MHZ, Macho SMA | RS Components." https://es.rs-online.com/web/p/antenas-de-telemetria/2150980 (accessed May 04, 2022).

[98]   "GY-BME280 bei az-delivery.de – AZ-Delivery." https://www.az-delivery.de/es/products/gy-bme280 (accessed May 04, 2022).

[99]   "Nooelec - Flamingo AM - Broadcast AM Bandstop Filter for Software Defined Radio (SDR) Applications." https://www.nooelec.com/store/flamingo-am.html (accessed Oct. 06, 2022).

[100]   M. I. Ryabova, D. V. Ivanov, and A. A. Kislitsin, "Developing methods and algorithms for studying polarization coherent bandwidth for the NVIS propagation," *2019 Systems of Signal Synchronization, Generating and Processing in Telecommunications, SYNCHROINFO 2019*, Jul. 2019, doi: 10.1109/SYNCHROINFO.2019.8813968.

[101]   Z. Zhang, M. Li, and X. Sun, "The influence of temporal factors to frequency of NVIS communication," *Proceedings of 2017 IEEE 7th International Conference on Electronics Information and Emergency Communication, ICEIEC 2017*, pp. 70–73, Oct. 2017, doi: 10.1109/ICEIEC.2017.8076514.

[102]   N. V. Ryabova, D. V. Ivanov, V. A. Ivanov, and A. A. Elsukov, "Processing Multicarrier Phase Coded Signals with OFDM on the USRP Platform for NVIS Sounding of HF Radio Channels," *2020 Systems of Signal Synchronization, Generating and Processing in Telecommunications, SYNCHROINFO 2020*, Jul. 2020, doi: 10.1109/SYNCHROINFO49631.2020.9166059.

[103]   P. Bergadà, R. M. Alsina-Pagès, and M. Hervás, "Polarization diversity in a long-haul transequatorial HF link from Antarctica to Spain," *Radio Sci*, vol. 52, no. 1, pp. 105–117, Jan. 2017, doi: 10.1002/2016RS006136.

[104]   J. Porte, J. M. Maso, J. L. Pijoan, and D. Badia, "Sensing System for Remote Areas in Antarctica," *Radio Sci*, vol. 55, no. 3, p. e2019RS006920, Mar. 2020, doi: 10.1029/2019RS006920.

[105]   W. C. Jakes and D. C. Cox, *Microwave Mobile Communications.* Wiley-IEEE Press, 1994.

[106]   M. J. Angling, P. S. Cannon, N. C. Davies, T. J. Willink, V. Jodalen, and B. Lundborg, "Measurements of Doppler and multipath spread on oblique high-latitude HF paths and their use in characterizing data modem performance," *Radio Sci*, vol. 33, no. 1, pp. 97–107, 1998, doi: 10.1029/97RS02206.

[107]   A. Gamal, A. Enginyeria, I. Arquitectura, and L. Salle, "Soundings of the ionospheric HF radio link between Antarctica and Spain," *TDX (Tesis Doctorals en Xarxa)*, Nov. 2013.

[108]   E. M. Warrington and A. J. Stocker, "Measurements of the Doppler and multipath spread of HF signals received over a path oriented along the midlatitude trough," *Radio Sci*, vol. 38, no. 5, p. 1080, Oct. 2003, doi: 10.1029/2002RS002815.

[109] J. M. Maso, J. Porte, J. L. Pijoan, and D. Badia, "Study of NVIS channel for USN protocol definition in antarctica," *Electronics (Switzerland)*, vol. 9, no. 6, 2020, doi: 10.3390/electronics9061037.

[110] J. Porte, J. M. Maso, J. L. Pijoan, and D. Badia, "Sensing System for Remote Areas in Antarctica," *Radio Sci*, vol. 55, no. 3, p. e2019RS006920, Mar. 2020, doi: 10.1029/2019RS006920.

[111] J. Porte, J. Maso, J. L. Pijoan, and D. Badia, "Design, implementation, and test of an SDR for NVIS communications," *International Journal of Circuit Theory and Applications*, vol. 47, no. 9, pp. 1502–1512, Sep. 2019, doi: 10.1002/CTA.2670.

[112] J. Porte, J. Maso, J. L. Pijoan, M. Miret, D. Badia, and J. Jayasinghe, "Education and e-health for developing countries using NVIS communications," *IEEE Region 10 Humanitarian Technology Conference, R10-HTC*, vol. 2018-December, Jan. 2019, doi: 10.1109/R10-HTC.2018.8629842.

[113] J. Male, J. Porte, T. Gonzalez, J. M. Maso, J. L. Pijoan, and D. Badia, "Analysis of the Ordinary and Extraordinary Ionospheric Modes for NVIS Digital Communications Channels," *Sensors 2021, Vol. 21, Page 2210*, vol. 21, no. 6, p. 2210, Mar. 2021, doi: 10.3390/S21062210.

[114] T. Gonzalez *et al.*, "SC-FDE Layer for Sensor Networks in Remote Areas Using NVIS Communications," *Electronics 2021, Vol. 10, Page 1636*, vol. 10, no. 14, p. 1636, Jul. 2021, doi: 10.3390/ELECTRONICS10141636.

[115] W. J. Kim, K. J. Cho, S. P. Stapleton, and J. H. Kim, "An efficient crest factor reduction technique for wideband applications," *Analog Integr Circuits Signal Process*, vol. 51, no. 1, pp. 19–26, Apr. 2007, doi: 10.1007/s10470-007-9038-8.

[116] M. Ojima and T. Hattori, "PAPR reduction method using clipping and peak-windowing in CI/OFDM system," in *IEEE Vehicular Technology Conference*, 2007, pp. 1356–1360. doi: 10.1109/VETECF.2007.290.

[117] "Crest Factor Reduction - RFmx SpecAn 19.1 Help - National Instruments." https://zone.ni.com/reference/en-XX/help/374264N-01/rfmxspecan/crest_factor_reduction/ (accessed Apr. 19, 2021).

[118] Polarjournal, "Chile plans fiber optic cable to Antarctica." https://polarjournal.ch/en/2021/11/30/chile-plans-fiber-optic-cable-to-antarctica/ (accessed Apr. 06, 2022).

[119] Polarjournal, "Submarine fiber optic cable to Antarctica planned." https://polarjournal.ch/en/2021/07/09/fiber-optic-submarine-cable-to-antarctica-planned/ (accessed Apr. 06, 2022).

[120] "Observatori de l'Ebre." https://www.obsebre.es/ca/ (accessed Oct. 06, 2022).

[121] G. Bitella *et al.*, "Geophysical techniques for plant, soil, and root research related to sustainability," *The Sustainability of Agro-Food and Natural Resource Systems in the Mediterranean Basin*, pp. 352–372, Jan. 2015, doi: 10.1007/978-3-319-16357-4_23/FIGURES/9.

[122] M. Grabiec, "GLACIAL ICE AND PERMAFROST DISTRIBUTION IN THE MEDENA KOTLINA (SLOVAK TATRAS) : MAPPED WITH APPLICATION OF GPR AND GST MEASUREMENTS," 2009.

[123] G. S. Baker, T. E. Jordan, and J. Pardy, "An introduction to ground penetrating radar (GPR)," *Special Paper of the Geological Society of America*, vol. 432, pp. 1–18, 2007, doi: 10.1130/2007.2432(01).

[124] B. A. Witvliet *et al.*, "Near Vertical Incidence Skywave Propagation: Elevation Angles and Optimum Antenna Height for Horizontal Dipole Antennas," *IEEE Antennas Propag Mag*, vol. 57, no. 1, pp. 129–146, Jul. 2015, doi: 10.1109/MAP.2015.2397071.

[125] "Barker & Williamson HF Antennas and Masts - Home Page." https://www.bwantennas.com/ (accessed Jul. 12, 2022).

[126] G. Zhang, G. Wei, Y. Zhou, and X. Feng, "Design of a Novel Embedded Shipborne HF Antenna," *2022 IEEE 5th International Conference on Electronics Technology (ICET)*, pp. 819–822, May 2022, doi: 10.1109/ICET55676.2022.9825318.

[127] M. Ignatenko and D. S. Filipovic, "On the Design of Vehicular Electrically Small Antennas for NVIS Communications," *IEEE Trans Antennas Propag*, vol. 64, no. 6, pp. 2136–2145, Jun. 2016, doi: 10.1109/TAP.2016.2547018.

[128] M. Ignatenko and D. S. Filipovic, "Electrically small half-loop for wideband HF on-the-move operation," *2016 IEEE/ACES International Conference on Wireless Information Technology, ICWITS 2016 and System and Applied Computational Electromagnetics, ACES 2016 - Proceedings*, May 2016, doi: 10.1109/ROPACES.2016.7465357.

[129] S. Bounsiar *et al.*, "How to Enable Delay Tolerant Network Solutions for Internet of Things: From Taxonomy to Open Challenges," *Proceedings 2019, Vol. 31, Page 24*, vol. 31, no. 1, p. 24, Nov. 2019, doi: 10.3390/PROCEEDINGS2019031024.

[130] J. J. P. C. (Ed.)) Rodrigues, *Advances in Delay-Tolerant Networks (DTNs): Architecture and Enhanced Performance*, 2nd ed. UK: Woodhead Publishing: Sawston, 2020. doi: 10.1016/B978-0-08-102793-6.00008-4.

[131] IAU, "Instituto Antartico Uruguayo." http://www.iau.gub.uy/?doing_wp_cron=1649321329.1357541084289550781250&lang=en (accessed Apr. 07, 2022).

[132] A. Mallorquí, A. Zaballos, A. Briones, A. J. Dietz, S. Roessler, and C. Amélie Baumhoer, "DTN Trustworthiness for Permafrost Telemetry IoT Network,"

Annex 1

NVIS Multicarrier Modulations for Remote-Sensor Applications

NVIS Multicarrier Modulations for Remote-Sensor Applications

Josep M. Maso (ID)**, Tomas Gonzalez** (ID)**, Jordi Male, Joaquim Porte** (ID)**, Joan L. Pijoan * and David Badia**

La Salle Campus, Ramon Llull University, 08022 Barcelona, Spain; josep.maso@salle.url.edu (J.M.M.);
tomas.gonzalez@salle.url.edu (T.G.); jordi.male@salle.url.edu (J.M.); joaquim.porte@salle.url.edu (J.P.);
david.badia@salle.url.edu (D.B.)
* Correspondence: joanlluis.pijoan@salle.url.edu

Abstract: The number of Internet of Things (IoT) devices has experienced a large growth during the last decade, as well as the data volume gathered from remote sensors. Satellites are still a suitable communication method and may be preferable for a remote ubiquitous sensor network (USN), which sometimes are located in places without much communications infrastructure where coverage is the principal drawback. Alternatively, the proposed solution for this article aims at a near-vertical incidence skywave (NVIS) channel for high frequencies (HF) with a low-cost platform, allowing a low-power transmissions coverage area up to 250 km for USN. The HF standards are focused on generic communication channels not being robust for NVIS communications. In this article we study and test an alternative based on orthogonal frequency-division multiplexing (OFDM) modulations to make them more robust and less dependent on the channel NVIS communications. For that purpose, we test the HF standard modulations and a designed OFDM modulation to prove the robustness of each. This study has been tested between Barcelona and Tarragona, using different transmission power levels and modulation orders.

Keywords: Remote Sensing; HF; NVIS; USN; OFDM; IoT; STANAG; MIL-STD 188 110 D

1. Introduction

It is not news that the number of sensors and mobile devices is increasing enormously every day in the current world. The infrastructure of the communications for these devices is very extended in areas with a high population. However, some areas in the world do not have such infrastructure due to complex orography, which makes communications between the transmitter and receptor almost impossible. Normally, the most extended way to communicate in these places is the use of satellite services, which do not need any terrestrial network infrastructure. Nowadays, the environmental impact of satellite deployments [1] and their high cost has made researchers discover new methods of communications especially with the aim of collecting data through remote sensors for several scientific studies.

Remote sensing became an extended study focus making use of new technologies such as light detection and ranging (LIDAR), artificial intelligence (AI) [2], machine learning [3], geocoding algorithms [4], deep convolutional neural networks [5] or multi-sensor fusion positioning [6], being part of some examples of the wide range of technologies that sensing uses.

As an alternative to satellite communications, the use of ionospheric reflection has been under study for several years even in scenarios such as Antarctica where there is almost no kind of infrastructure, and the deployment of network communications are practically unfeasible due to its complicated terrain [7]. Near-vertical incidence skywave (NVIS) offers an alternative solution in order to collect

data from remote sensors. NVIS consists in transmitting a signal which near vertically rebounds in the ionosphere for frequencies under 10 MHz (high frequency) giving 250 km area coverage with low-cost equipment and an easy deployment system [8] in comparison to satellite communications.

To maintain a standard for NVIS communications, high-frequency (HF) frame protocols MIL-STD 188 110C Appendix D [9] and STANAG [10] are used. These frame protocols are well designed but the results for shorter distances are not borne in mind setting aside significant effects that degrade the signal as multipath which are critical in the mornings and evenings because of the use of narrowband modulations. In scenarios with big multipath, the equalization becomes a very complex work. To avoid this effect, orthogonal frequency-division multiplexing (OFDM) modulation can bring a solution due to its characteristics of being very robust against the multipath and the equalization being very simple to implement in real time.

In this paper we present an alternative to the standards by the use of a wideband OFDM modulation for NVIS based on a low-cost and low-power platform for remote sensors, which can be a solution to multipath. This solution aims to improve NVIS communications and make a more robust system. To achieve this solution, this study has two principal goals: the proposal of a new ionospheric transmission configuration and to have the ideal trade-off between narrow-band modulations and OFDM in terms of power consumption for low-power systems. If we take into account the possible applications, the starting point is the battery consumption for remote sensors. For that reason, the input back off (IBO) plays an essential role in the OFDM modulation. This parameter lets us increase the average power cutting the peaks that the OFDM produces due to the subcarriers division and is more adequate for the ubiquity for portable sensors.

Moreover, to improve NVIS, the use of two different waves, known as the ordinary and extraordinary waves, can benefit the communication. These waves are caused birefringence nature of the ionospheric plasma in the presence of the geomagnetic field [11]. Also, these two characteristic waves affect the radio wave differently, creating two decorrelated channels. This decorrelation opens new horizons in our link, as polarization diversity appears as an improvement for the NVIS link when used combined with multiple antennas in reception. Therefore, this paper presents the application of polarization diversity in an NVIS single input multiple output (SIMO) scenario.

This article is organized as follows. In Section 2, we explain the developed low-cost system, including hardware, software, the OFDM design and the diversity technique to overcome results. In Section 3, we explain the test's design and the frame protocols performed. In Section 4, the comparison between modulations based on the results are shown. Finally, Section 5 gives the conclusions.

2. System Description

This section introduces the basis of the NVIS characteristics and the leading technologies present in the developed platform used to achieve the study, as different techniques are used in the optimization of the platform. Additionally, an overall vision of the components and software are explained.

2.1. Near-Vertical Incidence Skywave (NVIS)

NVIS propagation consists of the transmission of HF electromagnetic waves between 3 to 10 MHz with an angle above 70° to the ionosphere which can make this signal rebound and reach distances up to 250 km [8]. The rebounds of the waves are possible due to the solar radiation and the terrestrial magnetic field. The reflection depends on the ionization of the ionospheric layers and is strongly dependent on the frequency and solar activity. The achieved bit rates are not high, but enough for Internet of Things (IoT) devices, so NVIS can be a good alternative for a ubiquitous sensor network (USN), having a low cost due to the use of software defined radio (SDR) [5].

The main challenge of this kind of communications is the availability of the rebounds. This fact relies on the ionosphere layers, which are D, E and F. D appears during the day but prevents the rebounds under 10 MHz and attenuates the signal. The E layer is the first which allows the HF signals to rebound followed by the F layer, which is divided into F1 and F2. Both are present during the day,

101

but during the night the F1 disappears. The F2 due to its stability is the layer with which the test transmissions have been performed.

Lastly, the ionosphere with NVIS has some difficulties in the design because of the channel effects produced by the ionosphere rebounds as studied by Vilella [11], Jodalen [12], Hervas [13], and Cannon [14] but the proposed NVIS protocol overcomes that.

Also, this protocol has a SIMO technique which overcomes results that sustain the study of different polarization ways in order to receive the NVIS signal studied by Erhel [15]. In our case, the polarization diversity is used to make the modulation performance better.

A preliminary experimental approach of the noise level in channels between 3 and 24 KHz was studied by Bechet, Bechet and Miclaus [16], but the proposed solution takes the channel and noise estimation by the PN sequence which does a channel profile. Also, the equalization with this sequence became more efficient.

2.2. Overview of the System

The current platform allows a continuous transmission with a radius of 250 km because of the NVIS channel. Talking about costs and pollution, the developed NVIS platform is affordable compared to any satellite.

The system description is explained below, taking into account all different parts, and finally, a graphical scheme is shown in Figure 1. Mainly, the Red Pitaya is the core of the system, and is in charge of all high-speed RF signal-processing. In the other hand, the Raspberry Pi 3 is in charge of all base-band signal-processing.
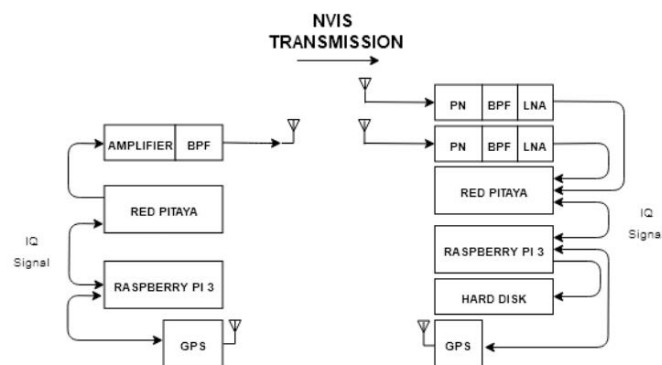
Figure 1. Near-vertical incidence skywave (NVIS) transmission scheme (transmitter in the left and receiver in the right).

- Software-Defined Radio (SDR)/Red Pitaya

SDR is key to the development of the platform [17] due to its scalability and is done through two Red Pitaya STEMLab 125-14 that contains field-programmable gate array (FPGA) Xilinx Zynq 7010 System on Chip (SoC). The low-cost Red Pitaya platform have two analogic digital converters (ADC) and two digital analogic converters (DAC) of 14 bit resolution allowing the transmission and reception of both ordinary and extraordinary waves. The SDR methodology, some settings such as the carrier frequency, bandwidth and modulation can be changed in a very dynamic way.

- Raspberry Pi 3

The time synchronization between transmitter and receiver is performed with GPS controlled as a peripheral from Raspberries Pi 3 [18]. In the transmitter side, the Raspberry has all the transmission

102

test signal files to be transmitted. All transmission signal files are sent to the Red Pitaya via Ethernet and transmitted when needed. For the reception, the process just explained works backwards. The Red Pitaya send the data received to the Raspberry, core that will gather all the information obtained in order to process it with data-processing software [19].

- Amplifier and Low Noise Amplifier (LNA)

For our lab tests, an amplifier of 48.5 dB is used in order to reach 50 dBm signal transmissions. Bonn BLWA 0103-250 class A is the chosen model, which can works correctly between 1.5 and 30 MHz [20]. In contrast, at the receiver side, the signal has to be preamplified to 30 dB by an LNA for a proper demodulation. In the final system, the amplifiers used are different, being more affordable.

- Filter

A band pass filter (BPF) is needed to limit the frequencies used for NVIS channel (3–10 MHz). Due to strong interferences in that band, we have used a 2 MHz BPF centered on 5.4 MHz to avoid the saturation of the ADC at the reception.

- Antenna

Our system needs to be easily deployed, and the election of the antennas is intended for this purpose as far as possible. The chosen antennas are an inverted V which have a gain of 6.8 dBi [21], with a simple installation using one single mast. A total of three identical antennas are needed in our scenario, all tuned to frequency of 5 MHz calculated from the revised ionograms of Observatori del Ebre [22].

One of the three antennas is placed in the transmitter, while the other two are set perpendicularly at the receiver with the purpose of receiving both right-handed circular polarization and left-handed circular polarization waves simultaneously. To receive both waves, the antenna configuration on the receiving requires a phasing network as we can see in Figure 2.
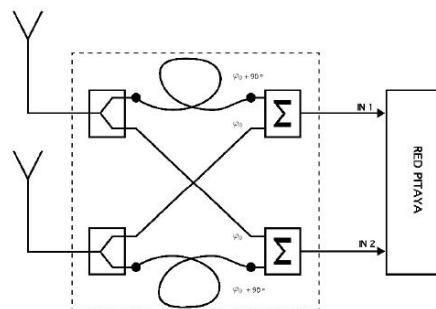
Figure 2. Phasing box of the receiver system.

The aforementioned phasing box was developed in order to perform the delays explained using coaxial cables. Each of the antenna inputs is divided into two identical signals with a radio frequency splitter, generating 4 signals (2 for each antenna). The paths followed by each antenna are identical. One of the cables is lengthened with a quarter wave phasing line, providing a 90° phase shift, while the other signal is connected directly to an RF combiner. This process is repeated identically for both antenna wires, resulting in an output of two dipole antennas with a phase difference of either +90° or −90° between each other. Equation (1) shows the unification of the two antennas which includes the non-phased wave in (2) and the 90° phased wave in (3). It is important to mention that this system

has been designed for a unique frequency. For wideband studies, the phasing network should be frequency adaptive and implemented in the FPGA.

$$\bar{E}(z,t) \; = \; \bar{E}x(z,t) \; + \; \bar{E}y(z,t) \tag{1}$$

$$\bar{E}x(z,t) \; = \; \bar{E}o \cdot \cos(wt \, - \, kz) \cdot x \tag{2}$$

$$\bar{E}y(z,t) \; = \; \bar{E}o \cdot \cos(wt \, - \, kz) + \frac{\pi}{2} \cdot y \tag{3}$$

2.3. Orthogonal Frequency-Division Multiplexing (OFDM)

The narrow-band modulations (PSK, FSK and QAM) studied in previous works are good enough for remote-sensing applications, but in low-multipath scenarios. Our OFDM proposal is suited to manage strong multipath with easy equalization methods. The study of this modulation lies in its capacity to avoid the multipath effect and the easy way to equalize it. It is known that in ionospheric communications the evening transmissions are plenty of multipath compared to the morning, being the OFDM an excellent option to avoid those effects [23].

The spectral efficiency is a good characteristic as well as the computational efficiency due to the FFT and IFFT. The modulation process is done by the IFFT of all the M-QAM or M-PSK symbols, which form the OFDM symbols. Equation (4) describes the IFFT process of the symbols where Nsc is the number of subcarriers and Sk is the modulated symbols in QAM/PSK. This process ensures data transmission in multiple parallel subtransmissions at lower speed, but in a robust way, which helps the stability of any communication system.

$$x[n] = \frac{1}{\sqrt{Nsc}} \sum_{k=0}^{k=Nsc-1} Sk \cdot e^{\frac{j2\pi n k}{Nsc}}, \, 0 \, \leq \, n \, \leq \, Nsc \tag{4}$$

As a drawback, the OFDM peak consumption is higher than any other narrow-band modulations because of the subcarrier division creates peaks having as a result a high peak to average power ratio (PAPR) which is the difference between the peak power and the average power.

The configuration of the OFDM to be transmitted in our tests is based to be the most similar as the HF standards to maintain the most similar comparison. The design of the OFDM configuration requires a previous study of the channel to define every parameter. This channel analysis and definition of the OFDM configuration for high multipath is defined in a previous article [24]. Taking account the designed OFDM, first of all, bandwidth of the OFDM signal is 3 KHz as the HF standards. The symbol length was calculated first with a value of 9.33 ms as in [24] to set the number of subcarriers. As a result of that, 28 subcarriers will be transmitted being one of them a DC null to avoid offset effects. The configuration designed makes every subcarrier to be about 107 Hz. Every frame packet is composed of 7 OFDM symbols with a duration of 86.31 ms, which are obtained due to the coherence time (10 s) [24]. One of the OFDM symbols is a pilot to estimate the channel to perform the zero-forcing equalization which is calculated as we can see in (6). The zero-forcing consists in applying the inverse of the estimated channel calculated with the pilot symbol. In (5) is shown a simple equation of a transmitted signal in which Y(f) means the signal affected by a channel, the X(f) refers to the raw signal and the H(f) means the channel response. The received pilot is compared to the transmitted one to take a value of how the channel changes and the OFDM symbols are multiplied by the inverse of the received channel response as in (6).

$$Y(f) \; = \; H(f) \cdot X(f) \tag{5}$$

$$C(f) \; = \frac{1}{Hest(f)} \tag{6}$$

The delay spread is a key measure of the multipath received, being the time between the first and the last path received. In [24] this was already calculated for an NVIS channel, and its value is 2.75 ms,

for that reason the cyclic prefix is calculated in relation to this value, adding a small leeway. Finally, 3 ms of copied useful data inserted at the beginning of the OFDM symbol (CP) avoid the interferences between neighbor symbols produced by the multipath of the channel. The application of this technique is the reason of why the OFDM is a good option to avoid the multipath intersymbol interference (ISI).

One of the weak points of the OFDM is the high PAPR, as mentioned, the OFDM modulation produces high peaks which reduce the average power of the modulation. Also, this is reduced by the IBO application to crop the peaks and then rising the average power. In [25] the IBO performance was analyzed, and it was concluded that the lowest values of IBO produce high in-band distortion that degrades the EVM, whereas the high values of IBO reduce the mean transmitted power.

The initial design is done with an IBO of 3 dB because the average power was too small compared to the narrow-band modulations. After doing the first comparison, more IBO values (4.5, 6, 7.5 and 9 dB) are studied to make the OFDM more efficient. The bits in use are calculated by multiplying the bits/symbol, the number of data OFDM symbols and the number of data subcarriers. Finally, the summarized configuration of the OFDM is shown in Table 1.

Table 1. Orthogonal frequency-division multiplexing (OFDM) configuration for NVIS transmission.

Bandwidth	3 KHz
Useful symbol length	$T_S = 9.33$ ms
Prefix cyclic length	$T_{CP} = 3$ ms
Number of subcarriers	$N_{SC} = 28$
Number of pilot OFDM symbols	$N_{SP} = 1$
Number of data OFDM symbols	$N_D = 6$
Number of subcarriers DC NULL	$N_{DC} = 1$
Number of symbols OFDM	$N_{SOFDM} = 7$
Time duration of OFDM packet	$N_{PT} = 86.31$ ms
Bits in packet	Bits = 324 bits
Input Back Off	3 dB
Modulation	QPSK
Equalization	Zero forcing
Bitrate of signal frame	2.139 Kbps

2.4. Polarization Diversity

Diversity techniques are being applied in many communication fields. Spatial diversity, frequency diversity and time diversity are methods applied in many frequency bands and scenarios. Polarization diversity is a diversity mode that may be applied in very specific environments and is based on two different channels with particular properties.

The ionosphere is an ionized layer of the atmosphere due to solar radiation. Its electrons vibrate at the frequency of the incoming waves, acting as small dipoles. These vibrations are usually elliptical in shape and occur in both directions. Because of this, the ionosphere creates two opposite channels due to the movement of the electrons. These channels are completely decorrelated and change the polarization of the wave to a circular one, even if the emitted signal is linearly polarized [26].

When having two isolated channels, multiple input multiple output (MIMO) appears as a method to exploit their multipath propagation. This work focuses on the ionospheric channel and the development of a SIMO system that benefits from the two characteristic waves, the ordinary and the extraordinary waves. Both MIMO and SIMO are valid solutions, with the MIMO being the one that can provide better results as more antennas are involved in the scenario and more techniques can be applied (space-time coding, for example). A SIMO scenario [27] demonstrated that the selection-combining (SC) technique helps to reach better results in terms of E_b/N_0.

Despite these gains, the HF antennas are too big and most of the times it is necessary to install a mast. The use of diversity-polarization makes sense in the receiver side because it can help to minimize the power consumption and the size of the transmitter antenna. This article studies the SC

and equal gain combining (EGC) techniques to outperform results. SC compares the two different signals received (two different channels) in terms of E_b/N_0 and then ignores the worse result. On the other hand, EGC makes the coherent sum of both channels to get an increase of the bit energy [27].

Geoscience and the complete understanding of how the atmosphere's layers work take a leading role in the development and implementation of telecommunication's applications. Remote sensing, for instance, can directly benefit from the ionosphere's studies by the application of techniques based on the ionospheric properties. This paper shows, for example the usage of polarization diversity as an improvement of a remote-sensing network.

3. Tests

In this section, we explain the area where we tested the different transmissions with an NVIS channel and the organization of the tests to be transmitted.

There were two different tests: the first one was dedicated to a simple comparison between the narrow-band and the multicarrier-band modulation to know the viability and efficiency respect narrow-band modulations, and the second one was to optimize the OFDM transmitted making use of the IBO which helps to find a power transmission for a low-consumption system which means smaller batteries.

3.1. Test Area

In La Salle University URL (Barcelona, Spain) there is an inverted V antenna acting as a transmitter NVIS node. The receptor is approximately 97 km away (Cambrils, Tarragona) where La Salle has a specific lab with the same antenna but making use of SIMO technique, so there are two of them and the phasing box. Figure 3 shows the link established within the line of sight between the transmitter and the receiver, as we can see at the profile elevation with an elevation peak of 546 m.
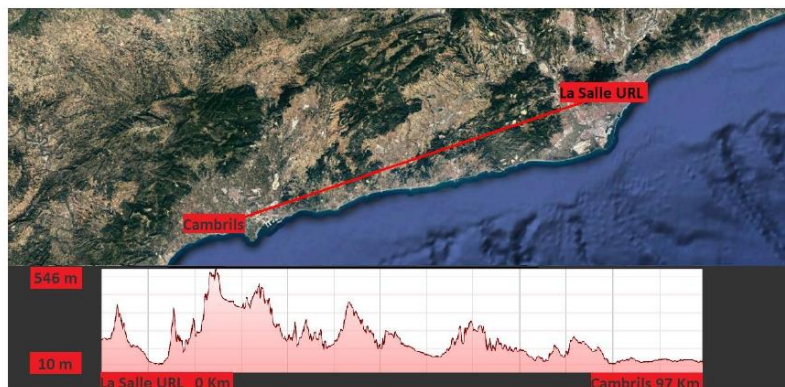
Figure 3. Barcelona-Cambrils link.

3.2. Frame Protocol and Tests Design

The tests follow a 10-minute plan, in which the first 5 min the platform does not transmit, and throughout the next 5 min, we increase the order of modulation for each modulation (from 2 to 32) after each minute. This process is repeated six times during one hour but increasing the transmission power by 3 dBs from 35 dBm to 50 dBm every 10 min. The summary is shown in Table 2.

Table 2. Testbench.

Order of Modulation	Peak Power	Minutes
2, 4, 8, 16, 32	35 dBm	05, 06, 07, 08, 09
2, 4, 8, 16, 32	38 dBm	15, 16, 17, 18, 19
2, 4, 8, 16, 32	41 dBm	25, 26, 27, 28, 29
2, 4, 8, 16, 32	44 dBm	35, 36, 37, 38, 39
2, 4, 8, 16, 32	47 dBm	45, 46, 47, 48, 49
2, 4, 8, 16, 32	50 dBm	55, 56, 57, 58, 59

Each transmission includes a 6th PN sequence with a resampling of 8 and 5 ms length as in [24] that is used to synchronize the demodulation of the frames. The PN sequence has been designed not to be affected by the delay spread and Doppler shift. A single-tone of 600 Hz of 60 ms length is used to correct the Doppler shift caused by the inaccuracy of the clocks of the Red Pitaya which generates a maximum Doppler of 17.5 Hz [24], higher than the ionospheric channel shift which values under 10 Hz. Taking into account a tone of 600 Hz in the worst case will be of 580 Hz due to the Doppler shift. To assure the measure, if we consider a 550 Hz received tone, the measure of it to correct the Doppler shift effect will be of 33 cycles. In the case of using a DC tone, for measuring 1 Hz of Doppler shift, the measure would consider only a 16th part of a cycle (60 ms), which is not enough for an accurate result. The entire tests have a fixed bandwidth of 3 kHz and a frequency of 5.4 MHz.

Each transmission contains 200 packets (50 for each modulation) of 162 symbols with a resample of 34 to achieve 3 KHz of channel bandwidth. In the Figure 4 below, the frame design is outlined. Each test transmission is composed of a frame that includes a PN sequence to synchronize each transmission, and then there are a single-tone and a PN sequence for every modulation packet. To maintain the time standards of each packet with the OFDM modulation, the narrow-band modulations are 87.04 ms in length and the multicarrier modulation is 86.31 ms in length. Once the packet is transmitted this process is repeated for the rest of the packets.
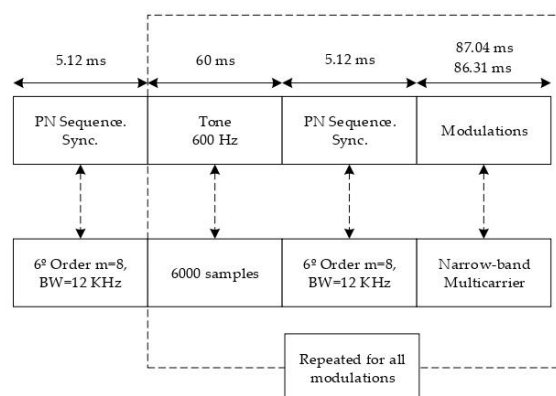
Figure 4. Frame design for each modulation.

A good point of study is the optimization of the average power of the OFDM due to the high peaks produced by the multiple subcarriers. This optimization allows the platform to have greater autonomy or smaller batteries to be integrated in low-power applications. Numerous techniques overcome the results of the OFDM bit error rate (BER) due to the increase of the average power. However, we opted for the IBO study.

The initial tests start with IBO = 3 dBs just to reduce the principal peaks and compared directly with narrow-band modulations. After that, there is a specific IBO sweep to obtain the optimal one (same structure as before), which also helps the reduction of power consumption indirectly. Is true that high values of IBO increase the average power (energy) and overcome the bit error, but thanks to that, the peak power could be decreased.

4. Results

The most relevant results obtained from the test performed will be shown in this section. We will analyze the BER obtained depending on the E_b/N_0, the cumulative distribution function (CDF) of BER for a specific E_b/N_0, the PAPR, average power and peak power obtained depending on the IBO, the CDF BER depending on the IBO and the improvement of the communication by using polarization techniques at the receiver system. These tests took around two weeks transmitting and receiving a total amount of 28 MB of data.

4.1. BER vs. E_bN_0

At first, we will analyze the BER obtained depending on the E_b/N_0 for each transmitted modulation and modulation order symbolized with M. These results show us the robustness of each modulation in front of the NVIS channel. The results are better when the line takes lower values.

4.1.1. BER vs. E_b/N_0 M = 4

In Figure 5, we can see the results obtained for the 4FSK, 4QAM and the OFDM designed with a 4QAM modulation. As we can see in the graphic, the OFDM is the most robust modulation to be transmitted. In the best case, for an E_b/N_0 of 18 dB we can obtain a BER of 6×10^{-5} by using an OFDM modulation, a BER of 10^{-3} by using a 4QAM and a BER of 6×10^{-3} by using a 4FSK. For a lower E_b/N_0 as 10 dB, we can see that the results are more similar with a BER of 4×10^{-3} for the OFDM, a BER of 8×10^{-3} for the 4QAM and a BER of 3×10^{-2} for the 4FSK.
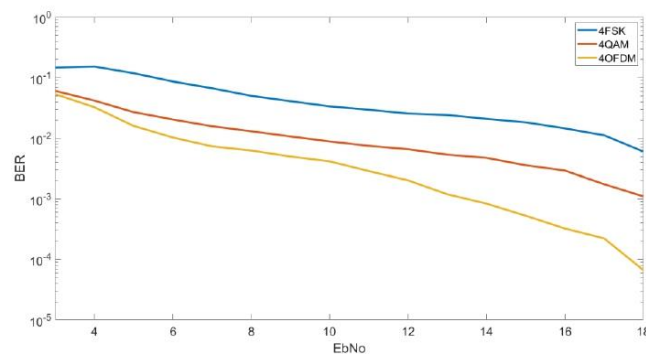
Figure 5. BER vs. E_b/N_0 M = 4.

4.1.2. BER vs. E_b/N_0 M = 8

In Figure 6, we can see the results obtained for the 8FSK, 8QAM and the OFDM designed with an 8QAM modulation. In this case the OFDM is shown again to be the most robust. For an E_b/N_0 of 10 dB we can obtain a BER of 4×10^{-3} by using an OFDM modulation, a BER of 2×10^{-3} by using an 8QAM and a BER of 8×10^{-1} by using an 8FSK. For a lower E_b/N_0 as 5 dB, we can see that we obtain a BER of 4×10^{-2} for the OFDM, a BER of 7×10^{-2} for the 8QAM and a BER of 2×10^{-1} for the 8FSK.
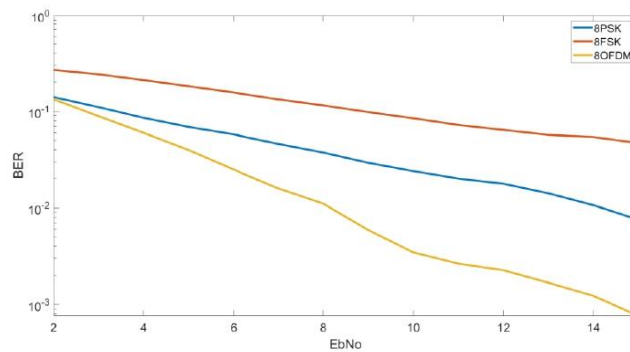
Figure 6. BER vs. E_b/N_0 M = 8.

4.1.3. BER vs. E_b/N_0 M = 16

In Figure 7, we analyze the results of 16FSK, 16QAM, 16PSK and the OFDM designed with a 16QAM modulation. In this case, OFDM is only the most robust modulation for high E_b/N_0 and 16QAM the most robust modulation for low E_b/N_0. As we can see for an E_b/N_0 of 10 dB we can obtain a BER of 2×10^{-2} by using an OFDM modulation, a BER of 3×10^{-3} by using a 16QAM, a BER of 7×10^{-2} by using an 8PSK and a BER of 2×10^{-1} by using a 16FSK. For lower E_b/N_0 as 5 dB, we can see that we obtain a BER of 6×10^{-2} for the 16QAM, a BER of 10^{-1} by using an OFDM, a BER of 10^{-1} for the 16PSK and a BER of 2×10^{-1} for the 16FSK.
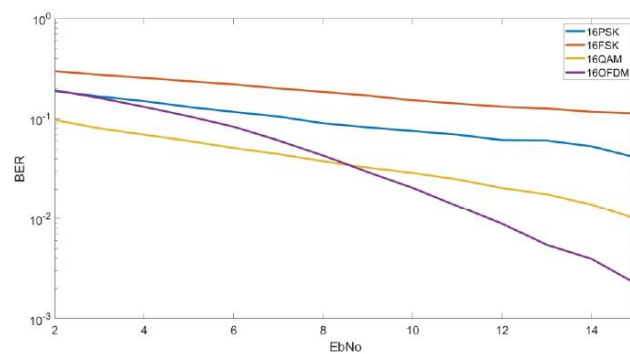
Figure 7. BER vs. E_b/N_0 M = 16.

4.2. BER Cumulative Distribution Function (CDF)

Once analyzed the BER depending on the E_b/N_0 it is important to analyze for each E_b/N_0 the CDF of the modulations depending on the order of modulation. By this test, we can obtain more information about the robustness of each modulation with low energy per bit and the probabilities of obtaining a low BER. All graphics of this section shows us in the Y-axis the probability of obtaining a BER lower than a value X_o represented on the X-axis. The results are better when the line is at the top left.

4.2.1. BER vs. E_b/N_0 = 5 dB M = 4

In Figure 8, we can see for a low E_b/N_0 of 5 dB the behavior of each modulation and robustness. We can see that the OFDM and QAM have the best results in a very similar way. The 4QAM have a

probability of 79% to obtain a BER lower than 2×10^{-3} and the OFDM have a probability of a 78% to obtain a BER lower than 3×10^{-3}. The 4FSK as we can see is highly affected by the low energy bit transmission with a probability of a 4% to obtain a BER lower than 2×10^{-3}. As we can see in this graphic, the OFDM is shown to be a little bit worse than the 4QAM even though in the graphic of Figure 5 it is shown to be more robust. As we can see at Figure 8 for higher BERs the OFDM is more robust than the QAM, for a BER lower than 10^{-1} we have a probability of 98% for the OFDM, a probability of 95% for the 4QAM and a probability of 64% for the 4FSK. For this reason, for a low E_b/N_0 of 5 dB, the OFDM obtains better results in terms of average but for transmission with the minimum errors it is better to use the 4QAM.

Figure 8. BER vs. $E_b/N_0 = 5$ dB M = 4.

4.2.2. BER vs. $E_b/N_0 = 5$ dB M = 8

In Figure 9, we can see the CDF for an E_b/N_0 of 5 dB and order of modulation 8. As we can see, in this case, the OFDM obtains the best results in comparison of the 8PSK and the 8FSK. To obtain a BER lower than 2×10^{-3} we have a probability of 56% for the OFDM and a probability of 45% for the 8PSK. For the 8FSK, we have a probability of a 1% to obtain a BER lower than 4×10^{-3}.
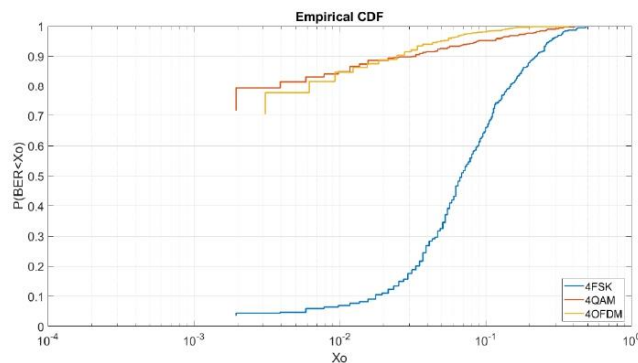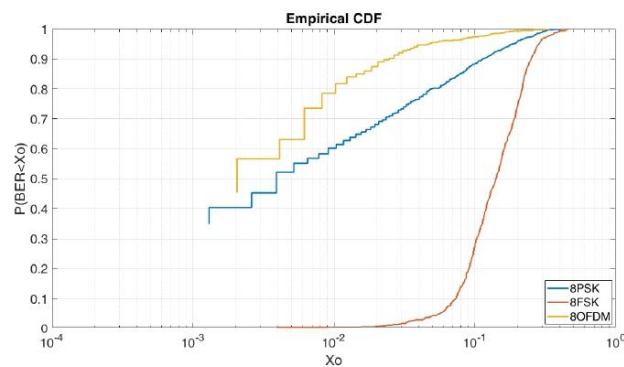

Figure 9. BER vs. $E_b/N_0 = 5$ dB M = 8.

4.2.3. BER vs. $E_b/N_0 = 5$ dB M = 16

In Figure 10, we can see the CDF for a E_b/N_0 of 5 dB and order of modulation of 16. In this case, contrary to Figure 9, 16QAM obtains the best results in comparison of the 16PSK, the 16FSK and the OFDM. As we can see, to obtain a BER lower than 5×10^{-3} we have a probability of 54% for the 16QAM, a probability of 10% for the 16PSK, and a probability of a 4% for the OFDM. At this figure, the OFDM is highly affected due to the increase of modulation order. Finally, in this case, the 16FSK has a probability of 10% to obtain a BER lower than 10^{-1}.
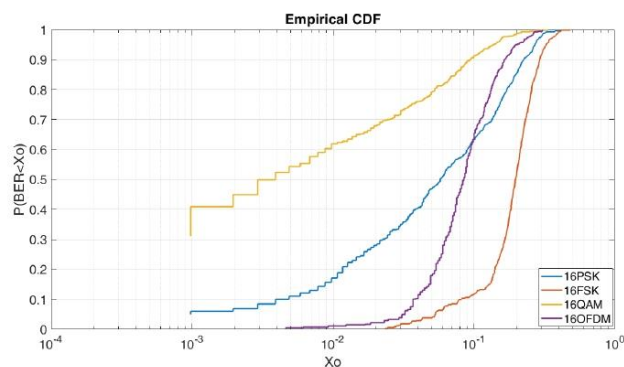
Figure 10. BER vs. $E_b/N_0 = 5$ dB M = 16.

4.2.4. BER vs. $E_b/N_0 = 8$ dB M= 4

Once the order modulations with a low E_b/N_0 of 5 dB are analyzed, we will analyze the same modulations with a E_b/N_0 of 8 dB. At Figure 11, we can see that the OFDM has better results than the 4QAM due to the increase of E_b/N_0. To obtain a BER lower than 6×10^{-3} we have a probability of 97% for the OFDM, a probability of 95% for the 4QAM and a probability of 61% for the 4FSK. For this E_b/N_0, we can see in Figure 11 that the OFDM always has better results than the 4QAM unlike the CDF of Figure 8.
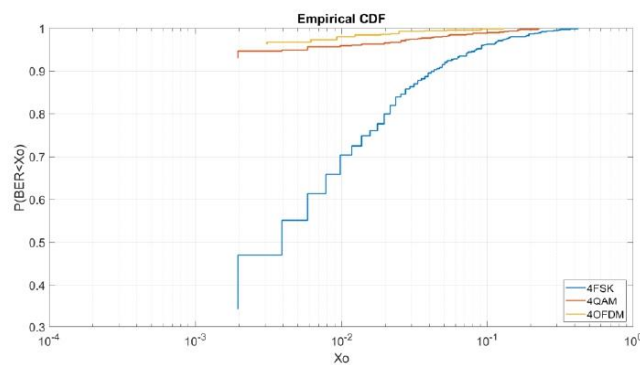
Figure 11. BER vs. $E_b/N_0 = 8$ dB M = 4.

111

4.2.5. BER vs. $E_b/N_0 = 8$ dB $M = 8$

At Figure 12, we can analyze again that the order 8 OFDM is more robust than the 8PSK and 8FSK. As we can see, to obtain a BER lower than 4×10^{-3} we have a probability of 95% for the OFDM, a probability of 88% for the 8PSK and a probability of 4% for the 8FSK.
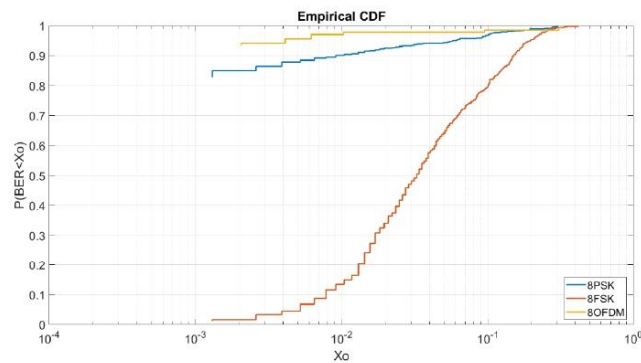
Figure 12. BER vs. $E_b/N_0 = 8$ dB $M = 8$.

4.2.6. BER vs. $E_b/N_0 = 8$ dB $M = 16$

At Figure 13, for a higher order modulation, the 16QAM is shown to be the best modulation to obtain high probabilities of low BER. In addition, we can observe that for a BER higher than 10^{-2} the OFDM has the same results as the 16QAM. For a lower BER, the 16QAM and the 16PSK are better. In Figure 13 we can analyze that to obtain a BER lower than 10^{-3} we have a probability of 70% for the 16QAM, a probability of 34% for the 16PSK and a probability of 30% to obtain a BER lower than 2×10^{-3} for the OFDM.

Figure 13. BER vs. $E_b/N_0 = 8$ dB $M = 16$.

For higher BER, to obtain a BER lower than 2×10^{-2} we have a probability of 87% to for the OFDM and 16QAM, a probability of 58% for the 16PSK and a probability of 3% for the 16FSK.

4.3. BER CDF vs. Power
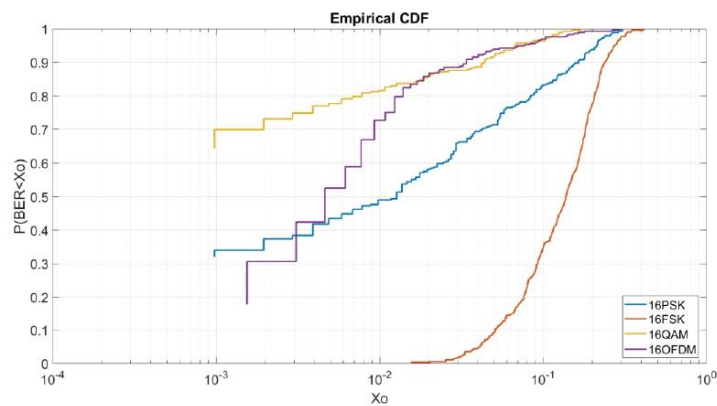
Taking into account the results obtained in Section 4.1 BER vs. E_b/N_0 and Section 4.2 BER CDF, we can analyze that the most robust modulations for order modulations 4 and 8 are the OFDM with a 4QAM and the OFDM with an 8PSK modulation. Despite the results, during a transmission with an average power, the analysis the E_b/N_0 received can have high variations. At Figure 14 we can analyze the CDF BER received signal for low power transmissions of 4QAM, 8PSK, OFDM with 4QAM and OFDM with 8PSK respectively with average power transmissions of 4.7 W, 5.1 W, 3.4 W and 3.7 W. Despite the similar average powers, the efficiency of the OFDM is 63% lower than the narrow-band modulations because of the low value of the IBO. As we can see in Figure 14, the graphic is based on the received signals between 20 UTC and 00 UTC, a range in which the channel presents high delay spreads of 2 ms affecting the robustness of narrowband modulations. To analyze the time range with a greater presence of multipath, we analyzed the ionograms of the Observatori de l'Ebre [22], and in Figure 15 we can distinguish the presence of the different ionosphere layers responsible for signal rebounds. The red line shows the possible reflection of the ordinary wave and the green line shows it for the extraordinary one. In Figure 15 we can see also the multipath produced with more than 8 paths.
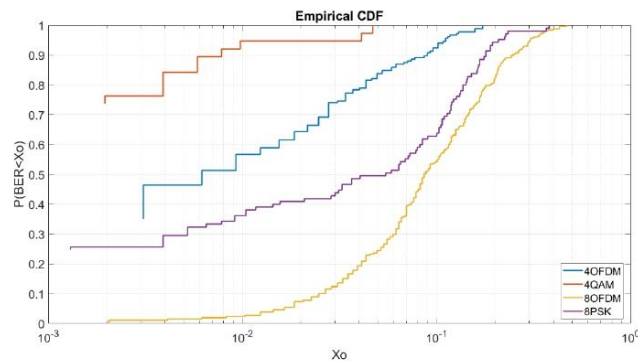

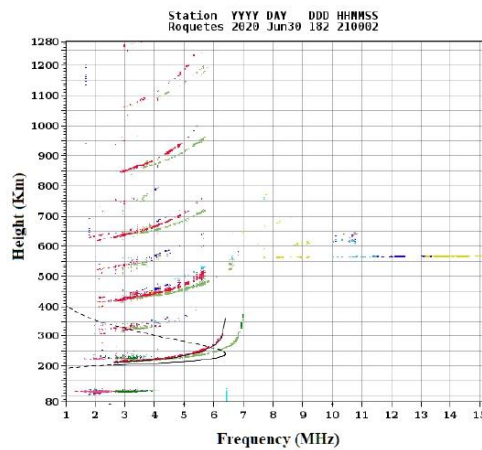**Figure 14.** BER CDF vs. Power.

Figure 15. Ionogram at 20 UTC.

At Figure 14, despite the multipath, the 4QAM is the most robust modulation in comparison with the OFDM. As we can see, we have a probability of 76% to receive a BER lower than 2×10^{-3}, the OFDM with a 4QAM modulation has a probability of 46% to receive a BER lower than 3×10^{-3}, the 8PSK have a probability 25% to receive a BER lower than 4×10^{-3} and the OFDM with an 8PSK has 1% to receive a BER lower than 4×10^{-3}. As we can see, the OFDM with a 8PSK is shown to be the less robust modulation due to the lack of power to achieve E_b/N_0 of 8 dB to maintain its robustness.

4.4. Input Back Offs (IBOs) Test

Taking into account the results obtained in Section 4.3 BER CDF vs. Power, the 4QAM was shown to be the most robust modulation followed by the OFDM with a 4QAM modulation. Through the results obtained, the OFDM results can be improved by the variation of the IBO. The OFDM tested in previous figures were configured with an IBO of 3 dB. To improve the robustness of OFDM in front of the 4QAM modulation, in the next sections we will study the best IBO design for the OFDM.

To achieve that goal, a simple IBOs sweep to find the optimal value has been simulated as is shown below. The simulations have been set with a Rayleigh distribution with an SNR of 0 dB and a second path delayed 250 ms from the first one with half of the power. In Table 3, we can see the BER results in terms of IBO in a simulation scenario.

Table 3. Simulated IBO test.

IBO (dBs)	BER
0	0.0863
1.5	0.0644
3	0.0494
4.5	0.0404
6	0.0331
7.5	0.0284
9	0.0273
10	**0.0267**
12	0.0295
15	0.0377
18	0.0448
21	0.0497
24	0.0554
27	0.0639

The results show that values of IBOs between around 9 and 10 dBs can reduce the BER around 46% in relation to the IBO of 3 dB, so a priori the increase of the IBO value from the initial one, must overcome the results of the tests already done. That improvement makes it possible to make the OFDM more robust than the 4QAM of Figure 14.

4.5. BER CDF vs. IBO

In a real scenario, we performed several tests to verify the simulated IBO results and analyzed the best option to apply. In addition, IoT needs to have a low power system, so we limit the real tests up to 5 W of average power. Different studies such as [28–30] show that OFDM IBOs are typical between 6 and 14 dBs. In Table 4, we can see the transmitted PAPR in terms of IBOs and the average power that is transmitted. In Equation (7), we can see how the PAPR is calculated, the maximum absolute voltage value of the signal divided into the average absolute voltage value PAPR is always expressed in dBs.

$$\text{PAPR} = 10 \log \left(\frac{\max |x(k)|^2}{E\left[|x(k)|^2\right]} \right) \qquad (7)$$

114

Table 4. Real IBO test.

OFDM Configuration	IBO	PAPR	Average Power
#1	4.5 dB	10.3 dB	2.3 W
#2	6 dB	9.1 dB	2.9 W
#3	7.5 dB	8.1 dB	3.7 W
#4	9 dB	7.2 dB	4.6 W
#5	4.5 dB	6.7 dB	2.5 W
#6	6 dB	5.8 dB	3.1 W
#7	7.5 dB	5.0 dB	3.7 W
#8	9 dB	4.4 dB	4.3 W

Through the realization of this test, at Figure 16 we can analyze the IBO tests results of real transmissions. As we can see, to obtain a BER lower than 3×10^{-3} we have a probability of 80% for the configuration #4, a probability of a 77% for the configuration #3 and a probability of a 71% for the configuration #2, #8 and #9. The rest of results obtained are lower to assure stable communication, as we can see, to obtain the same BER we have a probability of 63% for the configuration #1, we have a probability of 40% for the configuration #6, and we have a probability of 31% for the configuration #5.
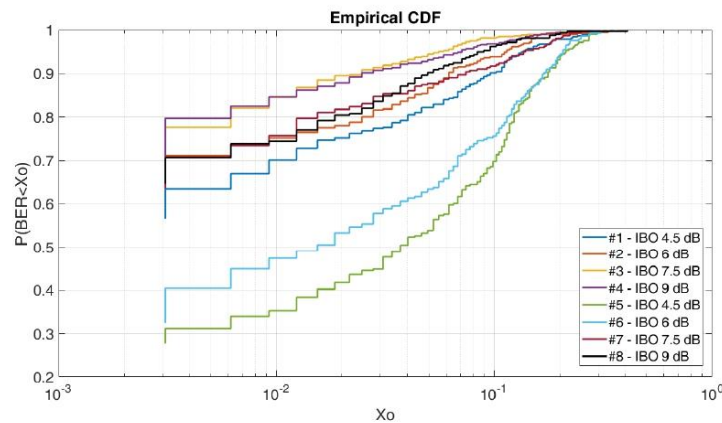
Figure 16. BER CDF vs. IBO.

By the variation of the IBO, we can analyze that the OFDM with a 4QAM modulation is more robust than the results achieved with the 4QAM narrowband modulation of Figure 14, the OFDM being more robust for a channel with the presence of a high delay spread.

4.6. Single Input Multiple Output (SIMO) Technique

Finally, by the results obtained, we can apply SIMO techniques by the addition of a second antenna at the receiver system. In Figure 17, we can see the results obtained by the ordinary wave, the extraordinary wave, and the use of SIMO techniques such as the SC technique and EGC technique. As we can see, the OFDM with a 4QAM modulation, an average power of 4.6 W and a SC technique can improve the probability of receiving a BER lower than 3×10^{-3} to a probability of 87% in front of the EGC which improves the probability to receive a BER lower than 3×10^{-3} to an 82%.

Figure 17. Single input multiple output (SIMO) technique.

5. Conclusions

Finally, we can conclude that OFDM overcomes narrow-band modulations in scenarios with high multipath such as mornings and evenings for NVIS communications. As we have studied, the OFDM is a good alternative but requires the IBO to be well confi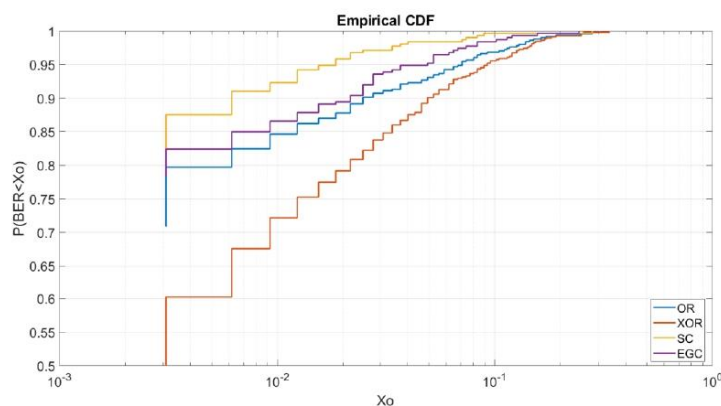gured to decrease the PAPR of the modulation signal. This factor is very important for remote sensing where the power consumption is a critical issue.

Through the study performed, in terms of robustness if we analyze the BER E_b/N_0 graphics, the OFDM modulation seems to be the best option with an IBO of 3 dB and a modulation order 4 in front of the narrowband modulations, as we have seen in Figure 5. Despite the results, if we focus on a certain value of E_b/N_0 and we analyze the BER on a CDF, the results change and the 4QAM seems to be the best option. As analyzed, the 4QAM modulation requires less E_b/N_0 to obtain better results as we can see at Section 4.2 BER CDF. That make sense of the challenge to obtain a robust low-power OFDM modulation due to the high PAPR and low average power for the same power transmissions. For that reason, one of the key issues of this study is the optimization of the OFDM using the IBO technique increasing the average power and consequently the average BER as we can see in Figure 16. The IBO technique as we have seen, offers a better efficiency for low-power OFDM modulations for remote sensors.

Furthermore, to make the NVIS communication more robust, as studied, the addition of a second antenna at the receiver system to apply SIMO techniques, can improve the link. By the use of the polarization technique using the ordinary and the extraordinary waves and the SC polarization technique, the BER results have been improved in a 9% the results obtained as we can see at Figure 17.

As analyzed, the mix of the OFDM and QAM depending on the channel scenario is the right approach, especially with the rapid changes of the ionosphere. Through the results obtained, in terms of applications, the OFDM can assure the use of NVIS communication for remote sensors in distances under 250 km, with low-power transmissions and a higher robustness than the HF standards modulations based on narrowband. We conclude that the study of multicarrier modulations benefits the robustness of NVIS communications giving a wide range of possibilities for sensors which need ubiquity to monitoring or sensing multiple facts.

Finally, through the results obtained we propose as the best option for NVIS remote sensing the use of an OFDM modulation for high multipath scenarios with 4QAM subcarriers and an average power transmission of 4.6 W. This configuration offers a bitrate of 2.139 Kbps and a probability of 80% to obtain a BER lower than 3×10^{-3}. In the case of adding a second antenna in the receiver system, the probability will increase to 87% to obtain a BER lower than 3×10^{-3}. In the case of need to reduce

the average power of the system more than 4.6 W, the receiver node will receive low E_b/N_0 signals. In this case, the use of a 4QAM will be more robust than the OFDM modulation.

In Table 5, we summarize different scenarios and the best modulation use for a robust transmission based on the results obtained in this article.

Table 5. Modulation depending on scenario.

Multipath	E_b/N_0	Modulation	SIMO Technique	Average Power	PAPR
High	Low	4-QAM	Selection Combining	4.7 W	4.8 dB
High	High	OFDM	Selection Combining	4.6 W	7.2 dB
Low	Low	4-QAM	Selection Combining	4.7 W	4.8 dB
Low	High	OFDM/4-QAM	Selection Combining	4.6W/4.7 W	7.2/4.8 dB

Author Contributions: Investigation, J.M.M., T.G., J.M., J.P., J.L.P. and D.B; Methodology, J.L.P. and D.B.; Software, J.M.M., T.G., J.M. and J.P.; Supervision, J.L.P. and D.B.; Validation, J.L.P. and D.B.; Writing—original draft, J.M.M., T.G., J.M. and J.P.; Writing—review and editing, J.M.M., T.G., J.M., J.P., J.L.P. and D.B. All authors have read and agreed to the published version of the manuscript.

Conflicts of Interest: The authors declare no conflict of interest.

References

1. Nikoghosyan, E.H. Ecology of Near-Earth Space. *arXiv* **2018**, arXiv:1812.10478.
2. Saibi, H.; Bersi, M.; Mia, M.B.; Saadi, N.M.; Al Boushi, K.M.S.; Avakian, R.W. *Applications of Remote Sensing in Geoscience Recent Advances and Applications in Remote Sensing*; IntechOpen: London, UK, 2018. [CrossRef]
3. Lary, D.J.; Alavi, A.H.; Gandomi, A.H.; Walker, A.L. Machine learning in geosciences and remote sensing. *Geosci. Front.* **2016**, *7*, 3–10. [CrossRef]
4. Lee, K.; Claridades, A.R.C.; Lee, J. Improving a Street-Based Geocoding Algorithm Using Machine Learning Techniques. *Appl. Sci.* **2020**, *10*, 5628. [CrossRef]
5. Alshaikhli, T.; Liu, W.; Maruyama, Y. Automated Method of Road Extraction from Aerial Images Using a Deep Convolutional Neural Network. *Appl. Sci.* **2019**, *9*, 4825. [CrossRef]
6. Han, J.; Park, C.; Kwon, J.H.; Lee, J.; Kim, T.S.; Jang, Y.Y. Performance Evaluation of Autonomous Driving Control Algorithm for a Crawler-Type Agricultural Vehicle Based on Low-Cost Multi-Sensor Fusion Positioning. *Appl. Sci.* **2020**, *10*, 4667. [CrossRef]
7. Pijoan, J.L.; Badia, D. Investigación a la Antártida: Comunicación a 12,500 Km con la ayuda de la Ionosfera–Ciènciaprop®. Available online: http://cienciaprop.fundaciocaixavinaros.com/conferencias/investigacion-a-la-antartida-comunicacion-a-12500-km-con-la-ayuda-de-la-ionosfera/ (accessed on 7 September 2020).
8. Davies, K. *Ionospheric Radio*; The Institution of Engineering and Technology (IET): Stevenage, UK, 1990.
9. MIL-STD-188C Appendix D. *Deparment of Defense Interface Standard: Interoperability and Performance Standards for Data Modems*; Department of Defense: Arlington, VI, USA, 2017.
10. North Atlantic Treaty Organization. *STANAG 4539. (n.d)*; North Atlantic Treaty Organization: Brussels, Belgium, 2015.
11. Parra, C.V. Comunicacions Avançades d'HF entre la Base Antàrtica Espanyola i l'Observatori de l'Ebre: Caracterització de Canal i Transmissió de Dades. 2008. Available online: https://dialnet.unirioja.es/servlet/tesis?codigo=84296&orden=1&info=link (accessed on 30 October 2020).
12. Jodalen, V.; Lundborg, B.; Jacobsen, B. Channel characteristics of HF NVIS paths in northern Scandinavia. In Proceedings of the Eighth International Conference on HF Radio Systems and Techniques, Guilford, UK, 10–13 July 2000; pp. 269–273.
13. Hervás, M.; Pijoan, J.L.; Alsina-Pagès, R.M.; Salvador, M.; Altadill, D. Channel sounding and polarization diversity for the NVIS channel. In Proceedings of the Nordic HF Conference, Faro, Sweden, 12–14 August 2013.

14. Cannon, P.S.; Angling, M.J.; Davies, N.C.; Wilink, T.; Jodalen, V.; Jacobson, B.; Lundborg, B.; Broms, M. Damson HF channel characterization—A review. In Proceedings of the. 21st Century Military Communications. Architectures and Technologies for Information Superiority, Los Angeles, CA, USA, 20–25 October 2000; Volume 1, pp. 59–64. [CrossRef]

15. Erhel, Y.; Lemur, D.; Oger, M.; le Masson, J.; Marie, F. Evaluation of Ionospheric HF MIMO Channels: Two complementary circular polarizations reduce correlation. *IEEE Antennas Propag. Mag.* **2016**, *58*, 38–48. [CrossRef]

16. Bechet, P.; Bechet, A.C.; Miclaus, S. HF urban noise level in variable channels of 3–24 kHz: A preliminary experimental approach. In Proceedings of the Loughborough Antennas & Propagation Conference, Loughborough, UK, 13–14 November 2017; Volume 2017. [CrossRef]

17. Porte, J.; Maso, J.M.; Pijoan, J.L.; Badia, D. Design, implementation, and test of an SDR for NVIS communications. *Int. J. Circuit Theory Appl.* **2019**, *47*, 1502–1512. [CrossRef]

18. Austin, R.; Bull, P.; Buffery, S. A raspberry Pi based scalable software defined network infrastructure for disaster relief communication. In Proceedings of the IEEE 5th International Conference on Future Internet of Things and Cloud, FiCloud, Prague, Czech Republic, 21–23 August 2017; pp. 265–271. [CrossRef]

19. Thomas, S.A.; Anusudha, K. Comparative analysis for various parametric attributes for an optimized DUC/DDC. In Proceedings of the International Conference on Inventive Computing and Informatics (ICICI), Coimbatore, India, 23–24 November 2017; pp. 206–209. [CrossRef]

20. Bonn Elektronik. Bonn Elektronik Power Amplifier 9kHz-40Ghz. Available online: https://www.bonn-elektronik.com/wp-content/uploads/2013/04/brochure.pdf (accessed on 13 February 2020).

21. Porte, J.; Pijoan, J.L.; Masó, J.M.; Badia, D.; Zaballos, A.; Alsina-Pagès, R.M. Advanced HF communications for remote sensors in Antarctica. In *Antartica—A Key to Global Change*, 1st ed.; IntechOpen: London, UK, 2019.

22. Observatori de l'Ebre. Available online: http://www.obsebre.es/es/ (accessed on 28 May 2020).

23. Alsina-Pagès, R.; Altadill, D.; Hervas, M.; Blanch, E.; Segarra, A.; Sans, X. Variation of Ionospheric Narrowband and Wideband Performance for a 12,760 km Transequatorial Link and Its Dependence on Solar and Ionospheric Activity. *Remote Sens.* **2020**, *12*, 2750. [CrossRef]

24. Maso, J.M.; Porte, J.; Pijoan, J.L.; Badia, D. Study of NVIS channel for USN protocol definition in Antarctica. *Electron* **2020**, *9*, 6. [CrossRef]

25. Bergadà, P.; Alsina-Pages, R.M.; Pijoan, P.L.; Salvador, M.; Regue, J.R.; Badia, D.; Graells, S. Digital transmission techniques for a long haul HF link: DSSS versus OFDM. *Radio Sci.* **2014**, *49*, 518–530. [CrossRef]

26. Greenman, M. An Introduction to HF Propagation and the Ionosphere. Available online: https://www.qsl.net/zl1bpu/IONO/iono101.htm (accessed on 8 September 2020).

27. Maso, J.M.; Male, J.; Porte, J.; Pijoan, J.L.; Badia, D. Ionospheric polarization techniques for robust NVIS remote sensing platform. *Appl. Sci.* **2020**, *10*, 3730. [CrossRef]

28. Zegeye, W.; Moazzami, F.; Dean, R. Peak-to-Average Power Ratio (PAPR) Reduction for OFDM. In Proceedings of the International Telemetring Conference, Las Vegas, NV, USA, 21–24 October 2019.

29. Aghdam, M.H.; Sharifi, A.A. PAPR reduction in OFDM systems: An efficient PTS approach based on particle swarm optimization. *ICT Express* **2019**, *5*, 178–181. [CrossRef]

30. Musabe, R.; Lionel, M.B.; Ushindi, V.M.; Atupenda, M.; Ntaganda, J.; Bajpai, G. PAPR reduction in LTE network using both peak windowing and clipping techniques. *J. Electr. Syst. Inf. Technol.* **2019**, *6*, 1–11. [CrossRef]

Annex 2

Analysis of the Ordinary and Extraordinary Ionospheric Modes for
NVIS Digital Communications Channels

Article

Analysis of the Ordinary and Extraordinary Ionospheric Modes for NVIS Digital Communications Channels

Jordi Male [ID]**, Joaquim Porte** [ID]**, Tomas Gonzalez** [ID]**, Josep M. Maso** [ID]**, Joan L. Pijoan *** [ID] **and David Badia**

La Salle Campus, Ramon Llull University, 08022 Barcelona, Spain; jordi.male@salle.url.edu (J.M.); joaquim.porte@salle.url.edu (J.P.); tomas.gonzalez@salle.url.edu (T.G.); josep.maso@salle.url.edu (J.M.M.); david.badia@salle.url.edu (D.B.)
* Correspondence: joanlluis.pijoan@salle.url.edu

Abstract: Sensor networks have become more popular in recent years, now featuring plenty of options and capabilities. Notwithstanding this, remote locations present many difficulties for their study and monitoring. High-frequency (HF) communications are presented as an alternative to satellite communications, being a low-cost and easy-to-deploy solution. Near vertical incidence skywave (NVIS) technology provides a coverage of approximately 250 km (depending on the frequency being used and the ionospheric conditions) without a line of sight using the ionosphere as a communication channel. This paper centers on the study of the ionosphere and its characteristic waves as two independent channels in order to improve any NVIS link, increasing its robustness or decreasing the size of the node antennas through the appliance of specific techniques. We studied the channel sounding of both the ordinary and extraordinary waves and their respective channels, analyzing parameters such as the delay spread and the channel's availability for each wave. The frequency instability of the hardware used was also measured. Furthermore, the correlation coefficient of the impulse response between both signals was studied. Finally, we applied polarization diversity and two different combining techniques. These measurements were performed on a single frequency link, tuned to 5.4 MHz. An improvement on the mean bit energy-to-noise power spectral density (E_b/N_0) was received and the bit error rate (BER) was achieved. The results obtained showed that the extraordinary mode had a higher availability throughout the day (15% more availability), but a delayed spread (approximately 0.3 ms mean value), similar to those of the ordinary wave. Furthermore, an improvement of up to 4 dB was achieved with the usage of polarization diversity, thus reducing transmission errors.

Keywords: HF; NVIS; SIMO; diversity combining; sounding; communication channel; ionosphere; STANAG; MIL-STD-188; polarization diversity; remote sensing

1. Introduction

The ionosphere has an essential function for our planet, which is the protection against external radiations. It has been studied for a long time both in a physical way and also as a communication channel [1,2], as the ionosphere behaves like a mirror for high frequency (3–30 MHz) signals. Using the ionosphere as a channel, and taking advantage of the benefits of signal reflection for HF, has wide use for emergency services and is also suitable for ubiquitous sensors networks (USN). In addition, it avoids the use of satellites and high infrastructure and operational costs.

The behavior of the ionosphere is under continuous research due to its difficult prediction. Observatories, using an ionosonde, examine the quantity of ions and electrons produced in the atmosphere to get information of the radio wave refraction, and the generation of different waves due to these reflections (the ordinary and the extraordinary waves [1,2]). There are studies such as those by the respective authors of [3–5], where a deterministic model of a narrowband and wideband HF channel was studied giving a prediction of quality parameters of ionospheric communications, but there was no distinction

between ordinary and extraordinary waves. Doppler and multipath measurements on oblique and vertical ionospheric paths were performed in studies by the respective authors of [6,7] and also in the Doppler And Multipath Sounding Network (DAMSON) project [8,9]. Moreover, another sounding of narrowband and wideband ionospheric communications, was done with oblique transmissions [10]. It is known that the availability of the ionosphere as a communication channel is not remarkable, since it depends on its ionization. Its behavior varies throughout the day, which implies that different transmission frequencies must be used due to the change of the critical frequency. Due to its low bandwidth and coherence time, the ionosphere is not a solution for high-speed data transmissions but, on the other hand, its channel characteristics are suitable for sensor network deployment.

In this article, we analyze the behavior of the ionosphere as a communication channel, using near vertical incidence skywave (NVIS) propagation and the transmission of different data frames. The transmit frequency used in our experiment was 5.4 MHz. NVIS propagation is based on the transmission of a signal with an incidence angle between 70° and 90° to the ionosphere. The properties of the ionosphere cause that signal to be reflected, obtaining a coverage of approximately a 250 km radius [11], which is a relevant fact for remote sensors or emergency communications for places without infrastructure [12]. The ionospheric reflection is frequency dependent, with typical frequencies ranging from 3 to 10 MHz. The coverage radius of 250 km corresponds with F_2-layer propagation.

In what follows, characteristics of the ionosphere and NVIS communications and polarization diversity are introduced in Section 2. The sounding system implemented is described in Section 3, where, in Section 3.1, the overall infrastructure is explained, the data frames designed and used are detailed in Section 3.2, and the test scenario is described in Section 3.3. Results of this study are presented in Section 4, and finally, the conclusions of this work are in Section 5.

2. The Ionosphere and Polarization Diversity

The ionosphere is one of the layers of the atmosphere that, thanks to its physical characteristics, allows the refraction of radio signals between 3 and 30 MHz. Specifically, the ionization of the ionosphere is the responsible of this signal refraction. The ionization of the outer layers of the atmosphere depends on the degree of solar activity, which follows cycles of approximately 11 years and presents sunspots as an indicator [1]. The condition of the ionosphere not only changes annually, but also depends on the season and the time of day. These variations make ionospheric communications very challenging, requiring a system that adapts to the state of the ionosphere at all times.

Communications through the ionosphere are classified according to the angle of incidence of the radio wave. NVIS communications are based on a 90° to 70° angle of incidence, and generate a coverage area of up to 250 km (depending on frequency and ionospheric conditions) from the point of transmission [11]. The focus of this article is to define the physical properties of the NVIS channel (Figure 1).
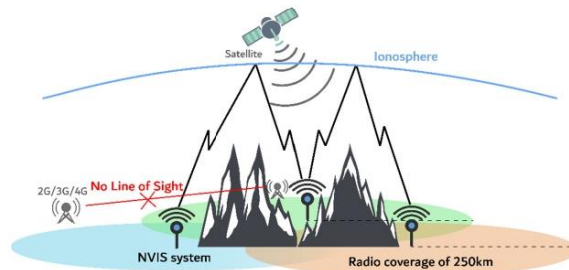

Figure 1. Near vertical incidence skywave (NVIS) link scenario.

The ionosphere presents multiple layers (D layer, E layer, and F layer, which splits into F_1 and F_2 layers during daytime), which depend on the sun's ionization [1]. NVIS communications can use both the E layer and the F_2 layer. Taking into account the distance between our nodes, and in order to maximize the received signal strength, we based our study on the F_2-layer propagation. Furthermore, the ionosphere is a birefringent medium. Two modes or propagation (ordinary and extraordinary) are formed as soon as the radio wave enters the ionized plasma in the presence of a magnetic field. The plane-polarized wave is decomposed into two different waves, and the direction of energy is deviated from the direction of propagation [1]. This partition creates two totally different propagation paths, resulting in two independent communication channels.

Specifically, when a radio wave reaches the ionosphere, the electrons in the layer start an elliptical movement [1]. As a result of this almost-circular spin, the radio wave has its polarization changed by the ionosphere. This leads to the return to the Earth of two different rays (the ordinary and extraordinary rays) with different properties, such as different critical frequencies, phase, amplitude, and arrival time [2]. Specifically, both of these waves have elliptical polarization and also have opposite rotation sense. For the Northern Hemisphere, the ordinary wave has the greater delay and left-hand circular polarization (LHCP), and the extraordinary wave presents the lesser delay and right-hand circular polarization (RHCP) [13]. These different properties can be used to improve telecommunication links, as polarization diversity techniques are an option in ionospheric channels.

The different polarizations and the usage of the ionospheric characteristic waves as two different communication channels allow for the usage of polarization diversity techniques to improve the robustness and throughput of the link. The concept of polarization diversity was first introduced by the authors of [14] in the 1950s. The work presented in Reference [15] was one of the first to use polarization diversity at the receiver achieving 9600 bps for a 1800 km skywave link. The authors of [16] highlighted the importance of using both ordinary and extraordinary waves for multiple-input multiple-output (MIMO) in the case of NVIS propagation, and the cross-correlation of both channels was analyzed for narrowband transmissions. A channel model for dual polarized MIMO communications was proposed in [17] and some high throughput testbeds are presented in [18,19], where the improved channel capacity was analyzed. Our team, after evaluating the polarization diversity for long-haul HF links between the Antarctic and Spain [20], is now considering the dual-polarized reception for a NVIS sensors network in order to decrease either the transmission power or the size of the antennas.

In order to improve the robustness of the NVIS link and apply polarization diversity techniques, a combination of the different signals that arrive at the receiver is needed. There are multiple methods of diversity combining, each one presenting different characteristics and gains. We studied two different techniques: equal-gain combining, a method that sums all the received signals coherently, and selection combining, a technique that selects the strongest signal received (a higher signal-to-noise ratio (SNR)) and ignores the other.

3. Sounding System

All the hardware used in order to carry out this work is presented in this section. Firstly, a description of the overall system is presented, explaining all the infrastructure and peripherals used. Secondly, the transmitted data frames are listed and detailed. Finally, the implemented link and the realized tests are described.

3.1. System Description

The system to perform this study relies on a software defined radio (SDR), which can be seen in Figure 2. The versatility of the SDR offers the possibility to adjust parameters for the adaptation of different scenarios. Our SDR was implemented with a field-programmable gate array (FPGA) combined with the Zynq-7010-SOC [21], which were placed in a Red Pitaya STEMlab 125-14 board [22]. This board makes all the computing operations possible, since it features analog-to-digital converters (ADC) and digital-to-

analog converters (DAC) with a resolution of 14 bits, all driven by a system clock of 125 MSPS. The Red Pitaya board was connected via Ethernet to a Raspberry Pi 3 [23], which saved the received files onto a hard disk and managed the different peripherals [24]. These connections are presented below:
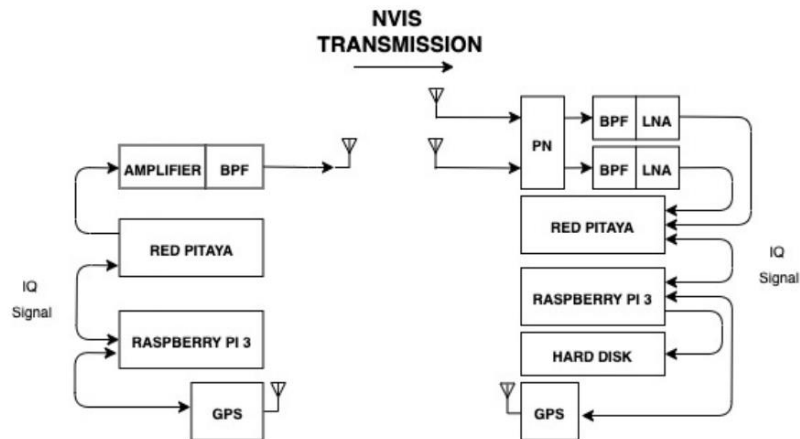

Figure 2. System block diagram.

- Antennas: At the transmitter site, an inverted vee (V-) antenna was used, which was placed in La Salle URL in Barcelona. At the receiver side in Cambrils, two orthogonal inverted-V antennas were located. Figure 3 displays a graphical representation of the orthogonal antennas located in Cambrils. The frequency is currently set to 5.4 MHz, a value based on ionogram studies [25]. The height of the antennas is 14.5 m and the length of their legs is 14 m.
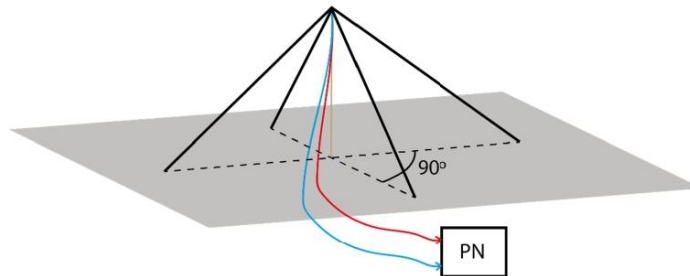
Figure 3. Diagram of the orthogonal inverted vee antennas in the receiver.

- Phasing Network: The two perpendicular inverted vee antennas worked together with a phasing network (PN; in Figure 2), which was in charge of shifting the phase of one of the two receiver antennas to make it possible to receive different and orthogonal polarizations [26]. The phasing network got a total of four wires, two from each antenna, as we duplicated the received signals using a radio frequency splitter (PDML-20A-100 from Merrimac Industries, Inc.). The route that both antennas followed was the same: one cable was lengthened with a quarter-wave phasing line to provide a 90° shift and connected to a radio frequency (RF) combiner (PDML-20A-100 from

Merrimac Industries, Inc.), and the other feed line was directly connected to a RF combiner. The output of the PN gave us a phase difference between the inverted vee antennas of either +90° or −90°. A block diagram of the phasing network is displayed in Figure 4.

Figure 4. Block diagram of the phasing network.

- Amplifier: In order to do the sounding an A-class amplifier was used in the transmitter side. The model chosen was the Bonn BLWA 0103-250, which achieves 250 W of maximum power with an input power of 0 dBm.
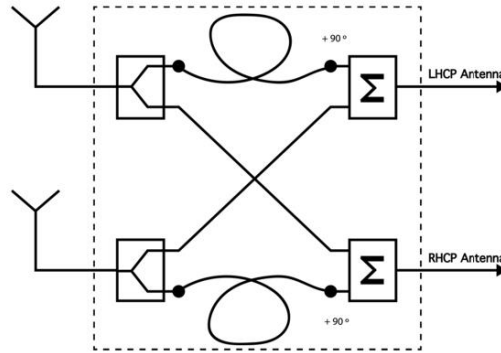- Low-noise amplifier (LNA): The model chosen was the ZFL-500LN+, with a minimum gain of 20 dB, a frequency range between 0.05 and 500 MHz, and an operating temperature between −20 °C and 70 °C.
- Filters: We used two band-pass filters (BPF) to avoid known interferences on both sides. On the transmitter side, we filtered the NVIS useful frequency range from 3 to 7 MHz. On the other side, we used a filter with a band pass between 4 and 6 MHz. Our system compensated for the phase delay of the BPF via software, as each data frame was corrected in both amplitude and phase before being demodulated and studied.
- GPS: A GPS was used to synchronize the transmitter and receiver in time (fundamental for the channel study performed). Time synchronization is essential to automate tests and data analysis. Our experiment had different signals sent, which depend on the minute of transmission. Thanks to the time synchronization, the transmitter knows which data file to send and the receiver tags it before saving it in order to analyze the data correctly. The transmitter and receiver were configured with extreme precision thanks to the GPS modules incorporated into the Raspberry. Furthermore, we also used PN sequences to detect the start of the received data structures and synchronize the transmitter and the receiver.

3.2. Data Frame Design

The correct definition of the data frame was essential for the experiment. We defined a level one frame of the Open Systems Interconnection model (OSI model), that consists of a physical structure of the transmitted data. We named this level one frame the "data frame". A poor definition of the data frame could imply intersymbol interference (ISI) and signal-to-noise ratio (SNR) fadings. Two different data frames were used to perform our tests, which were designed on the basis of earlier studies and the soundings of the ionospheric channel [27]. Figure 5 displays a graphical representation of the first type of signal sent (Frame number 1), which was composed by a total of 50 data groups (we named these structures "packets"), each formed by three different modulations: Phase-shift keying (PSK), frequency-shift keying (FSK), and quadrature amplitude modulation

(QAM). All the packets added a preamble that aims to mitigate the negative effects of the ionospheric channel and the frequency deviation between the transmitter and the receiver (the preamble is used to analyze and compensate the received signal's phase and amplitude via software). This preamble consisted of a 600 Hz tone and a sixth-order PN sequence, and it was located at the beginning of each of the 50 transmitted packets. The sampling speed of the system was 100 kS/s.
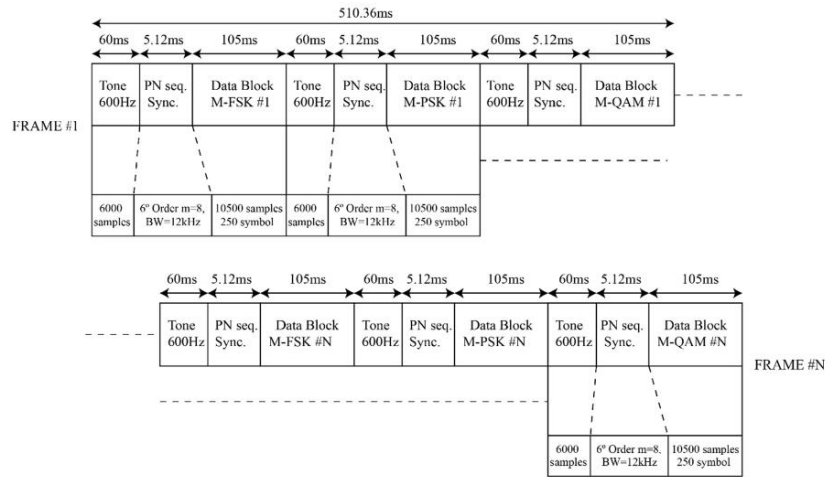

Figure 5. Data frame design [27].

Figure 5 exhibits the data frame's duration at both the sample and time levels. Analyzing all the packet segments and their respective lengths, it can be observed that the 600 Hz tone's duration was 6000 samples, the PN's sequence duration was 512 samples, and the modulated data transmitted corresponded to 10,500 samples. Furthermore, every data block contained 250 symbols with a resample of 42 (10,500 samples divided by 250 symbols), resulting in a bandwidth of 2.38 kHz per data block. On the other hand, the bandwidth used in the PNs was 12 kHz. This is because our frame had to respect the coherence time of the ionospheric channel, and in the design of the data frame, we did not want the PN sequences to have a significant influence. Our team decided to make the pseudo-random sequences shorter in time, resulting in a bandwidth of 12 kHz.

The data frame designed had a total duration of 510.36 ms, which was less than the most restrictive coherence time of the ionospheric channel (1.46 s) [28]. The total duration of the 50 packets sent was 25.518 s.

The first tone of the data frame was preceded by an extra block made of a PN sequence, intended to synchronize the system sample-wise.

All the data frames received were stored to be treated afterwards. The processing applied to each one of the data frames is explained as follows: First of all, the system identifies the data frame by correlating the signal received with the value of the PN sequence transmitted. If there are equispaced peaks in the result of this correlation, a data frame is identified. Once the system identifies the data frame, the first block encountered is the 600 Hz tone. This tone of a duration of 60 ms is key to identify and correct the channel's Doppler shift. In our system, the Doppler shift could not be studied as a frequency offset, as the Red Pitaya platform clocks have a low stability and create a relative frequency-drift effect that is higher than the ionospheric channel. Measures of the platform show that the maximum value of the frequency offset received, due to the low stability clocks, is about

125

$\pm$20 Hz [29]. The 600 Hz tone added to the data frame helps in identifying the frequency instability inserted by its variations between 580 and 620 Hz, approximately. Once the frequency offset is calculated, the received signal is corrected and this frequency offset is compensated for a correct demodulation of the signal.

The second block included in the data frame's preamble is the sixth-order PN sequence, whose function is to identify the start of the modulated data. The resampling of the PN sequence was about eight and had a total duration of 5.12 ms, as shown in Figure 5. The modulated data blocks were located just after the PN sequence.

As shown in Figure 6, a second data frame was designed for the study of the correlation coefficient between the ordinary and extraordinary channels and their respective delay spread. This second data frame consists of a group of equispaced PN sequences. The spaces between the known sequences do not present any kind of signal, and present a theoretical value of zero amplitude. The purpose of this design is the correct correlation of the PN sequences, as it is fundamental for the correct computation of the multipath values and the correlation coefficients between channels.
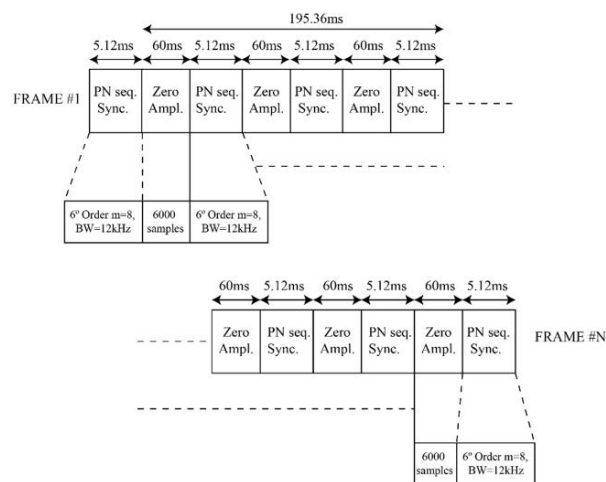

Figure 6. Second data frame design.

A key factor for our study was the separation between PN sequences, as it indicates the separation between the packets. This separation is the direct measurement cadence of our system. For the first data frame (Figure 5), a measurement was performed every 165 ms (6.06 Hz). For the second data frame used (Figure 6), a measurement was performed every 60 ms (16.17 Hz).

3.3. Test Scenario

To study the ionospheric channel, the research group installed a sounding system [29] between two points in the Catalonia region (Spain). These NVIS nodes established a link between La Salle University-URL Campus in Barcelona (41.41° N, 2.13° E) and a remote location in Cambrils, Tarragona (41.08° N, 1.07° E). Figure 7 presents a satellite picture of the terrain with the node locations highlighted in yellow. The distance between the two points without line of sight (LOS) was approximately 97 km, a value that is perfectly within the coverage area of an NVIS link. Surface wave signals did not affect our link thanks to the radiation pattern of antennas used in the experiment (their main beam is completely vertical, towards the sky) and the large distance between both points. This was verified as we transmitted different data frames throughout the whole day. During night, when

there is absence of ionospheric propagation at 5.4 MHz, we did not receive any signal in our receiver, thus confirming that surface waves do not affect our experiment. Figure 8 presents the elevation profile between the nodes.
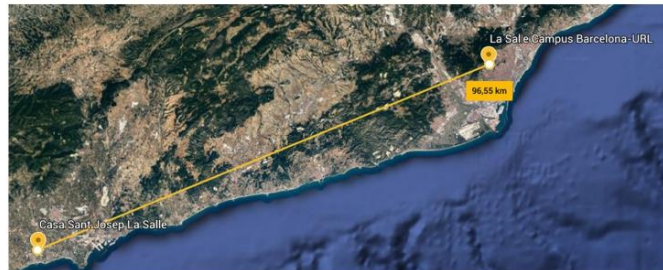

Figure 7. Location of the transmitter and receiver for the channel sounding.

Figure 8. Elevation profile of the NVIS link.

Because of the high interferences and electromagnetic noise in the HF band in Barcelona and its surroundings, the receiver was established in Cambrils. This configuration mini-mized the interferences in the receiving node, thus maximizing the robustness of the link.

The channel study presents a sounding of 12 complete days in December 2019. A total of 8308 files of 29.7 MB were studied, resulting in more than 240 GB of collected data. In one hour, a total of 30 tests were performed. The tests are the transmissions made on our link. These tests follow the format indicated by the experiment, which indicates the data structure to be sent, the transmission power, and the order of modulation sent. These tests followed two different experiments depending on which data frame they were transmitting (Figure 5 or Figure 6). As it can be observed in Table 1, the first data frame transmitted did a transmitting power sweep for five different modulation orders. This experiment is used to evaluate the SDR's frequency instability by computing the frequency shift of the signal received.

Table 1. Experiment for the first data frame (see Figure 5).

Modulation Order	Transmitting Power	Min
2, 4, 8, 16, 32	3 W	05, 06, 07, 08, 09
2, 4, 8, 16, 32	6 W	15, 16, 17, 18, 19
2, 4, 8, 16, 32	12 W	25, 26, 27, 28, 29
2, 4, 8, 16, 32	25 W	35, 36, 37, 38, 39
2, 4, 8, 16, 32	50 W	45, 46, 47, 48, 49
2, 4, 8, 16, 32	100 W	55, 56, 57, 58, 59

On the other hand, the second data frame (Table 2) did not present any modulated data (no modulation order implied) and was only transmitted at one transmitting power

127

value. This second data frame and its experiment are used to compute the correlation coefficient between both channels (correlation of the impulse responses of both channels), the availability (data frames detected throughout a day), and the delay spread (received multipath of the signal).

Table 2. Experiment for the second data frame (see Figure 6).

Transmitting Power	Min
50 W	05, 06, 07, 08, 09
	15, 16, 17, 18, 19
	25, 26, 27, 28, 29
	35, 36, 37, 38, 39
	45, 46, 47, 48, 49
	55, 56, 57, 58, 59

4. Ionospheric Channels Analysis

This section presents the detailed results obtained with the channel sounding performed. The availability of the ordinary and extraordinary NVIS Channels, their cross-correlation coefficient, and the delay spread are exhibited. Furthermore, the frequency offset caused by the SDR's frequency difference was also computed. The first three parameters (availability, correlation, and delay spread) were studied and computed using the second data frame (Figure 6), as they focus on data frame detection and PN sequence correlations. The remaining frequency instability was analyzed using the first data frame (Figure 5) as it was computed packet-wise. Finally, we analyzed the usage of polarizations diversity (the combining of the ordinary (O) and extraordinary (X) channels) and its improvement to the robustness of the NVIS link. Two different combining methods were used and studied: selection combining and equal-gain combining. All the results of this study are the product of observing the data sent over the 12 days. The data of all the days was put together in different graphs to analyze the behavior of our link in the described period.

First of all, the availability of the ordinary and extraordinary wave's channels was evaluated. Figure 9 displays the percentage of data frames detected at 5.4 MHz at the reception point in Cambrils. This data frame detection was based on the PN sequences received and their correlation with our known sequence. The availability was defined as follows: the total number of data frames received with respect to the total number of sent data frames. The maximum availability (number of transmitted data frames) was defined as the peak performance (corresponding to the 100% in our graph). The number of data frames detected for every hour was based on this factor and then displayed in the graph. Figure 9 states that the ionospheric channel is not active up until 7 Coordinated Universal Time (UTC) (8 a.m. Central European Time (CET)) and stops being active at 17 UTC time (6 p.m. CET). This result matches with the sunrise and the sunset in the month when the tests were performed (November/December), as it corresponds approximately to the hours of the activation and deactivation of the ionospheric channels. The best availability was between 7 UTC and 16 UTC (8 a.m. and 5 p.m. CET). This high availability corresponds to the day's highest amount of solar activity. Comparing the ordinary and extraordinary channels, it can be affirmed that the extraordinary channel clearly performed better. The extraordinary wave received reached a peak performance of data frames detected at 15 UTC. Two exceptional intervals (7 UTC and 16 UTC) can be identified in Figure 9, in which almost only the extraordinary wave propagated and right-hand circular polarization (RHCP) was received. The ordinary wave (LHCP) rarely propagated, resulting in availabilities between 30% and 40%. These intervals are known as "happy hours" [13]. At sunrise the ionization showed a steep gradient and, accordingly, the morning happy hour was short (typically 30 min at mid-latitudes in winter, our scenario). The evening happy hour often lasted more than an hour due to the slower ion recombination processes [13]. Consequently, the highest differences in availability between the two channels coincided with the happy hours mentioned. Figure 9 also exhibits the performance (percentage of data frames detected)

128

of both the ionospheric channels. The legend of the graph is defined as follows: OR is the performance of the ordinary wave, XOR is the performance of the extraordinary wave received, and OR and XOR refers to the total performance between both ordinary and extraordinary modes. The results are clearly better, achieving a result of 86% of the data frames detected from 7 UTC to 16 UTC.
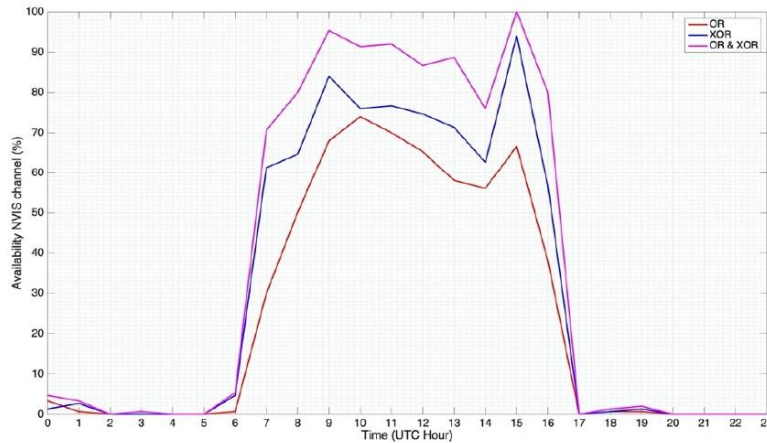

Figure 9. Availability of the Barcelona—Cambrils NVIS ionospheric channels.

The usage of both ionospheric channels at the same time resulted in the reception of simultaneous signals. If these signals are decorrelated (two channels are considered as not correlated when their cross-correlation coefficient value is lower than 0.7 [30]), an increase of SNR (signal-to-noise ratio) can be achieved. MIMO and single-input multiple-output (SIMO) links can benefit directly from this SNR gain, enabling link enhancement by the application of diversity techniques.

Figure 10 displays the cross-correlation coefficient between the ordinary wave's channel and the extraordinary wave's channel throughout the day. This value was computed by correlating the impulse responses of both channels. Before calculating the coefficient, the impulse responses were previously synchronized, so the delay between the received waves was not taken into account. A probability graph was exhibited in order to evaluate if both received signals were decorrelated enough, depending on the hour of the day. Analyzing the results, it can be stated that there is a probability of nearly 40% to achieve a correlation coefficient below 0.7 in the happy hour intervals. The SNR of the received signals in these intervals could be improved by the usage of diversity techniques.

In Figure 11, the delay spread of the ordinary and extraordinary waves can be analyzed, respectively. The multipath of the NVIS link between Barcelona and Cambrils was studied throughout the day. All the undesired paths limited our channel's coherence bandwidth, thus affecting the data frame design and the link's performance.

The figure displayed below only takes into account the well-demodulated data frames. If a data frame did not present enough SNR and the PN sequences were not correctly found, no multipath was computed. Therefore, the following graph was analyzed together with the channel's availability, presented above (Figure 9). Only the hours where both channels were active (7 UTC to 16 UTC) were taken into account for the delay spread study in order to have accurate results.
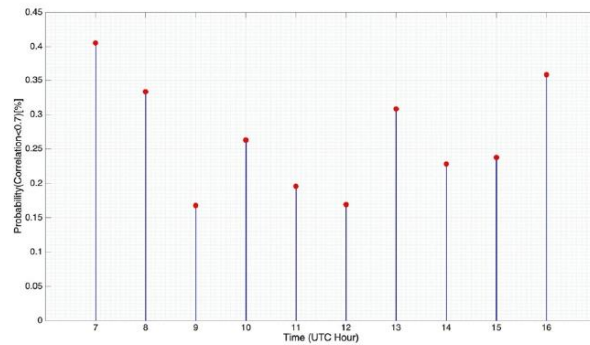
129

Figure 10. Probability (in %) of finding a cross-correlation coefficient below 0.7 between both channels.
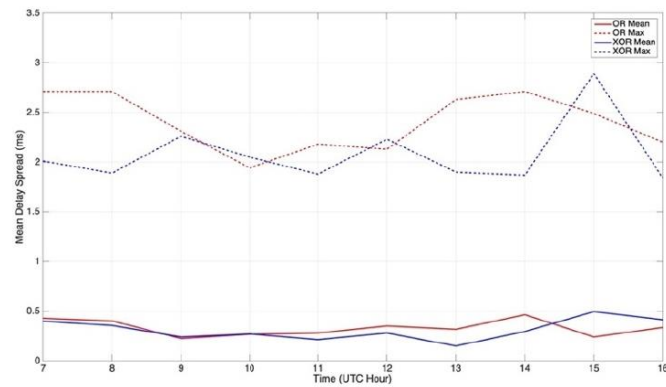

Figure 11. NVIS delay spread vs. time of the NVIS channels.

After carefully analyzing the delay spread of both channels, the highest value of the link was found to be 2.89 ms, corresponding to a coherence bandwidth of 346 Hz, and was provided by the extraordinary wave. On the other hand, the ordinary wave presented a peak value of 2.71 ms, corresponding to 369 Hz of coherence bandwidth. Both values implied receiving strong ISI among symbols in our system if we considered a time symbol of 0.42 ms (standards STANAG and MIL-STD-188 110, 2.38 kHz bandwidth). The coherence bandwidth of the ionospheric channel was thus defined as follows:

$$CB = 1/\sigma, \tag{1}$$

where σ corresponds to the delay spread. If we now study the less restrictive values, it can be observed that both waves often presented no multipath at all, as was observed in the mean values of the delay spread received (very low delay spread values). Therefore, the study of the mean value of the delay spread is key in our system design. The overall mean values of the delay spread of both channels were similar, presenting some differences if the graph was analyzed hour by hour. The differences in the multipath detected could only be observed if we compared all data frames individually, resulting in different instantaneous values. The mean value received of the ordinary wave was 0.33 ms, and the mean value received of the extraordinary wave was 0.31 ms. Taking into account the most-restrictive mean value (0.33 ms), which corresponds to a coherence bandwidth of 3 kHz (higher

than our used bandwidth; thus, our system overcame the ISI of the channel in almost all transmissions). Figure 12 displays the distribution of the delay spread of both ionospheric modes independently.
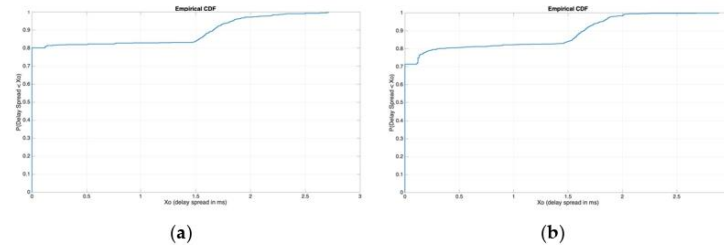

Figure 12. (**a**) NVIS delay spread distribution of the ordinary channel; (**b**) NVIS delay spread distribution of the extraordinary channel.

Another fundamental parameter to study for our NVIS system was the frequency offset that our link was affected by. This frequency variation depends on the movement between the transmitter and the receiver, which in our scenario should be produced by the displacement of the physical layers of the ionosphere. Notwithstanding this, the doppler shift caused by the ionosphere was negligible compared to the frequency variation that the clocks of the Red Pitaya platform produced. This shift was directly related to the temperature of the platform, which affected the clock's stability. The channel study performed in this research was implemented with rather cheap nodes, in a system where low-stability clocks are usual. Accordingly, a good data frame design and a good post-processing of the signals received was key to mitigate the negative effects of the usage of low-cost technologies.

Figure 13 exhibits a boxplot for all the hours throughout the day when the ionospheric channels are active. It can be appreciated that the maximum frequency offset received was -19.5 Hz and the minimum was -15 Hz, values that were remarkably higher than the ionospheric layer's Doppler shift (a value that can reach a maximum of 4 Hz, approximately [31]).
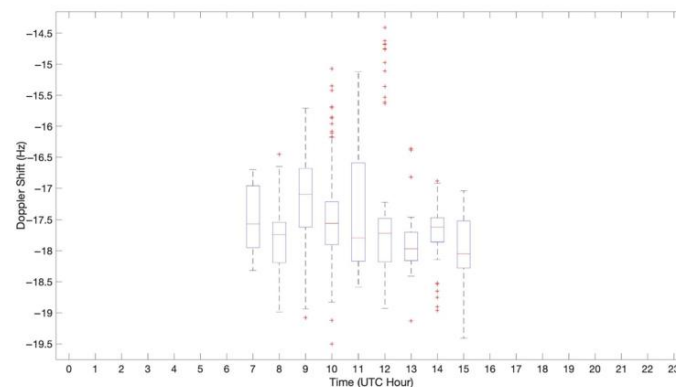

Figure 13. Frequency offset received vs. time.

Finally, we present the study of the combination of the ordinary and extraordinary wave's received. Tests on the bit error rate (BER) and bit energy-to-noise power spectral

density (E_b/N_0) of the system were performed to evaluate the improvement of the robustness achieved. The results of the fourth-order modulations with a transmit power of 50 W are presented below.

First of all, we measured the relationship between the E_b/N_0 received from the individual characteristic waves (ordinary and extraordinary) compared to the E_b/N_0 received as a result of the application of diversity combining techniques (selection combining and equal-gain combining). The E_b/N_0 of the signal received was computed as follows:

$$E_b/N_0 \text{ (dB)} = \text{SNR(dB)} + 10 \cdot \log 10(B) - 10 \cdot \log 10(Rb), \tag{2}$$

where Rb is the signal's bitrate (depends on the modulation order under test), B is the noise bandwidth of the measurement (2.3 kHz in our scenario), and SNR is the signal-to-noise ratio of the received signal.

Figure 14 presents the behavior of the ionospheric waves and their combining by the mean E_b/N_0 received throughout the day. Figure 14 only exhibits the 4QAM results in order to make the graph clearer. The 4PSK modulation presented almost identical performances in terms of E_b/N_0, while the 4FSK presented worse results. All three modulations are studied in terms of the BER in Figure 15. We can state that the selection combining (SC) technique presented a higher E_b/N_0 value than the individual ionospheric waves in all the studied hours. An improvement of up to 4 dB was achieved (at 12 UTC) while using this method. The equal-gain combining (EGC) technique also improved the performance of the link. An improvement of up to 3 dB was achieved (at 13 UTC), but there were certain times of the day (11 UTC, 14–16 UTC) when this technique did not improve the robustness of the link. Finally, we can also see that the mean E_b/N_0 received by the O and X modes differed by a maximum of 2 dB. Figure 14 compares the results obtained by using selection combining, equal-gain combining, the ordinary mode, and the extraordinary mode.
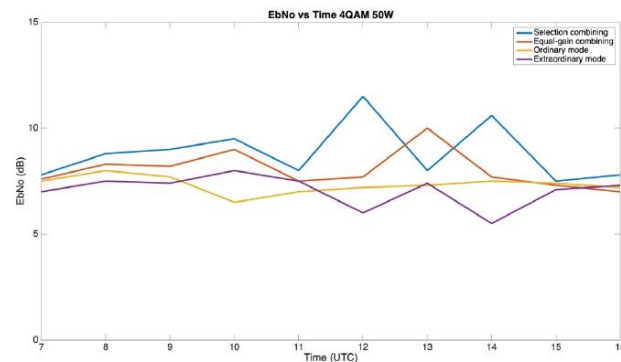
Figure 14. Received bit energy-to-noise power spectral density (E_b/N_0) for the 4QAM modulation at 50 W throughout the day.

Figure 15 presents the BER study performed in our link, specifically the fourth-order modulations with a transmitting power of 50 W. A clear improvement can be observed if we compare the characteristic waves individually with the combining of these techniques. The O and X (ordinary and extraordinary) modes had a 75% to 80% probability to achieve a BER lower than 10^{-4} when using the 4PSK and 4QAM modulations, respectively. If we used selection combining (SC), this probability improved up to 96% and 85%, respectively. On the other hand, if we used equal-gain combining (EGC), the probabilities to receive a BER lower than 10^{-4} improved to 82% for both modulations. The 4FSK modulation was the modulation with the worst performance. For the O and X waves, the 4FSK had a

55% to 57% of probability to achieve a BER lower than 10^{-4}, respectively. Using diversity combining, this probability improved up to 88% with SC and 59% with EGC.
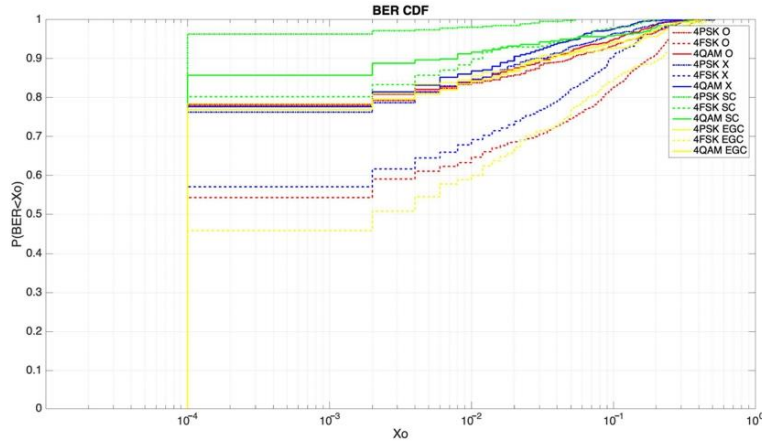

Figure 15. Cumulative distribution function (CDF) of the bit error rate for fourth-order modulations at 50 W.

5. Conclusions

In this work we present the single-frequency study of the two ionospheric characteristic waves as different communication channels. We analyzed the cross-correlation coefficient and the availability of both waves using nearly orthogonal polarized antennas. Similarly, we also studied the delay spread of both channels. We measured the frequency offset caused by the use of low-stability clocks on a low-cost system. Finally, we studied the BER and E_b/N_0 improvement of the system with the application of polarization diversity techniques, using selection combining and equal-gain combining. The research carried out in this work focused on two main objectives: the exploration of the feasibility of using polarization diversity techniques thanks to the decorrelation between the ordinary and extraordinary waves, and the study of the properties of each ionospheric channel for the optimization of the data frames in future studies and further channel characterization. From 17 UTC to 6 UTC, the lowest cross-correlation coefficient was found.

This work presents the comparison between all the parameters studied. Table 3 is exhibited below for a better understanding of these parameters.

Table 3. Channel study summary.

Parameter	Ordinary Wave			Extraordinary Wave		
	Max	**Min**	**Mean**	**Max**	**Min**	**Mean**
Availability (7 UTC to 16 UTC)	74%	30%	57.6%	94%	56.67%	72.2%
Delay Spread	2.71 ms	~0 ms	0.33 ms	2.89 ms	~0 ms	0.31 ms
SDR Frequency offset	−19.5 Hz	−14.5 Hz	−17.7 Hz	−19.5 Hz	−14.5 Hz	−17.7 Hz

The availability results showed that the extraordinary wave presented better results. Two "happy hour" [13] intervals were identified (sunrise and evening beginning), where the number of data frames detected by each ionospheric channel differed more. Another study realized in this work analyzed the usage of both signals simultaneously and the data frame detection between them both working together. The mean value of this new availability (from 7 UTC to 16 UTC) was 86%, increasing the results obtained by a singular

characteristic wave by more than 13%. These results encourage the study and application of diversity techniques and their combining at the receiver to increase the SNR of this NVIS link.

The delay spread (directly related to the multipath) of both channels was almost identical, a fact that allowed us to use the same coherence bandwidth for both channels. Having a huge value difference between both channels would imply the usage of the most restrictive data frames for the channel with the lower delay spread, not taking full advantage of the parameters of one channel.

The study of the Doppler shift was not performed properly because the system used a low-cost platform (higher frequency offset from the Red Pitaya clocks than the ionosphere's Doppler shift). Thus, well-designed data frame working together with a powerful post-processing of the signal are key to mitigate the channel's negative effect (up to ± 20 Hz in this work's infrastructure).

After analyzing the results obtained in the BER and E_b/N_0 studies, we can conclude that the application of polarization diversity implies an improvement in the robustness of the link. A higher E_b/N_0 and a lower BER were received using both selection combining and equal-gain combining. Selection combining presented the best results, improving the mean E_b/N_0 up to 4 dB compared to an individual ionospheric mode, and also remarkably lowering the BER results for the different modulations studied (4PSK, 4FSK, and 4QAM). Furthermore, we can also affirm that the ordinary and extraordinary waves were received with different mean E_b/N_0 values, which differed up to 2 dB.

According to our knowledge, no similar studies were performed for NVIS transmissions. The closest study for a channel like ours and the analysis of the different modes of the ionosphere was performed in [28] (a multifrequency study from 2012). Similar results were obtained in the multipath study for both the O and X modes. Our study, in addition, presented the availability of the different modes for NVIS transmissions and their correlation coefficients. The authors of [28] also presented a study of the BER improvement (up to 8% improvement) by the use of polarization diversity. Our system, on the other hand, improved the robustness of NVIS communications much more, up to 33% (4FSK at 50 W).

References

1. Davies, K. *Ionospheric Radio*; P. Peregrinus on Behalf of the Institution of Electrical Engineers: London, UK, 1990.
2. Budden, K.G. *The Propagation of Radio Waves*; Cambridge University Press: Cambridge, UK, 1985.
3. Watterson, C.; Juroshek, J.; Bensema, W. Experimental Confirmation of an HF Channel Model. *IEEE Trans. Commun.* **1970**, *18*, 792–803. [CrossRef]
4. Recommendation ITU-R. F.1487. *Testing of HF Modems with Bandwidths of up to about 12 kHz Using Ionospheric Channel Simulators*; International Telecommunications Union: Geneva, Switzerland, 2000.

5. Mastrangelo, J.; Lemmon, J.; Vogler, L.; Hoffmeyer, J.; Pratt, L.; Behm, C. A new wideband high frequency channel simulation system. *IEEE Trans. Commun.* **1997**, *45*, 26–34. [CrossRef]

6. Wagner, L.S.; Goldstein, J.A.; Rupar, M.A.; Kennedy, E.J. Delay, Doppler, and amplitude characteristics of HF signals received over a 1300-km transauroral sky wave channel. *Radio Sci.* **1995**, *30*, 659–676. [CrossRef]

7. Wagner, L.S.; Goldstein, J.A.; Meyers, W.D.; Bello, P.A. The HF skywave channel: Measured scattering functions for midlatitude and auroral channels and estimates for short-term wideband HF Rake modem performance. In Proceedings of the IEEE Military Communications Conference, "Bridging the Gap. Interoperability, Survivability, Security", Baltimore, MD, USA, 15–18 October 1989; Volume 3, pp. 830–839. [CrossRef]

8. Angling, M.J.; Cannon, P.S.; Davies, N.C.; Jodalen, V.; Lundborg, B.; Willink, T.J. Measurements of Doppler and multipath spread on oblique high-latitude HF paths and their use in characterizing data modem performance. *Radio Sci.* **1998**, *33*, 97–107. [CrossRef]

9. Cannon, P.S.; Angling, M.J.; Davies, N.C.; Wilink, T.; Jodalen, V.; Jacobson, B.; Lundborg, B.; Bröms, M. Damson HF channel characterisation—A review. In Proceedings of the 21st Century Military Communications. Architectures and Technologies for Information Superiority (MILCOM 2000), New York, NY, USA, 22–25 October 2002; Volume 1, pp. 59–64. [CrossRef]

10. Hervás, M.; Bergadà, P.; Alsina-Pagès, R.M. Ionospheric Narrowband and Wideband HF Soundings for Communications Purposes: A Review. *Sensors* **2020**, *20*, 2486. [CrossRef]

11. Witvliet, B.A.; Van Maanen, E.; Petersen, G.J.; Westenberg, A.J.; Bentum, M.J.; Slump, C.H.; Schiphorst, R. Near Vertical Incidence Skywave Propagation: Elevation Angles and Optimum Antenna Height for Horizontal Dipole Antennas. *IEEE Antennas Propag. Mag.* **2015**, *57*, 129–146. [CrossRef]

12. Porte, J.; Pijoan, J.L.; Masó, J.; Badia, D.; Zaballos, A.; Alsina-Pagès, R.M. Advanced HF Communications for Remote Sensors in Antartica. In *Antarctica—A Key To Global Change*, 1st ed.; IntechOpen: London, UK, 2019.

13. Witvliet, B.A. Near Vertical Incidence Skywave: Interaction of Antenna and Propagation Mechanism. Ph.D. Thesis, University of Twente, Enschede, The Netherlands, 2015.

14. Grisdale, G.; Morris, J.; Palmer, D. Fading of long-distance radio signals and a comparison of space- and polarization-diversity reception in the 6–18Mc/s range. *Proc. IEE Part B Radio Electron. Eng.* **1957**, *104*, 39–51. [CrossRef]

15. Jorgenson, M.B.; Johnson, R.W.; Moreland, K.W.; Serinken, N.; Chow, S.; Willink, T.J. Polarization diversity for HF data transmission. In Proceedings of the 7th International Conference on High Frequency Radio Systems and Techniques, Nottingham, UK, 7–10 July 1997; pp. 105–109. [CrossRef]

16. Witvliet, B.A.; Van Maanen, E.; Petersen, G.J.; Westenberg, A.J.; Bentum, M.J.; Slump, C.H.; Schiphorst, R. The importance of circular polarization for diversity reception and MIMO in NVIS propagation. In Proceedings of the 8th European Conference on Antennas and Propagation (EuCAP 2014), The Hague, The Netherlands, 6–11 April 2014; pp. 2797–2801. [CrossRef]

17. Enserink, S.; Köse, C.; Fitz, M.; Urie, M.; McCourt, R. A model for dual polarized HF MIMO communications. In Proceedings of the IEEE Military Communications Conference MILCOM, San Diego, CA, USA, 29 November–2 December 2015; pp. 1650–1655. [CrossRef]

18. Erhel, Y.; Lemur, D.; Oger, M.; Le Masson, J.; Marie, F. Evaluation of Ionospheric HF MIMO Channels: Two complementary circular polarizations reduce correlation. *IEEE Antennas Propag. Mag.* **2016**, *58*, 38–48. [CrossRef]

19. Umaisaroh, U.; Hendrantoro, G.; Mauludiyanto, A.; Fukusako, T. Capacity of 2×2 MIMO HF NVIS Channels With Linearly Polarized Horizontal Antennas. *IEEE Wirel. Commun. Lett.* **2019**, *8*, 1120–1123. [CrossRef]

20. Bergadà, P.; Alsina-Pagès, R.M.; Hervás, M. Polarization diversity in a long-haul transequatorial HF link from Antarctica to Spain. *Radio Sci.* **2017**, *52*, 105–117. [CrossRef]

21. Xilinx and Inc. Zynq-7000 SoC First Generation Architecture. 2012. Available online: www.xilinx.com (accessed on 2 November 2020).

22. Red Pitaya. Available online: https://www.redpitaya.com/ (accessed on 3 November 2020).

23. Buy a Raspberry Pi 3 Model B+—Raspberry Pi. Available online: https://www.raspberrypi.org/products/raspberry-pi-3-model-b-plus/?resellerType=home (accessed on 4 November 2020).

24. Austin, R.; Bull, P.; Buffery, S. A Raspberry Pi Based Scalable Software Defined Network Infrastructure for Disaster Relief Communication. In Proceedings of the 2017 IEEE 5th International Conference on Future Internet of Things and Cloud (FiCloud), Prague, Czech Republic, 21–23 August 2017; pp. 265–271. [CrossRef]

25. Digisonde 4D, Observatori de l'Ebre. Available online: http://dgs.obsebre.es:8081/ (accessed on 27 November 2020).

26. Witvliet, B.A.; Van Maanen, E.; Petersen, G.J.; Westenberg, A.J.; Bentum, M.J.; Slump, C.H.; Schiphorst, R. Measuring the Isolation of the Circularly Polarized Characteristic Waves in NVIS Propagation [Measurements Corner]. *IEEE Antennas Propag. Mag.* **2015**, *57*, 120–145. [CrossRef]

27. Porte, J.; Maso, J.M.; Pijoan, J.L.; Badia, D. Sensing System for Remote Areas in Antarctica. *Radio Sci.* **2020**, *55*. [CrossRef]

28. Hervás, M.; Pijoan, J.L.; Alsina-Pagès, R.M.; Salvador, M.; Altadill, D. Channel sounding and polarization diversity for the NVIS channel. In Proceedings of the Nordic HF Conference, Fårö, Sweden, 12–14 August 2013.

29. Maso, J.M.; Male, J.; Porte, J.; Pijoan, J.L.; Badia, D. Ionospheric Polarization Techniques for Robust NVIS Remote Sensing Platforms. *Appl. Sci.* **2020**, *10*, 3730. [CrossRef]

30. Jakes, W.C.; Cox, D.C. *Microwave Mobile Communications*; Wiley-IEEE Press: Hoboken, NJ, USA, 1994.

31. Ads, A.G.A.M. Soundings of the Ionospheric HF Radio Link between Antarctica and Spain. Ph.D. Thesis, Universitat Ramon Llull, Barcelona, Spain, 2013.

Annex 3

SC-FDE Layer for Sensor Networks in Remote Areas Using NVIS
Communications

electronics

MDPI

SC-FDE Layer for Sensor Networks in Remote Areas Using NVIS Communications

Tomas Gonzalez [ID], Joaquim Porte [ID], Jordi Male [ID], Joan Navarro [ID], Josep M. Maso [ID], Agustín Zaballos [ID], Joan L. Pijoan * and David Badia

La Salle Campus, Ramon Llull University, 08022 Barcelona, Spain; tomas.gonzalez@salle.url.edu (T.G.); joaquim.porte@salle.url.edu (J.P.); jordi.male@salle.url.edu (J.M.); jnavarro@salleurl.edu (J.N.); josep.maso@salle.url.edu (J.M.M.); agustin.zaballos@salle.url.edu (A.Z.); david.badia@salle.url.edu (D.B.)
* Correspondence: joanlluis.pijoan@salle.url.edu

Abstract: Despite high costs and lengthy deployments, satellite communications have traditionally been used to provide coverage in remote areas. However, given the fact that there is no radio infrastructure available in these areas, Near Vertical Incidence Skywave (NVIS) technology has positioned itself as an attractive alternative to communicate with low-power nodes in remote areas. This type of communication works in the HF frequency range complying with STANAG and MIL-STD standards, which define a physical layer for scenarios that differ from NVIS and low-power communication. The purpose of this paper was to present the definition of a new communication physical layer based on single-carrier frequency-domain equalization (SC-FDE) based on these standards but adapted to the ionospheric communication channel. This physical layer was compared to an OFDM-based layer from a previous study. The experiments performed show that this new approach achieves better results than OFDM in terms of a higher signal quality with a higher specific BER probability. Finally, this layer was also used in the theoretical design of an NVIS gateway to link sensor network devices spanning large-scale remote areas in a secure manner in the context of ubiquitous sensor networks (USN).

Keywords: remote sensing; HF; NVIS; IoT; OFDM; SC-FDE; SDR

1. Introduction

The use of sensor networks in remote areas plays a fundamental role in the development of applications such as fire detection and human rescue, among others. Monitoring these difficult-to-access areas and collecting in-field data have emerged as a popular research topic in the last 20 years [1,2]. This has motivated the conception of new distributed-computing paradigms such as the Internet of Things (IoT) or Ubiquitous Sensor Networks (USN) [1], in which several devices are deployed in a certain scenario and link together by means of a wireless (or not) network. There are many wireless technologies currently in use for IoT sensors [3]. Most of them (such as LoRa or Sigfox) rely entirely on already deployed infrastructure, which complicates their deployment in under-resourced or difficult-to-access areas. The most common way to install these networks for these kind of use-cases is using satellite communications. The main drawbacks of using satellites are their high installation cost [4,5] and their dependence on the satellite's orbit, which sometimes makes coverage difficult due to loss of line of sight (LOS) or low signal-to-noise ratio (SNR).

A cheaper and faster-to-deploy alternative without the need for LOS is Near Vertical Incidence Skywave (NVIS) that can be used to link nodes from a distributed sensor network spanning large-scale areas [6]. The NVIS technique is a good solution for deploying networks in infrastructureless (or remote) areas or in places where natural catastrophes have occurred. NVIS benefits from ionospheric reflection by transmitting high frequency (HF) signals with an angle of incidence between 70° and 90°. The ionosphere allows HF signals to bounce back due to ionization on some of its own layers, creating a coverage zone

of approximately 250 km (depending on many factors, such as the frequency or the time of day). Despite that, not all of the HF band can be used in a NVIS link [7] and the frequencies at which radio signals refract are between 3 MHz and 10 MHz [7]. Currently, NVIS nodes can be implemented on SDR platforms [8,9] and can achieve bit rates of up to thousands of bps (if higher data rates were needed, multiple antennas could be used to take advantage of the multipath effect or with multiple antennas using different channels [10,11]).

NVIS have to follow HF standards, which usually work with single carriers such as Quadrature Amplitude Modulation (QAM) or Phase-shift keying (PSK). These modulations require time-domain equalization to avoid multipath effects of the channel. Time-domain equalization is a computationally intensive implementation [12], which makes it unsuitable for low-cost platforms. Most current communications standards use the multicarrier scheme because of its adaptability and simple equalization [13]. These modulations have become widespread thanks to the exploitation of spectral bandwidth and the usage of mathematical expressions such as Fast Fourier Transform and the Inverse Fast Fourier Transform (FFT and IFFT) that optimize performance. For instance, Orthogonal Frequency-Domain Multiplexing (OFDM) was used in older versions of Wi-Fi [14]. Additionally, Orthogonal Frequency-Division Multiple Access (OFDMA) and Single-Carrier Frequency Division Multiple Access (SC-FDMA) are currently used for LTE and 5G in downlink (DL) and up-link (UL), respectively [15]. Indeed, recent studies confirm that such modulations could be used for resource-limited IoT devices [16–18].

Considering these modulations in the context of ionospheric communications, the study performed in [19] compared SC-FDE with OFDMA and SC-FDMA with ionospheric communications in an oblique way. In [20], an alternative solution with an OFDM transmission was proposed to avoid the complex equalization (OFDM requires frequency-domain equalization) for NVIS communications using the Zero Forcing (ZF) equalization method. The main drawback is that the subdivision of the bandwidth into subcarriers presents peaks in the envelope that cause a reduction in amplification capability.

The SC-FDE modulation has attracted significant interest in the field of research. In [21], a study of of SC-FDE synchronization technology in HF wireless communication using Minimum Mean Square Equalizer (MMSE) was proposed. In [22], an online Long Short-Term Memory (LSTM) estimator using HF Multiple-Input Multiple-Output (MIMO) SC-FDE systems was discussed. Furthermore, [23] proposed an efficient-channel parameters-estimation design for SC-FDE in HF wireless communications. This research endorsed the idea that SC-FDE can (1) be used for scenarios with challenging and noisy channels and (2) outperform OFDM in terms of power consumption by solving high Peak-to-average Power Ratio (PAPR) issues [24].

This paper defined a protocol for low-power NVIS communications that applies SC-FDE modulation to link nodes from wireless sensor networks deployed in remote areas. Compared with OFDM, SC-FDE improves the PAPR and reduces the complexity of transmitting nodes, as it is less sensitive to Inter-Block Interference (IBI) and Inter-Carrier Interference (ICI) caused by the multipath effect [25–27].

The outline of the paper is as follows. First, a background study and a summary of the theoretical concepts used in the protocol definition is provided in Section 2. Secondly, the use case is explained in Section 3 to contextualize and analyze the design of the system explained in Section 4 and the framework design is detailed and schematized in Section 4. Section 5 exhibits the tests results and, finally, Section 6 presents the conclusions.

2. Background Study

The following subsections outline the theoretical background regarding (1) the evolution of the HF communications, (2) NVIS history and current characteristics, and (3) the SC-FDE modulation to be analyzed.

2.1. HF Communications Evolution

HF communications started out as point-to-point and shortwave, and were mostly used by radio amateurs. Technical evolution and continuous research have led to these communications being used over long distances with several generations of advances. The first generation (1G) focused on narrowband systems with amplitude modulations for voice transmission with a 3 kHz channel (current standards as STANAG and MIL-STD keeps this channel bandwidth). Subsequently, attempts were made to improve performance with different modulations such as FSK, PSK, or QAM. The main drawback was the choice of frequency, as it was variant during the day. In the second generation (2G), microprocessors were introduced, and progress was made towards digital communications and signal processing. With this, point-to-multipoint communications were achieved. Finally, an interesting development was the Automatic Link Establishment (ALE), which allowed not to be in constant analysis of frequencies, but had a high cost of computing and very poor signal processing. The third generation (3G) improved the links, being faster and with a lower SNR. It also supported larger networks, and improved the efficiency of the entire network by separating channels for link establishment and traffic communications. The fourth generation (4G) already involves advances in artificial intelligence and broadband, and seeks the integration of systems with high data volumes and throughput [28,29].

2.2. NVIS

The use of NVIS communications dates back to the Vietnam War in the late 1960s. However, it is known that this type of communication had already been in use since 1939 at the advent of World War II, although not under this name. These communications were high-powered and were aimed primarily for voice transmission. In these systems, reference was already made to the use of antennas as horizontal dipoles to cover bands from 2 to 8 MHz with the objective of covering 24 h of operation due to the bouncing characteristics of the ionosphere using short waves [30]. In the overview of [31], a brief review of the history of NVIS is provided which starts with the discussion of the existence of the Hevyside layer by [32] as well as the Appleton and Builder experiment using the ionosphere as a refraction medium [33]. The reason for the use of these communications boils down to their rapid deployment and widespread supply.

The HF band has always been used for long distance communications with antennas at a low angle to the horizon. In this way, a coverage area of 250 km around the transmitter is produced. However, the link distance depends on the angle: the smaller the angle, the lower the Maximum Usable Frequency (MUF), mainly between 3 and 10 MHz [7]. Even so, the biggest disadvantage of this type of communication is the availability and behavior of the ionosphere due to the ionization of its own layers and solar activity. This implies that these communications will not be available during certain times at the same frequency. The use of multiband antennas can assure communication for an entire day. As an advantage, these communications are easy to install due to their antennas, they usually feature low-cost platforms, and they do not require the transmitter and receiver to have direct line of sight, allowing them to overcome large mountains, which makes them ideal for remote areas.

The antennas are usually wired and dipole types in order to optimize performance [7]. The horizontal dipole and the inverted Vee are the most frequently used antennas for NVIS, the latter being more interesting due to the need for a single mast [34].

To reduce the size of the antennas and to power the sensors with batteries, an efficient physical layer is required that can work with the lowest possible transmit powers and simple equalization.

2.3. SC-FDE

SC-FDE has the particularity of having the IFFT function in the receiver, which solves the main multicarrier modulation problems (high PAPR and low signal-to-noise ratio). The IFFT is performed at the receiver side together with the FFT [35]. This avoids the need for

precise frequency synchronization and for a linear amplifier. In addition, it has advantages such as having almost constant envelope characteristics, being considered a single carrier, and using a simple equalization as it is performed in the frequency domain [26]. Furthermore, it also maintains some of the advantages such as the integration of Cyclic Prefix (CP), where the multipath effect produced by ionospheric transmissions can be avoided, thus making the transmission more robust. Considering the ionosphere channel results in [36], the CP can be variably designed to fit the channel, resulting in higher efficiency without the need for multiple symbols to avoid multipath.

Figure 1 displays a block diagram of the OFDM modulation and the IFFT position change for the SC-FDE implementation. Serial bits are converted to symbols (Mapping), taking into account the modulation order after the parallel conversion. After that, the Cyclic Prefix is added to then convert all the symbols to serial again for transmission purposes. On the receiver side, the CP is removed and the FFT algorithm is applied. Then, the equalization is performed to compensate for the channel effects. Finally, the IFFT is applied along with the serial to parallel conversion in order to obtain the array of bits.
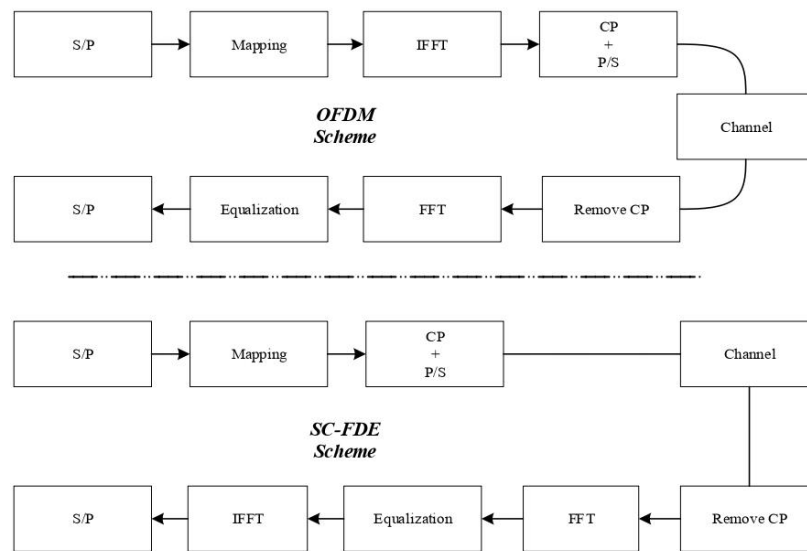

Figure 1. OFDM and SC-FDE schemes. Note the change of IFFT position between OFDM and SC-FDE.

In SC-FDE pilot schemes, values have a variation compared with other modulations. For example, OFDM can have a symbol full of pilots (all the subcarriers with the same value). In contrast, SC-FDE needs to have different pilot values due to the FFT, which converts these values to zero. Therefore, the root Zadoff-Chu sequence must be used, which is a sequence that presents different values but in-module are the same value [37].

SC-FDE modulation is noise-sensitive, so the equalization method can be improved by taking noise into account, as well as the effects of the channel.

Additionally, the study in [26] showed that other equalization types are better than the ZF. MMSE and Maximum Likelihood (ML) had the best performance. Nevertheless, the research performed in [38] showed that, despite being the one with the best results, the ML method is much more complex in computational terms. Therefore, it is also possible to estimate noise and use (1), which outperforms the (2) method when noise cannot be

considered negligible, although it is not as robust against Inter-symbol Interference (ISI) [39]. H_{est} is the channel effect estimation and σ^2 is the variance of the noise.

$$H_{mmse} = \frac{H_{est}*}{(|H_{est}|^2 + \sigma^2)} \qquad (1)$$

$$H_{zf} = \frac{1}{H_{est}} \qquad (2)$$

As noted above, multicarrier techniques produce peaks due to the division of the channel into subcarriers, which produces a high PAPR value. Many techniques, such as the Crest Factor Reduction (CFR) try to reduce this negative point. This commonly used technique uses different methods to reduce the peaks such as Clipping and Filtering, Peak Windowing, and Peak Cancellation, among others. Clipping is a very good option to reduce the PAPR due to its low computational cost and high effectiveness [40,41]. It consists of saturating the signal above a fixed threshold called Clipping Ratio (CR). It helps to increase the average power; however, one of its main drawbacks is that it introduces higher nonlinearity, causing out-of-band emissions and interference to the target link.

The clipping ratio is calculated in Equation (3) and illustrated in Figure 2. It shows an example of how the signal reacts to this technique. The signal x(n) maintains its value as long as it does not exceed a certain threshold. This threshold is set from the maximum peak power. If x(n) overcomes the threshold the signal value automatically becomes the CR value (x_clipping(n) in the figure).

$$y(n) = \begin{cases} x(n), \ \max(|x(n)| < \ CR \\ CR, \ \max(|x(n)| \geq \ CR \end{cases} \qquad (3)$$
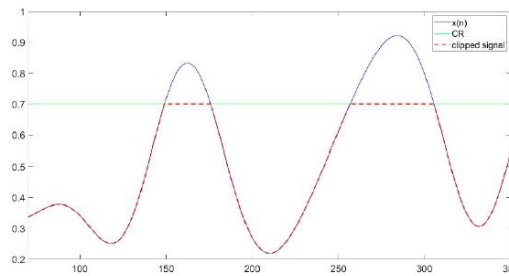

Figure 2. Clipping technique. The red line shows the original signal, and the blue line shows the clipped signal due to the threshold drawn in green [42].

3. Use Case

One of the great advantages of the NVIS technology is that it enables the rapid deployment of medium-distance (less than 250 km) communications with no line of sight at a very low cost. This results in a very convenient alternative when designing IoT environments for remote scenarios where sensing (and/or actuating) nodes are deployed to span large-scale areas and no other communication technologies are available.

In this case, as shown in Figure 3, the whole IoT scenario can best be viewed as a Ubiquitous Sensor Network [43] where sensors are grouped—by means of a concentrator/hub— around the NVIS node which, in turn, acts as a communication gateway to link with the nodes from neighboring IoT domains. In this way, the sensor network can use more standard communication technologies (e.g., Bluetooth, Wize) that are typically available in sensor devices. Additionally, following the principles of edge computing [44] and considering the limited bandwidth available at the NVIS link, this communication gateway can

also behave as an edge node where data are aggregated and summarized. If an Internet connection were available at any IoT domain, the NVIS node could also behave as a sink node to forward all the collected data elsewhere.
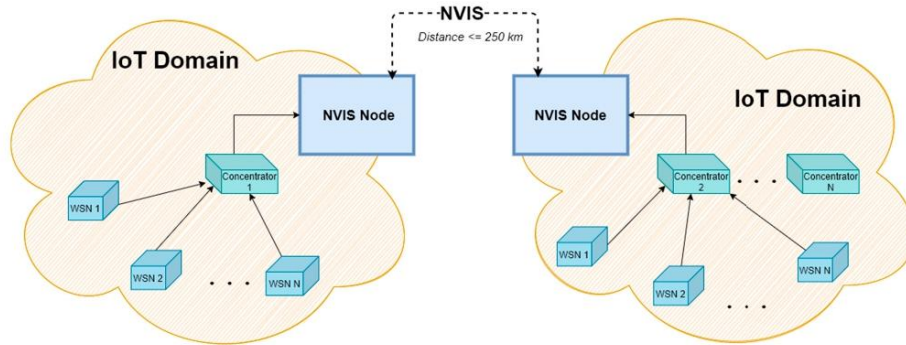

Figure 3. System model deployment.

4. System Design

In order to be able to establish a system adapted to the use case, we explain how the platform is composed and the design of the physical layer.

4.1. Platform Overview

The current platform is based on the concept of Software-Defined Sadio (SDR). SDR allows the independence of certain radio hardware components to operate independently as they are implemented by software. This fact offers many possibilities, especially when the transmitted protocols are not the same and some values (the carrier frequency, for example) need to be set several times for different scenarios.

The boards used for the signal processing were two Red Pitaya STEMLab 125-14 [45]. They present a ZYNQ SoC, including a field-programmable gate array (FPGA) and a central processing unit (CPU), an analog-digital converter (ADC) and a digital-analog converter (DAC). These converters present a resolution of 14 bits and are managed by a 125 MSPS clock.

The operating schemes of the Red Pitaya were based on two blocks: the processing system (PS) and the programmable logic (PL). On one side, the PS refers to the CPU, in which, in our case, an operating system (OS) is installed over this PS. This is where the configuration files are located and the peripherals, such as the external memory, are managed. On the other hand, the PL manages all the upsampling and downsampling, making use of the DUC/DDC converters that have been programmed using mainly FIR and CIC filters. The convergence of the two worlds is done through the RAM which, thanks to the direct shared memory (DMA), allows the transmission of data from the PS to the PL. In this case, the PS shares the data to be processed with the DMA, and the DMA passes the data to the PL through a FIFO memory where the DUC/DDC performs all the processing.

A microprocessor is connected to the Red Pitaya, which is in charge of time synchronization and the management of different peripherals. In addition, it is responsible for saving the raw files for transmission and also saving the received files for further post-processing. The microprocessor model chosen was the Raspberry Pi 3 [46].

A class-A amplifier was chosen to transmit signals with amplitude or phase changes that require linearity. The chosen model was a Bonn BLWA 0103-250 [47], which works at frequencies within the NVIS band and performs well in terms of efficiency. It was

143

connected to the output of the Red Pitaya and enabled output powers above 54 dBm, although we should mention here that we did not use more than 25 W in our tests.

On the receiver side, an amplifier was used only to preamplify the signal by 30 dB without degrading its SNR. In addition, a Low Noise Amplifier (LNA) was used to perform proper demodulation. A Band Pass Filter (BPF) on both sides prevented external interference at frequencies around our carrier frequency. The carrier frequency was set to 5.4 MHz due to previous ionosphere behavior analysis. At the transmitter side, a horizontal dipole was used, and two inverted Vees were used at the receiver due to the straightforwardness of their installation, together with a respectable gain of 6.8 dB [48]. Having two antennas on the receiver increases the availability of communications by taking advantage of both the Ordinary and Extraordinary skywaves and using them to apply the Single Input Multiple Output (SIMO) technique, but in this case, we just used the Ordinary skywave due to its higher gain [49].

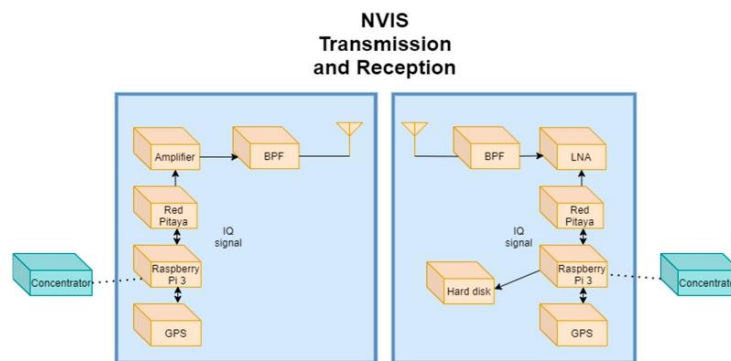Figure 4 exhibits an overview of the whole system in a schematic way.

Figure 4. Near-vertical incidence skywave (NVIS) transmission scheme (transmitter on the left and receiver on the right).

4.2. Frame Design

In other NVIS studies, such as [8,9,49–51], narrowband modulations have proven that communications are quite reliable in a wide range of scenarios. So far, HF standards (military or otherwise) have used 3 kHz channels with single-carrier modulations such as PSK and QAM. An OFDM protocol was designed and tested in [47] for low-power applications with this same channel bandwidth.

The SC-FDE design follows almost the same structure as OFDM, only the SC-FDE concept distributes the symbols shorter in the time domain but longer in the frequency domain. The symbol length was calculated by simply dividing the symbol length defined in [20] by the number of subcarriers defined due to the coherence bandwidth. We kept the same CP due to the maximum delay spread of 3 ms. In fact, the study performed in [36] concluded that Delay Spread values for the Ordinary channel reached around 2.7 ms during the ionosphere availability. However, if we consider the mean, the values were about 0.5, so this fact caused the CP to have a very large error margin.

Finally, we used six SC-FDE symbols and only one extra symbol to obtain known sequences in order to have enough samples to perform an equalization. For our case, we chose the MMSE equalization, which is ideal for low SNR because it balances the channel and noise estimation.

With this configuration, a bit-rate of almost 4 kbps (2% more than the OFDM) and PAPR around 2 dB (more than 5 dB less than the OFDM) could be achieved, taking into account that it could have been even higher if the CP were variable and set to the mean Delay Spread (Ds) of the channel at a given time.

In Table 1, all the parameters of the SC-FDE design are summarized. Additionally, they are compared to the OFDM design proposed in [20] since they have a similar configuration.

Table 1. SC-FDE parameters.

Parameters	SC-FDE Values	OFDM Values
Bandwidth	3 kHz	3 kHz
Useful symbol length (TS)	0.33 ms	9.33 ms
Prefix cyclic length (TCP)	3 ms	3 ms
Number of subcarriers (NSC)	28	28
Number of symbols (Nsymbol)	7	7
Number of pilot/symbol	1	1
Number of data symbol	6	6
Packet duration	87.64 ms	86.31 ms
Bits in packet	336 bits	324 bits
Modulation	QPSK	QPSK
Equalization	MMSE	ZF
Bitrate of signal frame	3.833 kbps	3.753 kbps

5. Experimental Evaluation

In this section, we explain the tests that have been carried out to verify the behavior of the modulation depending on the power transmission considering the transmission success.

In this case, we wanted to evaluate a sweep of each Bit-error rate (BER) value and obtain its probability of occurrence. Moreover, to check how the channel and noise affect each modulation, many measures can be assessed, such as the Error Vector Magnitude (EVM), which measures the quality of the signals by looking at the deviation of the points from the ideal constellation due to the effects of the channel. Other alternatives include the Modulation Error Rate (MER), which is related to the EVM when average power is compared, or more commonly the BER-E_bN_0. In our research, we analyzed the BER-E_bN_0, a parameter that provides a quick overview of the received signal's performance.

For the tests, we decided to first check the success rate of the SC-FDE and decided to optimize the transmission power by adopting the clipping technique. In addition, we compared the BER/E_bN_0 with the OFDM, FSK, and QAM from the study performed in [20].

5.1. Test Area

The NVIS transmitter was located in La Salle Campus Barcelona (Spain). It has a horizontal dipole set at 5.4 MHz. The receiver, which consists of an inverted Vee, was located approximately 100 km away (Cambrils, Tarragona). Between these locations, there was no Line Of Sight (LOS) considering the elevation of the profile, which is more than 500 m high. The NVIS link is shown in Figure 5.

Figure 5. NVIS link between LaSalle Campus, BCN and Cambrils, Tarragona. The highest peak is located at 573 m above sea level.

5.2. Test Design

To test our system, a new protocol was defined following the same structure as in [20,48] but with the addition of the SC-FDE modulation. The frequency was fixed at 5.4 MHz.

A total of 50 frames were transmitted, each of which composed of a group of four packets. All frames started with an initial 6th Pseudorandom Noise (PN) sequence with re-sampling of 8 and having a length of 5 ms. This was used to do the packet synchronization.

Each packet was then composed by grouping a 60 ms tone, another 5 ms PN sequence, and one of the four modulations. The tone included in each packet allowed the Doppler shift of each modulation to be corrected. This effect is due to the Red Pitaya's clocks, which can provoke deviations of up to 10 Hz by side, so a total of 20 Hz of Doppler shift and the PN allows for the identification each modulation. Finally, this was repeated four times (once for each modulation) to form the frame.

IoT devices are usually remote, and battery usage requires low power consumption; therefore, transmission power must be minimized [52]. Knowing that the OFDM studied in [20] had sufficient performance around 12 W, our SC-FDE system was evaluated for 6, 12, and 25 W.

After this first approach, a second test rig was designed to perform the consumption optimization. A sweep of clipping values from 3 dB to 8 dB has been performed.

6. Results

This section presents the results achieved when comparing the transmission power to observe the cumulative distribution function (CDF) and OFDM along with the PAPR. The CDF graphs consist of different BER values on the abscissa axis (Xo in the figure) and the probabilities of obtaining them displayed at the ordinate axis (P(BER<Xo)).

6.1. BER CDF

Figure 6 exhibits a CDF graph of the BER computed in the received signals. It can be observed that having a peak power of 6 W, the probabilities of receiving a BER under 10^{-2} were remarkably high (more than 90%), but also a good performance to have a BER of 10^{-3}, which is over 70%. With regard to the 12 W test, the SC-FDE showed very good results, obtaining probabilities of over 80% for BER 10^{-3} and more than 90% for BER under 10^{-2}. Finally, for the same test with a peak power of 25 W, it can be observed that SC-FDE outperformed the other models, having probabilities of almost 90% to have BER 10^{-3} and around 95% for BER under 10^{-2}. As a first conclusion, it can be stated that the SC-FDE provides high yields for low power, especially around 12 W.
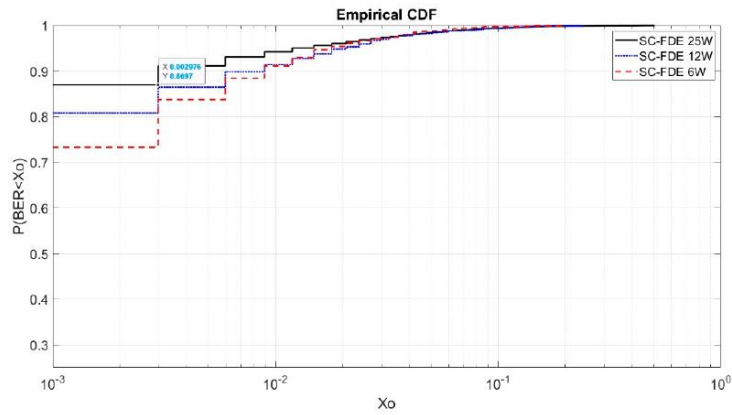
146

Figure 6. CDF plot of SC-FDE modulation with 6 W, 12 W, and 25 W of peak power.

6.2. BER vs. E_b/N_o

On the other hand, Figure 7 presents the relationship between received power (EbNo) and the BER obtained along with the FSK, QAM, and OFDM studied in [20].
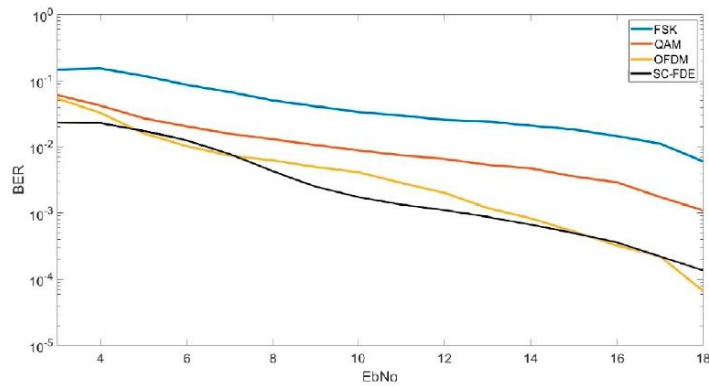

Figure 7. BER vs. EbNo comparison between FSK, QAM, OFDM, and SC-FDE.

FSK and QAM need higher EbNo than the OFDM and SC-FDE, which show very similar results. For BER of 10^{-3}, the SC-FDE needs 1 dB less than the OFDM, but for BER 10^{-4}, the OFDM needs 17.5 dB and the SC-FDE needs more than 18 dB.

6.3. CR Sweep

Taking into account these results and in a bid to raise the average power, a CR sweep was studied, with values starting at 3 dB with 1 dB steps up to 8 dBs. The higher the CR, the higher the Error Vector Magnitude (EVM) due to the saturation produced by the signal limitations. Despite having a higher EVM, the BER could be better due to the average power increase. The trade-off between power consumption and BER results must be considered.

147

As shown in Figure 8, we analyzed the CR tests with a transmitting power of 6 W. A significant difference can be observed when CRs were applied and when they were omitted. Initially, a probability of about 70% for a BER of 10^{-3} with a CR of 3 dB was obtained. If a CR of 6 dB was applied, a probability of more than 85% for a BER of 10^{-3} could be attained.
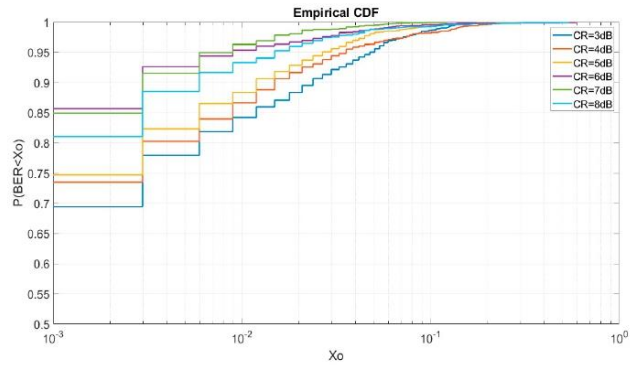

Figure 8. 6 W SC-FDE CR sweep CDF.

The graph below also shows how the CDF increases when the CR is higher. By dropping the peaks produced by the multicarrier splitting, the SNR and MER improved. However, from 6 dB (which is the best CR value) the CDF started to decrease again. This result was produced by the signal limiting, as the high-power peaks disappear and, therefore, relevant data was lost. This is the point where the EVM was large enough, and the increase of average power did not help due to the large in-band distortion.

6.4. CR Sweep 12 W

Figure 9 displays the same test of a peak power of 12 W. The results are quite similar, and only present some variations.
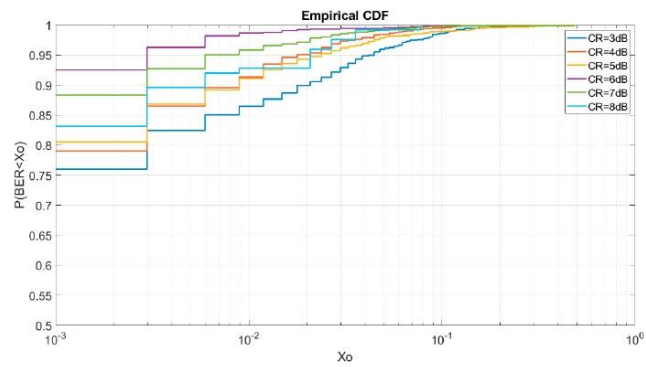

Figure 9. 12W SC-FDE CR sweep CDF.

6.5. CR Sweep 25 W

Figure 10 presents the results of the CR sweep for a peak power of 25 W. The point here is that the changes compared to 12 W were not that significant. For the low CR values,

148

the increase of the performance was relevant. By contrast, the high values did not change so much.
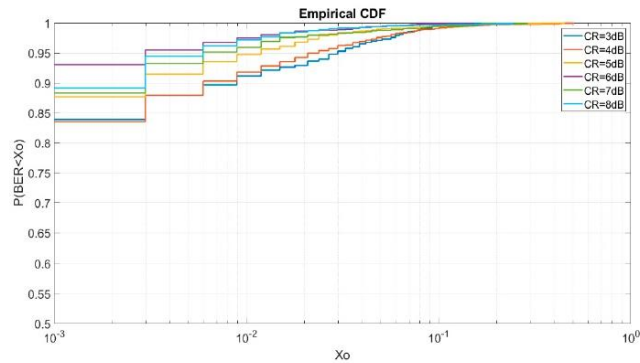

Figure 10. 25 W SC-FDE CR sweep CDF.

Results from Figure 10 show that 25 W is not worth implementing due to the higher consumption and near-identical behavior of 12 W. Comparing the three power scenarios, the BER-consumption ratio makes the 12 W the best configuration, saving the 6 W for more ideal scenarios without large multipaths or almost-null noise.

7. Conclusions

In this work we presented an analysis of the SC-FDE with the objective of improving the performance of NVIS communications following the STANAG and MIL-STD standards.

This study was carried out using two NVIS nodes 100 km apart. From the results of these transmissions, we can conclude that the SC-FDE together with an MMSE equalization obtains a much higher success rate than OFDM studied previously under the same conditions [20], making it much more efficient. As seen in the plots, this physical layer achieved a success rate of 93% BER 10^{-3} for the SC-FDE using the appropriate CR values at the expense of needing higher E_bN_0. With the same probability, the ODFM under the same conditions could only meet BER 10^{-2}. Apart from that, taking the best configuration of both, the OFDM needed a CR of 9 dB and the SC-FDE needed 3 dB less signal saturation. Moreover, by having the CP, the protection against the multipath effect is quite relevant. In addition, the CP set at the limits can be 33% more efficient in the case of no having multipath and slightly better if the symbol used to equalize has fewer pilot symbols. Finally, this physical layer will allow the use of low power amplifiers for battery-powered sensors, or use compact antennas with controlled losses of up to 10 dB. As an application, this protocol can be used as a platform for transmitting data collected from IoT devices and is suitable for USN thanks to the defined low transmitting powers. A disadvantage to take into account is that the bitrate in this type of communication is not particularly high, but it is not critical because remote sensors do not need high rates, but rather a strong communication robustness.

In future works, an exhaustive study of OFDM and SC-FDE together with their multiple access techniques (OFDMA and SC-FDMA) will be conducted, optimizing this physical layer, in order to try to define a complete uplink and downlink of NVIS technology. We will also study different bandwidths outside the standards in order to achieve higher bitrates.

Author Contributions: Investigation, T.G., J.P., J.M., J.L.P. and D.B.; methodology, J.L.P. and D.B.; software, T.G., J.P. and J.M.; supervision, A.Z., J.M.M., J.N., J.L.P. and D.B.; validation, J.L.P. and D.B.;

writing—original draft, T.G., J.P. and J.M.; writing—review & editing, T.G., J.P., J.M., J.N., J.M.M., A.Z., J.L.P. and D.B. All authors have read and agreed to the published version of the manuscript.

Conflicts of Interest: The authors declare no conflict of interest.

Abbreviations

ADC	Analog-Digital Converter
BER	Bit-error rate
BPF	A Band Pass Filter
CDF	Cumulative Distribution Function
CFR	Crest Factor Reduction
CP	Cyclic Prefix
CPU	Central Processing Unit
CR	Clipping Ratio
DAC	Digital-Analog Converter
DL	Downlink
Ds	Delay Spread
EVM	Error Vector Magnitude
FFT	Fast Fourier Transform
FPGA	Field-programmable gate array
HF	High Frequency
IBI	Inter-Block Interference
ICI	Inter-Carrier Interference
IFFT	Inverse Fast Fourier Transform
IoT	Internet of Things
ISI	Inter-symbol Interference
LNA	Low Noise Amplifier
LOS	Line of Sight
LSTM	Long Short-Term Memory
LTE	Long-Term Evolution
MER	Modulation Error Rate
MIMO	Multiple Input Multiple Output
ML	Maximum Likelihood
MMSE	Minimum Mean Square Equalizer
MUF	Maximum Usable Frequency
NVIS	Near Vertical Incidence Skywave
OFDM	Orthogonal Frequency Division Multiplexing
OFDMA	Orthogonal Frequency-Division Multiple Access
PAPR	Peak-to-average Power Ratio
PN	Pseudorandom Noise
PSK	Phase-shift keying
QAM	Quadrature Amplitude Modulation
SC-FDE	Single-Carrier Frequency-domain Equalization
SC-FDMA	Single-Carrier Frequency Division Multiple Access
SDR	Software Defined Radio
SIMO	Single Input Multiple Output
SNR	Signal-to-noise ratio
UL	Uplink
USN	Ubiquitous Sensor Networks
USN	Ubiquitous Sensor Network
ZF	Zero Forcing

References

1. Bagula, A.; Zennaro, M.; Inggs, G.; Scott, S.; Gascon, D. Ubiquitous sensor networking for development (USN4D): An application to pollution monitoring. *Sensors* **2012**, *12*, 391–414. [CrossRef]
2. Wang, J.; Lim, M.K.; Wang, C.; Tseng, M.L. The evolution of the Internet of Things (IoT) over the past 20 years. *Comput. Ind. Eng.* **2021**, *155*, 107174. [CrossRef]
3. Gazis, V.; Gortz, M.; Huber, M.; Leonardi, A.; Mathioudakis, K.; Wiesmaier, A.; Zeiger, F.; Vasilomanolakis, E. A survey of technologies for the internet of things. In Proceedings of the IWCMC 2015—11th International Wireless Communications and Mobile Computing Conference, Dubrovnik, Croatia, 24–28 August 2015; Institute of Electrical and Electronics Engineers Inc.: Piscataway, NJ, USA, 2015; pp. 1090–1095. [CrossRef]
4. Smallsat Launch Services Feel Pricing Pressure-SpaceNews. Available online: https://spacenews.com/smallsat-launch-services-feel-pricing-pressure/ (accessed on 20 May 2021).
5. The Cost of Building and Launching a Satellite | Globalcom Satellite Phones. Available online: https://globalcomsatphone.com/costs/ (accessed on 20 May 2021).
6. Porte, J.; Briones, A.; Maso, J.M.; Pares, C.; Zaballos, A.; Pijoan, J.L. Heterogeneous wireless IoT architecture for natural disaster monitorization. *Eurasip J. Wirel. Commun. Netw.* **2020**, *2020*, 184. [CrossRef]
7. Witvliet, B.A.; van Maanen, E.; Petersen, G.J.; Westenberg, A.J.; Bentum, M.J.; Slump, C.H.; Schiphorst, R. Near Vertical Incidence Skywave Propagation: Elevation Angles and Optimum Antenna Height for Horizontal Dipole Antennas. *IEEE Antennas Propag. Mag.* **2015**, *57*, 129–146. [CrossRef]
8. Porte, J.; Maso, J.; Pijoan, J.L.; Miret, M.; Badia, D.; Jayasinghe, J. Education and e-health for developing countries using NVIS communications. In Proceedings of the IEEE Region 10 Humanitarian Technology Conference, R10-HTC, Malambe, Sri Lanka, 6–8 December 2019; Institute of Electrical and Electronics Engineers Inc.: Piscataway, NJ, USA, 2019. [CrossRef]
9. Porte, J.; Maso, J.; Pijoan, J.L.; Badia, D. Design, implementation, and test of an SDR for NVIS communications. *Int. J. Circuit Theory Appl.* **2019**, *47*, 1502–1512. [CrossRef]
10. Daniels, R.C.; Peters, S.W. A new MIMO HF data link: Designing for high data rates and backwards compatibility. In Proceedings of the Proceedings-IEEE Military Communications Conference MILCOM, San Diego, CA, USA, 18–20 November 2013; pp. 1256–1261. [CrossRef]
11. Daniels, R.C.; Peters, S.W.; Heath, R.W. HF MIMO NVIS measurements with co-located dipoles for future tactical communications. In Proceedings of the IEEE Military Communications Conference MILCOM, San Diego, CA, USA, 18–20 November 2013; pp. 1250–1255. [CrossRef]
12. Kuschnerov, M.; Piyawanno, K.; De Man, E.; Chouayakh, M.; Spinnler, B.; Alfiad, M.; Napoli, A.; Lankl, B. Data-aided single-carrier coherent receivers. In Proceedings of the Conference Proceedings-Lasers and Electro-Optics Society Annual Meeting-LEOS, Belek-Antalya, Turkey, 4–8 October 2009; pp. 638–639. [CrossRef]
13. Fazel, K.; Kaiser, S. Multi-Carrier and Spread Spectrum Systems: From OFDM and MC-CDMA to LTE and WiMAX | Wiley eBooks | IEEE Xplore. Available online: https://ieeexplore.ieee.org/book/8039579 (accessed on 29 April 2021).
14. Narasimhamurthy, A.B.; Banavar, M.K.; Tepedelenliouglu, C. OFDM Systems for Wireless Communications. *Synth. Lect. Algorithms Softw. Eng.* **2010**, *2*, 1–78. [CrossRef]
15. Navita, A.; Amandeep, N. Performance analysis of OFDMA, MIMO and SC-FDMA technology in 4G LTE networks. In Proceedings of the 2016 6th International Conference-Cloud System and Big Data Engineering, Confluence 2016, Noida, India, 14–15 January 2016; Institute of Electrical and Electronics Engineers Inc.: Piscataway, NJ, USA, 2016; pp. 554–558. [CrossRef]
16. Choi, J. Single-Carrier Index Modulation for IoT Uplink. *IEEE J. Sel. Top. Signal. Process.* **2019**, *13*, 1237–1248. [CrossRef]
17. Iraqi, Y.; Al-Dweik, A. Efficient Information Transmission Using Smart OFDM for IoT Applications. *IEEE Internet Things J.* **2020**, *7*, 8397–8409. [CrossRef]
18. Hussein, A.; Elgala, H. *Lightweight Multi-Carrier Modulation for IoT*; Broadband Access Communication Technologies XII; International Society for Optics and Photonics: San Francisco, CA, USA, 2018; p. 105590W. [CrossRef]
19. Hervás, M.; Alsina-Pagès, R.M.; Pijoan, J.L.; Salvador, M.; Badia, D. Advanced modulation schemes for an Antarctic Long Haul HF Link: Performance comparison between SC-FDE, OFDMA and SC-FDMA in a hostile environment. *Telecommun. Syst.* **2016**, *62*, 757–770. [CrossRef]
20. Maso, J.M.; Gonzalez, T.; Male, J.; Porte, J.; Pijoan, J.L.; Badia, D. NVIS multicarrier modulations for remote-sensor applications. *Sensors* **2020**, *20*, 6232. [CrossRef] [PubMed]
21. Boyuan, X.; Weizhang, X. Research of the SC-FDE synchronization technology in HF wireless communication. In Proceedings of the 2013 IEEE 8th Conference on Industrial Electronics and Applications, ICIEA 2013, Melbourne, Australia, 19–21 June 2013; pp. 1420–1423. [CrossRef]
22. Wang, Z.; Pu, F.; Yang, X.; Chen, N.; Shuai, Y.; Yang, R. Online LSTM-Based Channel Estimation for HF MIMO SC-FDE System. *IEEE Access* **2020**, *8*, 131005–131020. [CrossRef]
23. Duan, H.; Yu, X.; Hou, Y. Efficient channel parameters estimation design for SC-FDE in HF wireless communications. In Proceedings of the 2015 8th International Congress on Image and Signal Processing, CISP 2015, Shenyang, China, 14–16 October 2015; Institute of Electrical and Electronics Engineers Inc.: Piscataway, NJ, USA, 2015; pp. 1338–1342. [CrossRef]
24. Myung, H.G. Introduction to Single Carrier FDMA-IEEE Conference Publication. Available online: https://ieeexplore.ieee.org/document/7099187 (accessed on 22 April 2021).

25. Yoshizawa, S.; Tanimoto, H.; Saito, T. SC-FDE vs. OFDM: Performance comparison in shallow-sea underwater acoustic communication. In Proceedings of the 2016 International Symposium on Intelligent Signal Processing and Communication Systems, ISPACS 2016, Phuket, Thailand, 24–27 October 2016; Institute of Electrical and Electronics Engineers Inc.: Piscataway, NJ, USA, 2016. [CrossRef]

26. Pancaldi, F.; Vitetta, G.M.; Kalbasi, R.; Al-Dhahir, N.; Uysal, M.; Mheidat, H. Single-Carrier Frequency Domain Equalization [A focus on wireless applications]. *IEEE Signal Process. Mag.* **2008**. [CrossRef]

27. Si, L.; Yu, X.; Yin, H.; Xu, W. Compressive sensing-based channel estimation for SC-FDE system. *Eurasip J. Wirel. Commun. Netw.* **2019**, *2019*, 16. [CrossRef]

28. Wang, J.; Ding, G.; Wang, H. HF communications: Past, present, and future. *China Commun.* **2018**, *15*, 1–9. [CrossRef]

29. Johnson, E.E. *Third-Generation and Wideband HF Radio Communications*; Artech House: Norwood, MA, USA, 2013.

30. Austin, B.A. Near vertical incidence skywaves in World War II: An historical perspective. In Proceedings of the 8th International Conference on High-Frequency Radio Systems and Techniques, Guildford, UK, 10–13 July 2000; IET: Piscataway, NJ, USA, 2000; pp. 225–229. [CrossRef]

31. Witvliet, B.A.; Alsina-Pagès, R.M. Radio communication via Near Vertical Incidence Skywave propagation: An overview. *Telecommun. Syst.* **2017**, *66*, 295–309. [CrossRef]

32. Appleton, E.V.; Barnett, M.A.F. On some direct evidence for downward atmospheric reflection of electric rays. *Proc. R. Soc. Lond. Ser. Contain. Pap. Math. Phys. Character* **1925**, *109*, 621–641. [CrossRef]

33. Appleton, E.V.; Builder, G. The ionosphere as a doubly-refracting medium. *Proc. Phys. Soc.* **1933**, *45*, 208–220. [CrossRef]

34. Witvliet, B.A. Near Vertical Incidence Skywave: Interaction of Antenna and Propagation Mechanism. Available online: https://www.researchgate.net/publication/284264255_Near_Vertical_Incidence_Skywave_-_Interaction_of_Antenna_and_Propagation_Mechanism_PhD_Thesis (accessed on 20 May 2021).

35. Gomes, R.; Al-Daher, Z.; Hammoudeh, A.; Sobaihi, K.; Caldeirinha, R.; Fernandes, T. Performance and evaluation of OFDM and SC-FDE over an AWGN propagation channel under RF impairments using simulink at 60 GHz. In Proceedings of the 2014 Loughborough Antennas and Propagation Conference, LAPC 2014, Loughborough, UK, 10–11 November 2014; Institute of Electrical and Electronics Engineers Inc.: Piscataway, NJ, USA, 2014; pp. 685–689. [CrossRef]

36. Male, J.; Porte, J.; Gonzalez, T.; Maso, J.M.; Pijoan, J.L.; Badia, D. Analysis of the Ordinary and Extraordinary Ionospheric Modes for NVIS Digital Communications Channels. *Sensors* **2021**, *21*, 2210. [CrossRef]

37. De Figueiredo, F.A.P.; Mathilde, F.S.; Cardoso, F.A.C.M.; Vilela, R.M.; Miranda, J.P. Efficient frequency domain zadoff-chu generator with application to LTE and LTE-A systems. In Proceedings of the 2014 International Telecommunications Symposium, ITS 2014-Proceedings, Sao Paulo, Brazil, 17–20 August 2014; Institute of Electrical and Electronics Engineers Inc.: Piscataway, NJ, USA, 2014. [CrossRef]

38. Trimeche, A.; Sakly, A.; Mtibaa, A. FPGA Implementation of ML, ZF and MMSE Equalizers for MIMO Systems. *Procedia Comput. Sci.* **2015**, *73*. [CrossRef]

39. Hervás, M.; Pijoan, J.L.; Alsina-Pagès, E.M.; Salvador, M.; Badia, D. Single-carrier frequency domain equalisation proposal for very long haul HF radio links. *Electron. Lett.* **2014**, *50*, 1252–1254. [CrossRef]

40. Kim, W.J.; Cho, K.J.; Stapleton, S.P.; Kim, J.H. An efficient crest factor reduction technique for wideband applications. *Analog Integr. Circuits Signal. Process.* **2007**, *51*, 19–26. [CrossRef]

41. Ojima, M.; Hattori, T. PAPR reduction method using clipping and peak-windowing in CI/OFDM system. In Proceedings of the IEEE Vehicular Technology Conference, Baltimore, MD, USA, 30 September–3 October 2007; pp. 1356–1360. [CrossRef]

42. Crest Factor Reduction-RFmx SpecAn 19.1 Help-National Instruments. Available online: https://zone.ni.com/reference/en-XX/help/374264N-01/rfmxspecan/crest_factor_reduction/ (accessed on 19 April 2021).

43. Watch, T. Ubiquitous Sensor Networks (USN) ITU-T Technology Watch Briefing Report Series, No. 4. 2008. Available online: http://www.itu.int/md/T05-NGN.GSI-DOC-0266/en (accessed on 18 May 2021).

44. Yu, W.; Liang, F.; He, X.; Hatcher, W.G.; Lu, C.; Lin, J.; Yang, X. A Survey on the Edge Computing for the Internet of Things. *IEEE Access* **2017**, *6*, 6900–6919. [CrossRef]

45. Red Pitaya-Stemlab Swiss Army Knife for Engineers. Available online: https://www.redpitaya.com/ (accessed on 20 May 2021).

46. Raspberry Pi 3 Model B+–Raspberry Pi. Available online: https://www.raspberrypi.org/products/raspberry-pi-3-model-b-plus/ (accessed on 13 April 2021).

47. Bonn, E. Bonn Elektronik BLWA 0103-250 1.5.30 MHZ. Available online: http://frontend.bonn-elektronik.com/pdfsheet.php?modellreihe=140&smid=354&lang=eng (accessed on 2 June 2021).

48. Maso, J.M.; Porte, J.; Pijoan, J.L.; Badia, D. Study of NVIS channel for USN protocol definition in antarctica. *Electronics* **2020**, *9*, 1037. [CrossRef]

49. Maso, J.M.; Male, J.; Porte, J.; Pijoan, J.L.; Badia, D. Ionospheric polarization techniques for robust NVIS remote sensing platforms. *Appl. Sci.* **2020**, *10*, 3730. [CrossRef]

50. Maso, J.M.; Porte, J.; Pijoan, J.L.; Badia, D. Internet of Things Communications for Remote Sensors in Antarctica Using NVIS. 2019. Available online: https://www.researchgate.net/publication/335774336_Internet_of_things_communications_for_remote_sensors_in_Antarctica_using_NVIS (accessed on 20 April 2021).

51. Porté, J.; Lluis Pijoan, J.; Masó, J.; Badia, D.; Zaballos, A.; Maria Alsina-Pagès, R. Advanced HF Communications for Remote Sensors in Antarctica. In *Antarctica—A Key to Global Change*; IntechOpen: London, UK, 2018.
52. Nikoukar, A.; Raza, S.; Poole, A.; Gunes, M.; Dezfouli, B. Low-power wireless for the internet of things: Standards and applications. *IEEE Access* **2018**, *6*, 67893–67926. [CrossRef]